Aerodynamic Model Identification of the Flying-V Using Flight Data

Kevin Siemonsma

Technische Universiteit Delft

TU Delft Delft University of Technology

Challenge the future

AERODYNAMIC MODEL IDENTIFICATION OF THE FLYING-V USING FLIGHT DATA

by

Kevin Siemonsma

to obtain the degree of Master of Science
at the Delft University of Technology,
to be defended publicly on Wednesday October 5th, 2022 at 09:30.

Student number:	4271917
Project Duration:	January 7th 2021 - October 5th 2022
Thesis committee:	Dr.ir. C.C. de Visser, TU Delft, Chair & Supervisor
	Dr.ir. E. van Kampen, TU Delft, Examiner
	Dr.ir. R. Vos, TU Delft, Examiner

TU Delft

Executive summary

The Flying-V is a new aircraft which breaks with the conventional tube and wing layout. This "Flying-Wing" layout promises an increased aerodynamic efficiency of 25% compared to the Airbus A350.

This research focuses on developing a new aerodynamic model using flight data for a 4.6% scaled version of the Flying-V. This model can be used to get better insights in the handling characteristics and stability of the novel aircraft.

Flight data gathered in eight test flights. The two-step method used consists of first, the state estimation using an Iterated Extended Kalman Filter(IEKF), and second the polynomial model structure is determined using a stepwise regression algorithm. Using the state estimate a stepwise regression performed a model structure estimation. The longitudinal models generally also perform better, with an average RRMSE of 13.2% compared to 13.4% for the lateral models. In addition, more higher order terms were needed for the lateral models. This indicates that more informative data is needed to model the lateral system behaviour. For C_X it is found that the current thrust model is not adequate. The model for the pitching moment gave a large deviation from the model that was found during wind tunnel tests. Finally, for C_n a clear relationship with β could not be found. This is likely due to the relatively small rudder and short arm of the Flying-V.

Preface

This thesis develops a new aerodynamic model of the Flying-V. In addition, this model is used to get an insight in the handling during the flight tests. The thesis is divided into two main sections: the scientific paper and the literature study. The thesis is concluded with the conclusions of the research and recommendations for further research.

This thesis is the final milestone of my Aerospace Engineering master program.

I would like to take this opportunity to express my gratitude to my family and Borui Song who were always there to support me. Finally I wish to thank my supervisor Coen de Visser for guiding me thought the final part of my master and providing me with new insights and different perspectives on the topics of this thesis.

Contents

Nomenclature

Abbreviations

SS_R	Sum of squares of the regression
MSE	Mean squared error
PSE	Predicted squared error
RLI	Resin Liquid Infusion
RRMSE	Relative root mean square
TAS	True Airspeed
VLM	Vortex Lattice Method

Symbols

α	Aerodynamic angle of attack	$[rad]$
β	Aerodynamic sideslip angle	$[rad]$
δ_a	Aileron deflection	$[rad]$
δ_e	Elevator deflection	$[rad]$
δ_r	Rudder deflection	$[rad]$
λ_i	Estimated sensor bias	$[-]$
$\overline{c}$	Mean aerodynamic chord	$[m]$
$\overline{q}$	Dynamic pressure	$[Pa]$
ϕ	Body axis angle around the x-axis	$[rad]$
ψ	Body axis angle around the z-axis	$[rad]$
σ^2	Variance	
θ	Body axis angle around the y-axis	$[rad]$
θ_i	Model parameter of regressor i	$[-]$
A_i	Acceleration in i-direction	$[m/s^2]$
C_D	Drag coefficient	$[-]$
C_L	Lift coefficient	$[-]$
C_l	Moment coefficient around x-axis	$[-]$
C_m	Moment coefficient around y-axis	$[-]$
C_n	Moment coefficient around z-axis	$[-]$
C_X	X-force coefficient	$[-]$
C_Y	Y-force coefficient	$[-]$
C_Z	Z-force coefficient	$[-]$
F_a	Aerodynamic reference frame	$[-]$

F_b	Body-fixed reference frame	[−]
T_C	Thrust force coefficient	$[T/\overline{q}S]$
V_{TAS}	True Airspeed	$[m/s]$
b	Wing span	$[m]$
D	Propeller diameter	$[m]$
J	Advance ratio	$[V/nD]$
L	Moment around x-axis	$[Nm]$
M	Moment around y-axis	$[Nm]$
m	Mass	$[kg]$
N	Moment around z-axis	$[Nm]$
n	Propeller rotational velocity	$[RPS]$
p	Rotational velocity around the x-axis	$[rad/s]$
q	Rotational velocity around the y-axis	$[rad/s]$
r	Rotational velocity around the z-axis	$[rad/s]$
S	Wing surface area	$[m^2]$
T	Thrust force	[−]
u	Velocity in x-direction	$[m/s]$
v	Velocity in y-direction	$[m/s]$
w	Velocity in z-direction	$[m/s]$
X	Force in x-direction	$[N]$
Y	Force in y-direction	$[N]$
y	Estimated output vector	
Z	Force in z-direction	$[N]$
z	Sensor measurement output vector	

I

INTRODUCTION

1 Introduction

From the iconic Douglas DC3 to the state-of-the-art Airbus A350, for the past ninety years, air transportation has been reliant on aircraft with a tube and wing layout. To improve fuel efficiency, the Flying-V was proposed by Benad [2015], which breaks with the conventional tube and wing layout. This "flying wing" configuration where passengers and cargo will be placed inside the wing offers multiple advantages according to Martinez-Val [2007], like reduced fuel consumption and noise levels at take-off and landing. Studies have shown an aerodynamic efficiency increase of 25% compared to the Airbus A350[Faggiano et al., 2017]. This significant improvement in efficiency sparked great interest in the industry and from TU Delft[1]. Here, more aerodynamic analysis and optimisations were performed [Faggiano et al., 2017; R.Viet, 2019; Palermo, 2019; Empelen, 2020; Johnson, 2021]. In addition, preliminary aerodynamic models have also been developed. Cappuyns et al. [2019] made an initial model using computational methods. Later Garcia [2019], continued by developing a model using wind tunnel data.

This study is focused on exploring the possibilities of using in-flight experimental data of a 4.6% scaled Flying-V model. The goal is to estimate a new aerodynamic model which can be used to replicate the behaviour of the Flying-V. The knowledge gained from this new model will be compared to the previously estimated wind tunnel models. In addition, this model will also give new insights on the behaviour and stability of the Flying-V.

1.1. Research Objective

The goal of this study is to estimate a new aerodynamic model using in-flight data which can closely resemble the flight characteristics of a 4.6% scaled Flying-V.

> "The aim of this research is to contribute to the development of the Flying-V, by generating a new aerodynamic model using the available in-flight test data. This model can give new insights on the behaviour of the Flying-V."

To aid the process of generating a new model and investigating the in-flight behaviour of the Flying-V, several research questions are formulated. The first question is

> Which methods are most suitable for aerodynamic system identification of the Flying-V using the available experimental flight data and information gained from previous studies?

This question is the starting point of the investigation. Using the knowledge gained from wind tunnel tests and restrictions of the flight tests a good indication of a suitable estimation method can already be determined.

> What influence does the amount of input parameters and the individual parameters have on the model behaviour?

The second question focuses on analysing the influence of the parameters on the model. Different parameters can have a different improvement on the model quality. In addition, certain parameters can indicate certain system behaviour of the Flying-V. Which leads to the final question.

> What new information on handling and stability of the Flying-V can be gathered compared to the wind tunnel models?

This final research question targets both the quantitative and qualitative performance of the in-flight model compared to the wind tunnel models. It is known that wind tunnel experiments have their limitations. So the flight experiments may give information on parts where the wind tunnel experiments could not.

[1] https://news.klm.com/klm-and-tu-delft-present-successful-first-flight-flying-v/ [visited 9-9-2021]

1.1.1. OUTLINE

This thesis report has three main parts, Part I, the research paper, Part II, the literature survey and Part III the overall conclusion of this thesis.

Part I contains the contributions to the research in the form of a research paper. The Part II, contains the literature survey where background information on the project is presented, followed by an investigation into state- and parameter estimation methods and finally information on what is already available on information on the Flying-V. The final part, Part III, contains the overall conclusion of this research.

II

Research Paper

Aerodynamic Model Identification of a Sub scale Flying-V using In-flight Data

K. Siemonsma
Control & Simulation Aerospace Engineering, TU Delft

An aerodynamic model of a 4.6% scaled version of the Flying-V is estimated using flight data gathered in eight test flights. The two-step method used consists of first, the state estimation using an Iterated Extended Kalman Filter(IEKF), and second the polynomial model structure is determined using a stepwise regression algorithm. Using the state estimate a stepwise regression performed a model structure estimation. The longitudinal models generally also perform better, with an average RRMSE of 13.2% compared to 13.4% for the lateral models. In addition, more higher order terms were needed for the lateral models. This indicates that more informative data is needed to model the lateral system behaviour. For C_X it is found that the current thrust model is not adequate. The model for the pitching moment gave a large deviation from the model that was found during wind tunnel tests. In addition, for C_n a clear relationship with β could not be found. Both of this is likely due to the relatively low level of excitations present in the data set.

I. Introduction

From the iconic Douglas DC3 to the state-of-the-art Airbus A350, for the past ninety years, air transportation has been reliant on aircraft with a tube and wing layout. To improve fuel efficiency, the Flying-V was proposed[1], which breaks with the conventional tube and wing layout. This "flying wing" configuration where passengers and cargo will be placed inside the wing offers multiple advantages[2], like reduced fuel consumption and noise levels at take-off and landing. Studies have shown an aerodynamic efficiency increase of 25% compared to the Airbus A350[3]. This significant improvement in efficiency sparked great interest in the industry and from TU Delft[1]. Here, more aerodynamic analysis and optimisations were performed [3–7]. In addition, preliminary aerodynamic models have also been developed. First only using computational methods [8]. Later a new model was developed using wind tunnel data[9].

This study is focused on exploring the possibilities of using in-flight experimental data of a 4.6% scaled Flying-V model to estimate an aerodynamic model. The following sections dive into the Flying-V project itself and the scaled model used for this research.

A. Background

In this section, a brief background on the Flying-V project is presented. In subsubsection I.A.1 a summary on the research done can be found. Then subsubsection I.A.2, the layout of the scaled version on the Flying-V used for this project.

[1] `https://news.klm.com/klm-and-tu-delft-present-successful-first-flight-flying-v/`[visited 9-9-2021]

1. Flying-V Project

The Flying-V was first proposed in 2015[1]. This revolutionary new aircraft is comparable to an Airbus A350-900. However, initial simulations have shown that the new shape is estimated to have a 10% higher L/D and a 2% lower empty weight. Moreover, in the design, the engines are mounted on top of the aircraft, reducing the noise level as compared to the reference aircraft.

At the TU Delft, the development of the Flying-V was continued. An initial optimisation was performed at the cruise condition of Mach 0.85 and a lift coefficient (C_L) of 0.26 at an altitude of 13,000m[3]. A key adjustment made to the design was to increase the outer wing sweep from 15° to 30° to reduce high local Mach numbers on the wing and improve the lift distribution. Moreover, this also improved the L/D ratio from 22.8 to 23.5. Finally, this newly optimised design was compared to the NASA Common Research Model. With an L/D of 18.9, it was found that the Flying-V is 25% more efficient than the reference model.

After the aerodynamic optimisation, the flight characteristics were analysed[4]. Experiments were conducted on a 4.6% scaled model in the Open Jet Facility at the Delft University of Technology. Using balance measurements it was shown that at untrimmed configuration the wind tunnel model has a maximum lift coefficient of 1.09 at 41 degrees angle of attack. The same measurements concluded that the stability derivative of the pitching moment is negative up to an angle of attack of 20°, measured at the quarter mean aerodynamic chord. Furthermore, the trimmed flight was investigated. It was found that due to trim limitations the centre of gravity location is limited between 1.345 and 1.425 meters behind the nose. An optimal centre of gravity location of 1.365 meters behind the nose was found when approach was taken into account. At this trimmed condition, the stall speed was found to be at $14.8m/s$ at an angle of attack of 28.5°.

Continuing with experimenting in the wind tunnel, the static stability and control characteristics were researched[5]. At an angle of attack range from $-10°$ to 35° deep-stall characteristics were not observed, meaning that at least within this range control surfaces will stay effective. Also, it was found that the position of the optimal centre of gravity for maximised lift coefficients occurs at 1.336 meters from the nose. The maximum lift coefficient in clean configuration at horizontal steady flight is 0.7. It is concluded that statically stable flight can be achieved with a maximum lift coefficient of 0.7 at the most forward centre of gravity location of 1.33 meters and 0.6 with the centre of gravity at the most aft location of 1.39 meters from the nose.

The wind tunnel data was also used to estimate a first aerodynamic model using experimental data[9]. It was found that in general global polynomials achieve appropriate prediction performance. This model structure was determined by using a Modified Stepwise Regression. Deficiencies were found due to the large range of measured angles of attack. Therefore, splines were used to estimate a continuous model with a better fit. Unfortunately, it was not possible to compare these results with other Flying-V model data, since these were not available at the time. The estimated models did provide the possibility to determine thrust and control surface settings required for level flight at different airspeeds and flight angles. An analysis into the centre of gravity range was also included.

The previous wind tunnel experiments did not include any engines on the scaled model. The investigation of the effects on the performance when engines are integrated was the following step[6]. It was found that this integration generates additional lift due to jet inference. However, an increase in drag has also been observed. Moreover, C_{m_α} gets influenced by the addition. Between 5° and 12.5° C_{m_α} is negative, while it is positive between 12.5° and 22.5°. In addition, an initial thrust model was formulated using isolated wind tunnel data, resulting in the following expression

$$T_C = 0.025J^{-2} + 0.011J^2 - 0.0297 \quad \text{Where} \quad J = \frac{V_\infty}{nD} \tag{1}$$

Here V_∞ is the free stream airflow velocity, n is the rotational velocity in RPS and D is the rotor

diameter.

Finally, winglets were added to the wind tunnel model[7]. An analysis of the effects of a winglet and rudder deflection was done since these are integrated into the winglets. For angels below 10°, it was found that the lift coefficient slightly increases with about 0.0035 per degree and for higher angles decreases by about 0.016 per degree. The drag coefficient increases by about 0.004 per degree for angels below 28°. In addition, a winglet also reduces the maximum untrimmed L/D ratio from 14.4 to 12.3 at 10° angle of attack and increases the pitching moment. The rudder deflections have also been found to reduce the lift coefficient, with a maximum of 0.0024.

2. Flying-V Layout

The layout of the full scale Flying-V is presented in this section. In Table 1 the important physical parameters of the Flying-V can be found and in figs. 1a to 1d multiple views of the Flying-V are presented[2].

Parameter	Value	Unit
Length	55	[m]
Wingspan	65	[m]
Height	17	[m]
Pax	314	[−]
Fuel capacity	140.000	[l]
Cargo Capacity	160	[m^3]
Design Mach number	0.85	[−]
Cruise altitude	43,000	[ft]

Table 1. Design parameters of the full-scale Flying-V [8]

B. Scaled Flying-V

In the previous sections, subsection I.A, the full-scale Flying-V is briefly discussed. For this research, a downsized version of the Flying-V is used. This section elaborates on the aircraft which is being used for flight testing. In subsubsection I.B.1 information on the manufacturing and physical sizing of the Flying-V can be found. All the onboard systems are discussed in subsubsection I.B.2.

1. Physical Layout

For the flight test a 4.6% scaled model is used, so the test model complies with the legal weight limitation of 25kg for drones in the Netherlands. The Flying-V is constructed from glass fibre using Resin Liquid Infusion (RLI) with epoxy, in a negative mould. At the leading and trailing edges, Airex C70.75 foam panels are used. The ribs and spars are water jet cut from honeycomb reinforced glass fibre panels, see Fig. 2. The physical parameters of the scaled Flying-V can be found in Table 2.

[2]`https://www.tudelft.nl/en/ae/flying-v/`

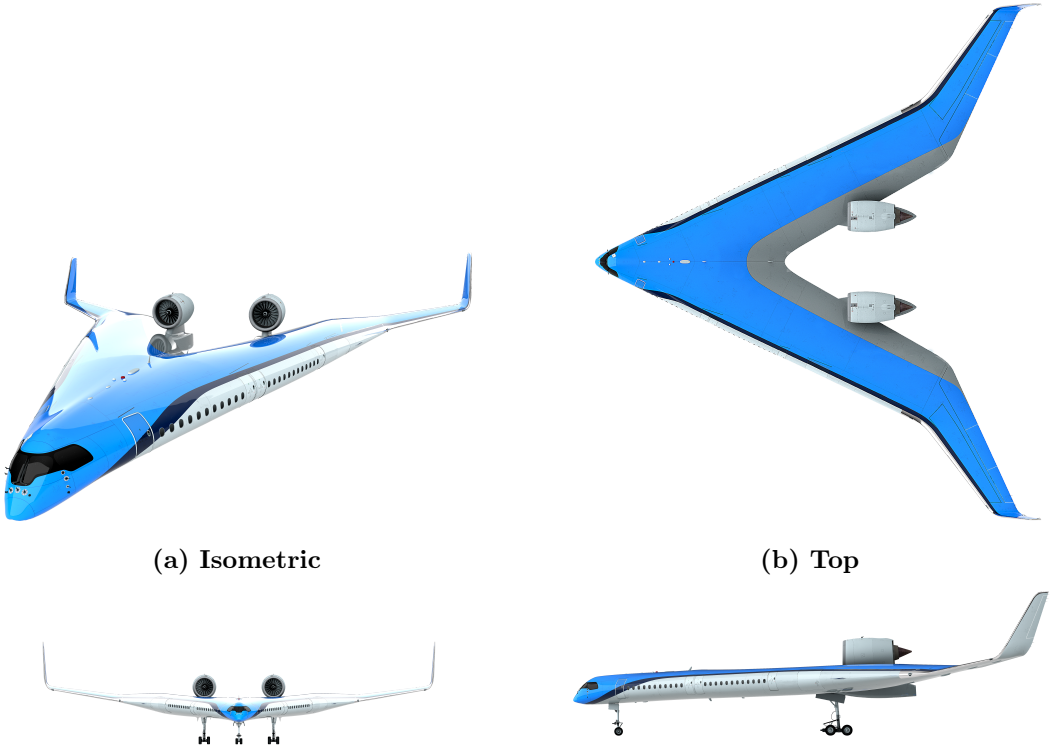

(a) Isometric **(b) Top**

(c) Front **(d) Left**

Figure 1. Renderings of the Flying-V

2. Onboard Systems

The test model has various systems onboard. These systems can be split up into two categories, flight control devices and onboard sensors.

The flight control devices are responsible for the control surfaces and engine. The control surfaces are the elevons and rudders. In Fig. 3, CS1, CS2 and CS3 are the elevons. The rudders are integrated into the winglets.

The specifications of the servos used to move the control surfaces can be found in Table 3. Both the two engines comprise of an electric motor and a ducted fan. The specifications can be found in Table 4.

Various sensors are used to measure the state of the aircraft. Two systems are responsible for the collection of the data, the build-in sensors of the Pixhawk 4 autopilot system[3] and the Aeroprobe Voyager[4]. The Pixhawk 4 uses the internal GPS and INS to estimate the position and Euler angles. The Aeroprobe Voyager, gathers aerodynamic parameters such as airspeed and aerodynamic angles. Table 5 gives an overview of the sensors and the standard deviations provided by the manufacturer or literature[10].

C. Outline

This thesis report has two main parts, Part I, the research paper and Part II, the literature survey.

[3] `https://docs.px4.io/master/en/flight_controller/pixhawk4.html`

[4] `http://www.aeroprobe.com/micro-air-data-computer-models/`

	Value	Unit
Mass	22.947	kg
S	1.866	m^2
$\overline{c}$	0.817	m
b	2.9	m
I_{xx}	6.165	kgm^2
I_{yy}	7.442	kgm^2
I_{zz}	13.289	kgm^2
I_{xy}	0.024	kgm^2
I_{yz}	-0.002	kgm^2
I_{xz}	0.397	kgm^2
$x_{cg}/\overline{c}$	34.02	%
$x_{ref}/\overline{c}$	25	%

Table 2. Physical parameter of the scaled Flying-V

Part I is set out as follows. In section II the flight test data and flight path reconstruction using an Iterated Extended Kalman Filter are discussed. Continuing on that, the methodology behind the aerodynamic model identification is explained in section III. Then finally, the results of the methods can be found in section IV. In Part II the literature survey is presented.

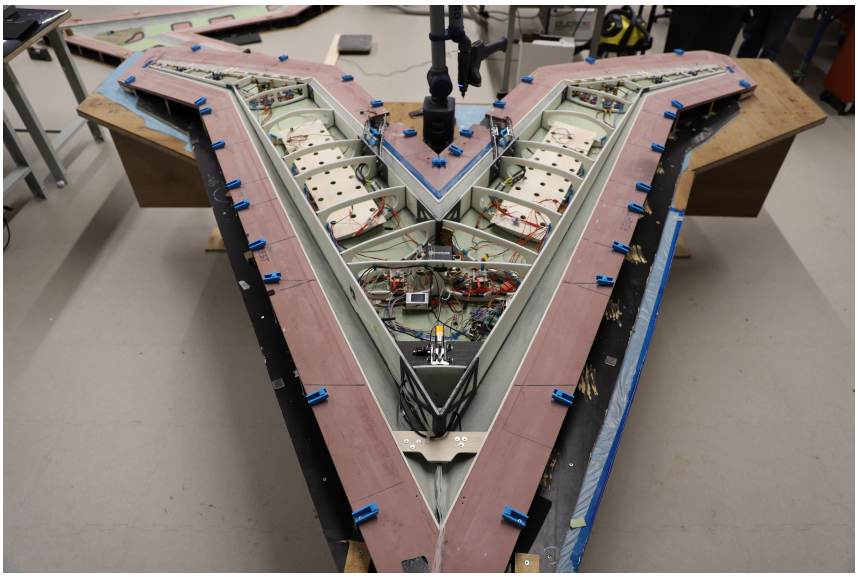

Figure 2. Flying-V during assembly

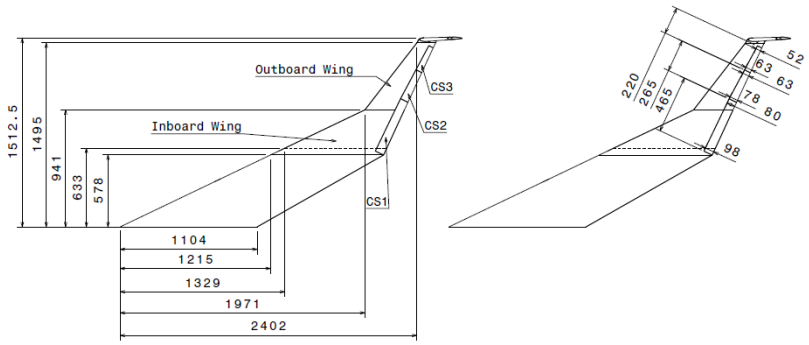

Figure 3. Half wing Flying-V sizing [7]

				Unit
Manufacturer	Hitec Multiplex	Hitec Multiplex	Hitec Multiplex	-
Model	D954SW	D89MW	HS-5070MH	-
Control surface	Inboard (CS1)	Middle (CS2) Rudder	Outboard (CS3)	-
Max torque range	18-29	5.3-8.5	3.0-3.7	kg/cm
Operating voltage range	4.8-7.4	4.8-7.4	6.0-7.4	V
Idle current	30	30	3	mA
No load operating current	500	300	240	mA
Stall current	5200	2900	1300	mA
Speed (Seconds to 60°)	0.19-0.12	0.17-0.11	0.14-0.12	s

Table 3. Servo Specifications

	Value	Unit
Manufacturer	Schubeler Jets	-
Model number fan	DS-86-AXI HDS	-
Model number electric motor	HET800-68-685kV	-
Diameter	120	mm
Thrust static	60	N
Max. Thrust	86	N
Max voltage	52	V
Max current	108	A
Max RPM	33000	RPM

Table 4. Ducted fan specifications [6]

Symbol	Sensor	System	Standard Deviation	Unit
A_x	Accelerometer	Pixhawk 4	$1.294 \cdot 10^{-2}$	m/s^2
A_y	Accelerometer	Pixhawk 4	$1.324 \cdot 10^{-2}$	m/s^2
A_z	Accelerometer	Pixhawk 4	$2.012 \cdot 10^{-2}$	m/s^2
p	Gyroscope	Pixhawk 4	$7.026 \cdot 10^{-4}$	rad/s
q	Gyroscope	Pixhawk 4	$6.325 \cdot 10^{-4}$	rad/s
r	Gyroscope	Pixhawk 4	$6.218 \cdot 10^{-4}$	rad/s
ϕ	GPS/INS	Pixhawk 4	0.3	$^\circ$
θ	GPS/INS	Pixhawk 4	0.3	$^\circ$
ψ	GPS/INS	Pixhawk 4	0.8	$^\circ$
V_{TAS}	Air Data Probe	Aeroprobe Voyager	1	m/s
α	Air Data Probe	Aeroprobe Voyager	1	$^\circ$
β	Air Data Probe	Aeroprobe Voyager	1	$^\circ$

Table 5. Sensor noise statistics

II. Flight Path Reconstruction

A two-step method is applied to determine the an aerodynamic model using flight data. The first step is the flight path reconstruction, where a Kalman filter is used to estimate the states needed for the second step, the model identification step. This chapter contains an elaboration on the state estimation step. First a brief description is given on the data acquisition. Second, the method and results of the state estimation are discussed.

A. Flight data

Between June 22nd, 2021 and June 25th, 2021 a total of eight flight tests were carried out. An overview of the weather on those days can be found in table 6. The Flying-V is equipped with an Aeroprobe Voyager Digital Air Data Computer (DADC) and a Pixhawk 4 autopilot, which are responsible for the acquisition of the measurement data.

Date	Data sets	Temperature $[°C]$	Wind speed $[m/s]$	Wind Direction $[°]$
22-06-2021	1	14.5	3.7	24
23-06-2021	2, 3	14.6	2.5	14
24-06-2021	4, 5	15.0	1.4	352
25-06-2021	6, 7, 8	14.8	2.2	193

Table 6. Average weather statistics on test flight days[5]

It is important to mention that on June the 24th, 2021 the side slip angle was measured incorrectly due to sensor issues. Therefore, the data sets gathered on this day will not be used for lateral analysis.

The test flights usually consisted of various circles at different altitudes. In the later flights, (Flights 4-8) special identification manoeuvres were performed. During these flights, the pilot gave more extreme inputs, in order to generate more valuable data for system identification.

B. State estimation

The data gathered during the test flights contains noise. Sensor noise statistics provided by the manufacturers will enable an Iterated Extended Kalman filter (IEKF) to perform a state estimation. The IEKF is a nonlinear state estimation method based on the linear Kalman filter. The theory on how the linear Kalman filter and Extended Kalman filter work can be found in section VII.

In the regular EKF the perturbation equations are linearised around the nominal state. In the IEKF the nominal states are recursively updated in order to reduce the linearisation error. These iterative steps happen after step four of the EKF, as described in section VII, and are done as follows:

5) Measurement equation Jacobian recalculation:

$$H_x(\underline{\eta}_i) = \frac{\delta}{\delta \underline{x}} h(\underline{\eta}_i, \underline{u}(t), t) \tag{2}$$

6) Kalman gain recalculation:

$$K_{k+1}(\underline{\eta}_i) = P_{k+1,k}(\underline{x}(t), \underline{u}(t), t) H_x^T(\underline{\eta_i}) \left[H_x(\underline{\eta_i}) P_{k+1,k}(\underline{x}(t), \underline{u}(t), t) H_x^T(\underline{\eta_i}) + R_{k+1} \right]^{-1} \tag{3}$$

[5]URL https://weerverleden.nl/ [cited 31/03/2022]

7) Measurement update, update state estimate:

$$\underline{\eta}_{i+1} = \underline{\hat{x}}_{k+1,k} + K_{k+1}(\underline{\eta}_i)\big(\underline{z}_{k+1} - \underline{h}(\underline{\eta}_i, \underline{u}_{k+1}) - H_x(\underline{\eta}_i)(\underline{\hat{x}}_{k+1,k} - \underline{\eta}_i)\big) \tag{4}$$

$$\underline{\hat{x}}_{k+1,k+1} = \underline{\eta}_l \tag{5}$$

The iteration continues until it reaches the following performance measure:

$$\frac{\left\|\underline{\eta}_l - \underline{\eta}_{l-1}\right\|}{\left\|\underline{\eta}_{l-1}\right\|} \leq \varepsilon \tag{6}$$

After the iterative part, the covariance matrix will be calculated the same way as with the EKF with Eq. 76. A flowchart visualising each step of the IEKF can be found in Fig. 24a.

The following equations of motions are used

$$f(\underline{x}(t), \underline{u}(t), t) = \begin{bmatrix} \dot{u} \\ \dot{v} \\ \dot{w} \\ \dot{\phi} \\ \dot{\theta} \\ \dot{\psi} \\ \dot{\lambda}_x \\ \dot{\lambda}_y \\ \dot{\lambda}_z \\ \dot{\lambda}_p \\ \dot{\lambda}_q \\ \dot{\lambda}_r \end{bmatrix} = \begin{bmatrix} A_{x_{cg}} + \lambda_x - (q+\lambda_q)w + (r+\lambda_r)v - g\sin(\theta) \\ A_{y_{cg}} + \lambda_y - (r+\lambda_r)u + (p+\lambda_p)w + g\cos(\theta)\sin(\phi) \\ A_{z_{cg}} + \lambda_z - (p+\lambda_p)v + (q+\lambda_q)u + g\cos(\theta)\cos(\phi) \\ p + \lambda_p + (q+\lambda_q)\sin(\phi)\tan(\theta) + (r+\lambda_r)cos(\phi)\tan(\theta) \\ (q+\lambda_q)\cos(\phi) - (r+\lambda_r)\sin(\phi) \\ (q+\lambda_q)\sin(\phi)\sec(\theta) + (r+\lambda_r)\cos(\phi)\sec(\theta) \\ 0 \\ 0 \\ 0 \\ 0 \\ 0 \\ 0 \end{bmatrix} \tag{7}$$

Here λ_i is the estimated sensor bias, it is assumed that these sensor biases are time-invariant. The acceleration equations for $\dot{u}$, $\dot{v}$ and $\dot{w}$ take the accelerometer measurements into account. However, the accelerators are not located in the centre of gravity therefore the following correction equations are included in the IEKF

$$A_{x_{cg}} = A_{x_{pixhawk}} + (x_{cg} - x_{ac})\left(q^2 + r^2\right) - (y_{cg} - y_{ac})(pq - \dot{r}) - (z_{cg} - z_{ac})(pr + \dot{q}) \tag{8}$$

$$A_{y_{cg}} = A_{y_{pixhawk}} + (y_{cg} - y_{ac})\left(r^2 + p^2\right) - (z_{cg} - z_{ac})(qr - \dot{p}) - (x_{cg} - x_{ac})(qp + \dot{r}) \tag{9}$$

$$A_{z_{cg}} = A_{z_{pixhawk}} + (z_{cg} - z_{ac})\left(p^2 + q^2\right) - (x_{cg} - x_{ac})(rp - \dot{q}) - (y_{cg} - y_{ac})(rq + \dot{r}) \tag{10}$$

In these equations the subscript cg indicates the position of the centre of gravity and subscript ac the position of the sensor. The measured distances from the nose and centre line for the centre of gravity and sensor locations are:

$$x_{cg} = 1305 \text{ mm} \qquad x_{pixhawk} = 384 \text{ mm} \tag{11}$$

$$y_{cg} = 0.946 \text{ mm} \qquad y_{pixhawk} = 0 \text{ mm} \tag{12}$$

$$z_{cg} = 34.645 \text{ mm} \qquad z_{pixhawk} = 55 \text{ mm} \tag{13}$$

The sensor equations are defined as

$$h(\underline{x}(t), \underline{u}(t), t) = \begin{bmatrix} A_{x_{pixhawk}} \\ A_{y_{pixhawk}} \\ A_{z_{pixhawk}} \\ p \\ q \\ r \\ \phi \\ \theta \\ \psi \\ V_{TAS} = \sqrt{u^2 + v^2 + w^2} \\ \alpha = \tan^{-1}(\frac{w}{u}) \\ \beta = \tan^{-1}(\frac{v}{\sqrt{u^2+w^2}}) \end{bmatrix} \tag{14}$$

1. Assumptions

Several assumptions were made for the state estimation:

- The measurement noise variance matrix, R, consists of the noise statistics provided by the sensor manufacturers or found in literature[10], see Table 5.
- The process noise matrix, Q, is determined using trial and error. The best converging output was given when $Q = 0.10 \cdot I$.
- In eqs. (8) to (10) $\dot{p}$, $\dot{q}$ and $\dot{r}$ cannot be determined directly. To estimate these, p, q and r are filtered with a 5 Hz lowpass filter and the time derivative of these filtered signals is taken.
- Thrust is calculated using the thrust model estimated using wind tunnel experiments[6].

C. State Estimation Results

The IEKF was performed on all eight flights. In fig. 4 the result of the state estimation for an attempted 3211 manoeuvre is shown. The duration of each of the 3211 input sequence was reduced to a 1-0.5-0.3-0.3 manoeuvre. For the angle of attack (α), it is clear that a small bias and delay is present between the measured and predicted results. The bias is also present in the pitch angle (θ). This is most likely due to a fuselage-induced angle of attack. A large difference is found for the sideslip angle (β). For this flight, the operators noted that the sideslip angle sensor did not perform accordingly and did not give reliable results. Therefore, the predicted estimate of β is the best available estimate.

For the estimated biasses (λ_i) it was found that these are not constant, as for example for flight 5 can be seen in fig. 5. This means that the sensor bias is dependent on external factors. It is likely that this occurs because the sensors are relatively small and not as accurate as sensors on a full-scale airliner or a fixed wind tunnel setup. The biases for multiple initial conditions converge quickly after a few seconds as can be seen in fig. 6. The estimation results for the eight data set is displayed in Fig. 7, the other data sets can be found in section VIII.

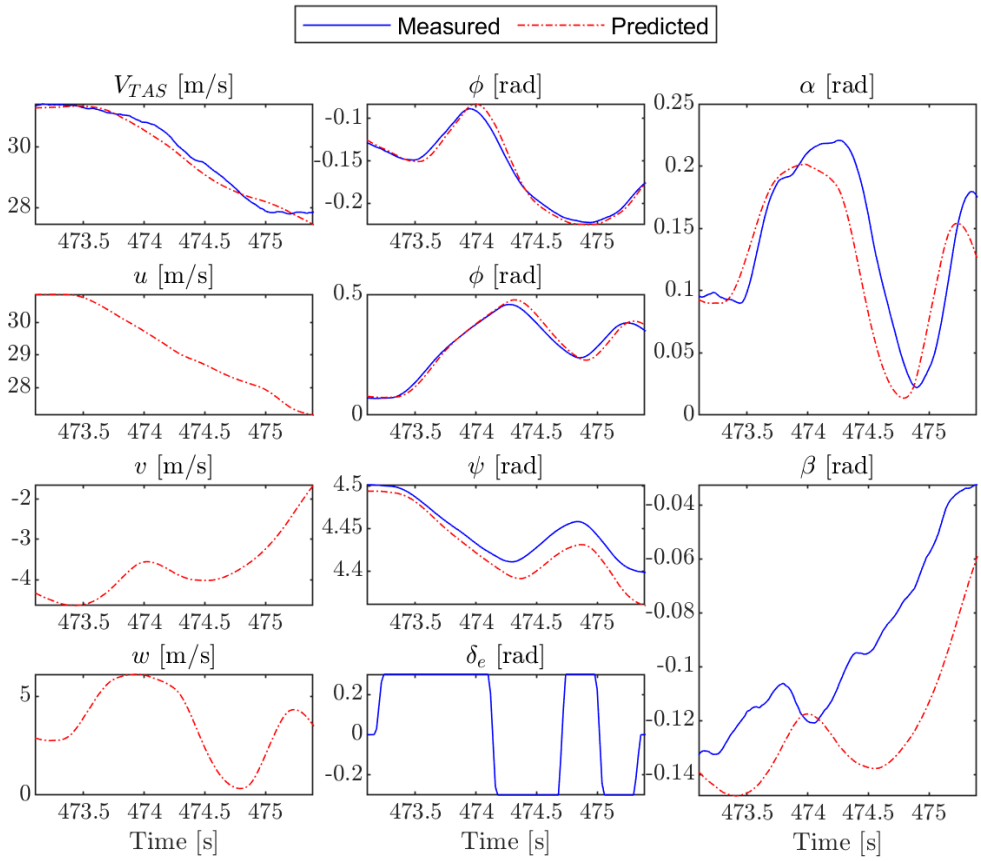

Figure 4. Reconstructed states (u, v, w, ϕ, θ, ψ) and observed parameters (V_{TAS}, α, β) for a longitudinal δ_e 3211 manoeuvre in the fifth flight.

D. Data Coverage

The data is manually picked for both the longitudinal and lateral directions to contain the most information for each case. The main focus was to extract the identification manoeuvres for training the model. However, to ensure safe flight operations the operators decided not to explore the full flight envelope and stay within the predictable boundaries. This is where the Flying-V remains easy to control. Therefore, only a limited amount of these manoeuvres were performed. In order to enrich the data set, other motions containing large pilot inputs and excitations were selected. For this, the source of the excitation was also taken into account. For example, take-off and landing were ignored since these involved aerodynamic effects such as ground effect, turbulence from the ground and the airplane touching the ground. In order to visualise the limitations of the aerodynamic model, a convex hull is formed around the data points. This is used to estimate the model, this can be seen in figs. 8 and 9. In these figures the α-β, α-V_{TAS} and β-V_{TAS} ranges are displayed. The convex hull surrounding the estimation data signifies the region of validity. Outside of this region, the accuracy of the model decreases.

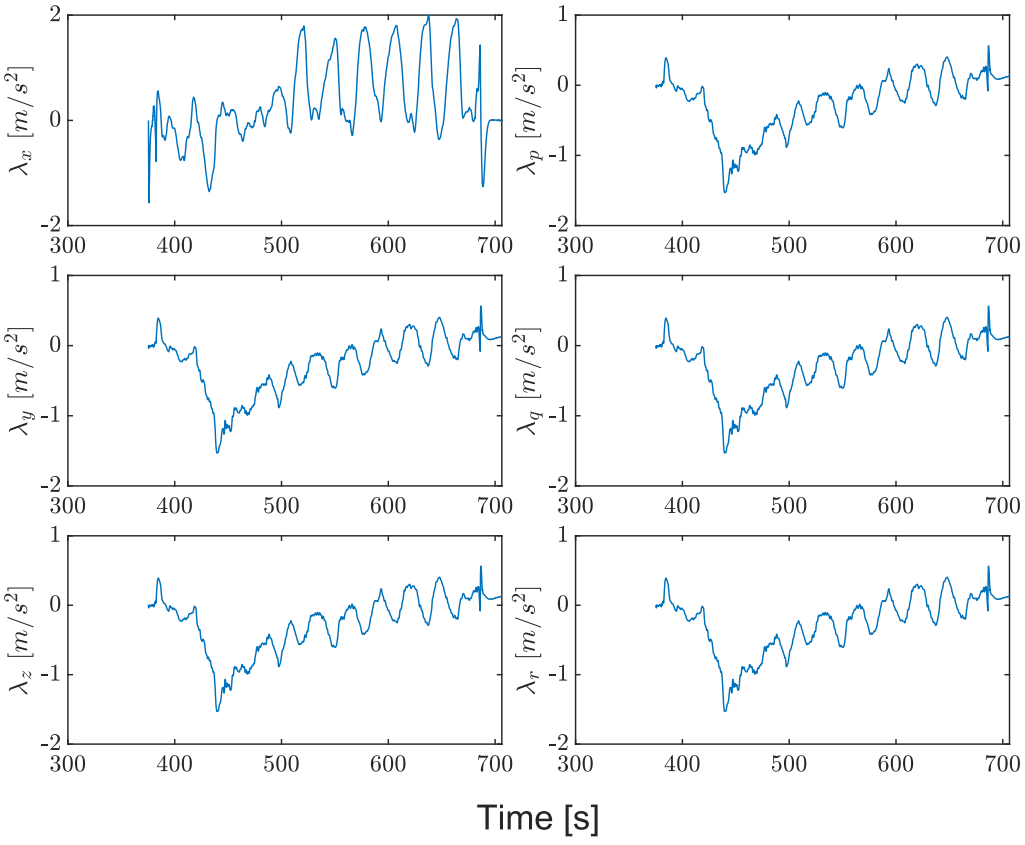

Figure 5. Linear and rotational sensor biases for flight 5

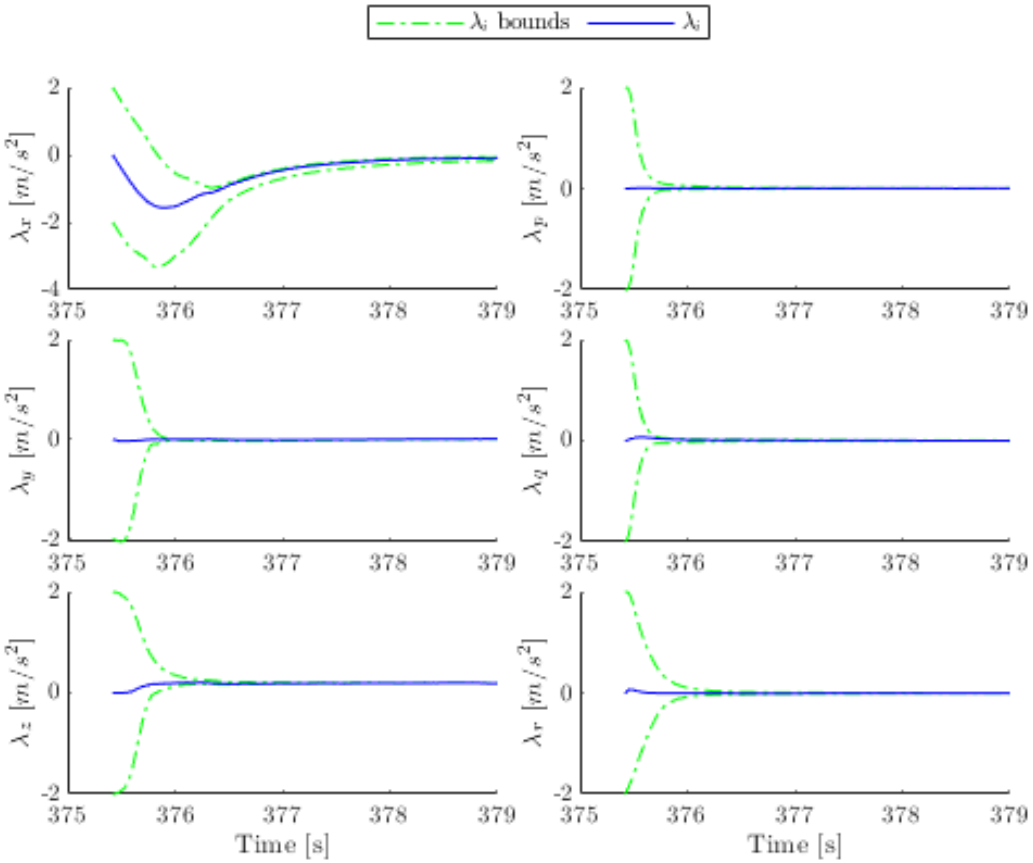

Figure 6. Convergence of biases for different initial conditions for flight 5

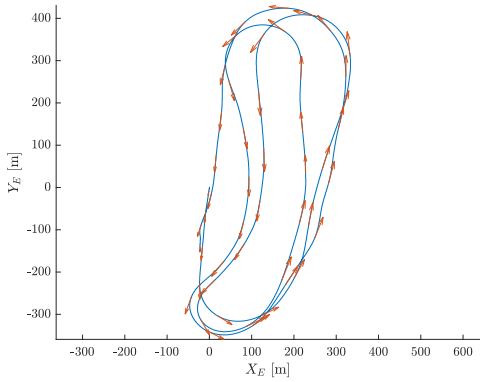

(a) **X-Y position**

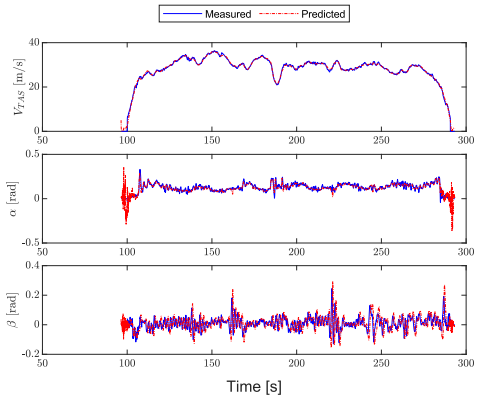

(b) V_{TAS}, α **and** β

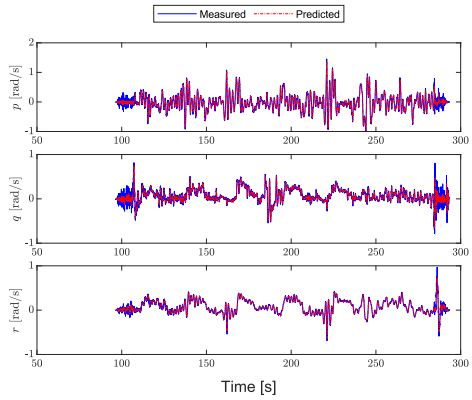

(c) p, q **and** r

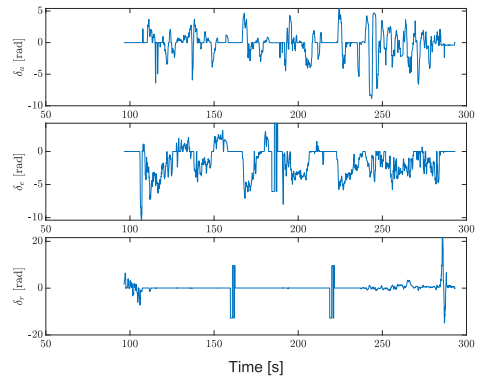

(d) δ_a, δ_e **and** δ_r

Figure 7. Set 8

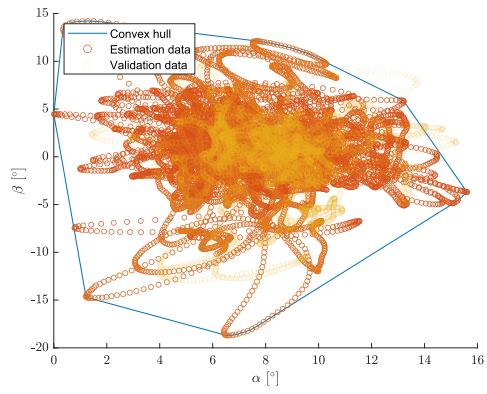

(a) α-β **range of training and validation data data**

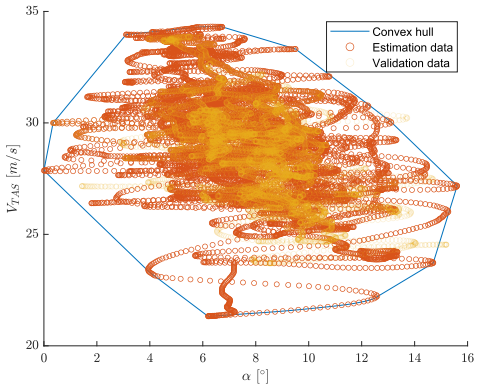

(b) α-V_{TAS} **range of training and validation**

Figure 8. Longitudinal data range

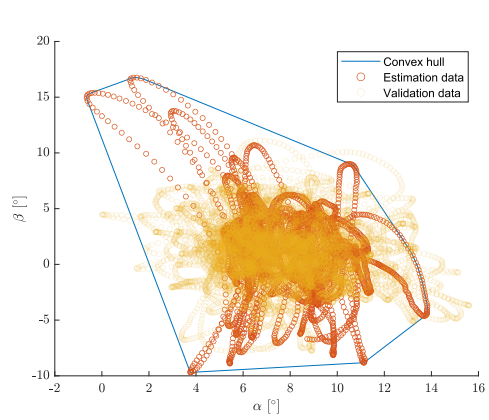

(a) α-β range of training and validation data data

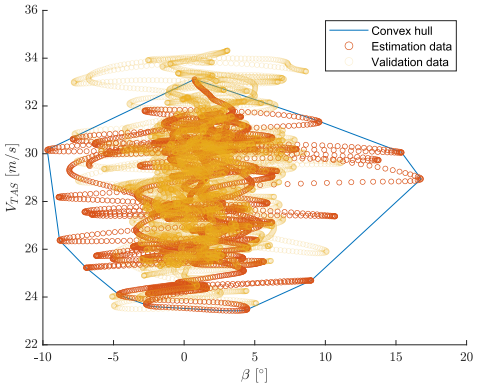

(b) β-V_{TAS} range of training and validation

Figure 9. Lateral data range

III. Aerodynamic model identification

This chapter explains the method for the aerodynamic model identification. First, a description of the basic shape of the model function is presented. Second, the estimation and model structure determination methods are described. Finishing up with a validation of the presented method.

A. Aerodynamic Model Definition

1. Model postulation

In previous research it was found that nonlinear unstable behaviour occurs at high angle of attacks. During the flight tests performed for this research these angles of attack were avoided. Therefore, a polynomial model will be used to represent the aerodynamic model of the Flying-V. The basic polynomial form of this model is

$$y = \theta_0 + \sum_{j=1}^{n} \theta_j x_j \tag{15}$$

Where n is the number of regressors, x_j are the regressors and θ the model parameters. This polynomial form can be used for both the force and moment representation. Adding higher order regressor terms to the polynomial may aid the model performance. These contain behaviour which is not directly available from the first order terms. To incorporate these higher order terms, the expression of eq. (15) can be changed to

$$\mathbf{y} = \theta_0 + \sum_{j=1}^{n} \theta_j \mathbf{p}_j \tag{16}$$

or in vector form

$$\mathbf{y} = X \cdot \theta \tag{17}$$

where $X = [1, p_1, p_2, ..., p_n]$.

Here $\mathbf{P}_j$ are functions of the independent variables [11]. y is the dependent variable.

2. Coefficient Definition

The aerodynamic force and moment coefficients in each Cartesian direction are defined as:

$$C_X(x) = \frac{X - T}{\bar{q}S} \qquad C_l(x) = \frac{L}{\bar{q}Sb} \tag{18}$$

$$C_Y(x) = \frac{Y}{\bar{q}S} \qquad C_m(x) = \frac{M}{\bar{q}S\bar{c}} \tag{19}$$

$$C_Z(x) = \frac{Z}{\bar{q}S} \qquad C_n(x) = \frac{N}{\bar{q}Sb} \tag{20}$$

Where

$$\bar{q} = \frac{1}{2}\rho V^2 \tag{21}$$

Here X, Y, Z are the body-axis components of the forces experienced by the airframe. Similarly, L, M, N are the body-axis components of the moment on the airframe. These are defined as:

$$X = A_X \cdot m \tag{22}$$
$$Y = A_Y \cdot m \tag{23}$$
$$Z = A_Z \cdot m \tag{24}$$

$$L = \dot{p} \cdot I_{XX} + p \cdot q(I_{ZZ} - I_{YY}) - (p \cdot q + \dot{r})I_{XZ} \tag{25}$$
$$M = \dot{q} \cdot I_{YY} + r \cdot p(I_{XX} - I_{ZZ}) - (p^2 - r^2)I_{XZ} \tag{26}$$
$$N = \dot{r} \cdot I_{ZZ} + p \cdot q(I_{YY} - I_{XX}) - (q \cdot r - \dot{p})I_{XZ} \tag{27}$$
$$\tag{28}$$

Here the moment of inertia, I_{nn} are measured using the CAD model and can be found in Table 2. The thrust force T is defined as:

$$T = \frac{T_C}{\overline{q}S} \tag{29}$$

As explained in subsubsection III.A.1 the model will consist of dependent and independent variables. The dependent variables are the force and moment coefficients. The independent variables, also regarded as regressors, will be the aerodynamic inputs. These consist of the translational velocities, rotational velocities and inputs. These are

$$\overline{x} = \begin{bmatrix} u & v & w & p & q & r \end{bmatrix}^T \tag{30}$$

and

$$\overline{u} = \begin{bmatrix} \delta_a & \delta_e & \delta_r \end{bmatrix}^T \tag{31}$$

Since the forces and moments are expressed as non-dimensional coefficients the aerodynamic variables will be non-dimensionalised using the following relations:

$$\hat{u} = \frac{u}{V_{TAS}} \qquad \alpha = \frac{w}{V_{TAS}} \qquad \beta = \frac{v}{V_{TAS}} \tag{32}$$
$$\hat{p} = \frac{pb}{2V_{TAS}} \qquad \hat{q} = \frac{q\bar{c}}{V_{TAS}} \qquad \hat{r} = \frac{rb}{2V_{TAS}} \tag{33}$$

This leads to the following non-dimensional state equation

$$x = \begin{bmatrix} \hat{u} & \alpha & \beta & \hat{p} & \hat{q} & \hat{r} \end{bmatrix}^T \tag{34}$$

The pilot inputs, $\overline{u}$, have the following definitions:

- δ_a
  - $\delta_a = \frac{\delta_{a,L} + \delta_{a,R}}{2} > 0$ When left aileron,$\delta_{a,L}$, is up, and right aileron,$\delta_{a,R}$, is down.
- δ_e
  - $\delta_e > 0$ when elevator, δ_e, is down.
- δ_r

– $\delta_r > 0$ when both left and right rudders,δ_e, are right.

To improve on the simplicity of the model the following assumptions are made[12]:
- Aircraft is a rigid body.
- Aircraft mass is constant.
- Earth is non-rotating.
- Earth is flat.
- Gravity is constant.
- Thrust acts perpendicular to the x-axis.

B. Model Structure Determination

Not every independent variable in the polynomial will have a significant effect on the model. So, a stepwise regression is used to determine the model structure. This is done by determining which regressors contain the most relevant information. This method consists of two parts namely, Forward Selection and Backwards Elimination.

Forward Selection This method starts with only the independent constant term θ_0. One by one new terms will be added to the model. The order in which regressors are added to the regression depends on the simple correlation between the orthogonalised regressor ξ_j and z, this correlation is defined as

$$r_{jz} = \frac{\sum_{i=1}^{N} \left[\xi_j(i) - \bar{\xi_j}\right] \left[z(i) - \bar{z}\right]}{\sqrt{S_{jj} S_{zz}}} \tag{35}$$

Where S_{jj} is the centred sum of squares for ξ_j, calculated as:

$$S_{jj} = \sum_{i=1}^{N} \left[\xi_j(i) - \bar{\xi_j}\right]^2 \tag{36}$$

and the centred sum of squares for S_{zz} is calculated as:

$$S_{zz} = \sum_{i=1}^{N} [z(i) - \bar{z}]^2 \tag{37}$$

When the partial F-statistic of the regressor with the highest absolute simple correlation exceeds the predefined entry value, F_{in}, the regressor enters the model. The partial F-statistic is defined as

$$F_0 = \frac{SS_R\left(\hat{\boldsymbol{\theta}}_{p+j}\right) - SS_R\left(\hat{\boldsymbol{\theta}}_p\right)}{s^2} \tag{38}$$

Here $SS_R(\hat{\boldsymbol{\theta}}_p)$ is the sum of squares of the regression with p terms. Furthermore, $SS_R\left(\hat{\boldsymbol{\theta}}_{p+j}\right)$ is the sum of squares of the existing model with p terms and the jth regressor added. s^2 is the fit error variance which is computed as

$$s^2 \equiv \hat{\sigma}^2 = \frac{\boldsymbol{v}^T \boldsymbol{v}}{(N - p - 1)} = \frac{\sum_{i=1}^{N} [z(i) - \hat{y}(i)]^2}{(N - p - 1)} \tag{39}$$

In this equation, it is assumed that the jth term is included in the regression. The addition of terms will continue until new regressors cannot pass F_{in} or all available regressors are added to

the model. This goes on either until all regressors are added or until the partial F-statistic entry requirement cannot be satisfied anymore.

Backward Elimination Backward elimination is the opposite of forward selection. Backward elimination starts with all the regressors already in the regression equation. In this case, the partial F-statistic of each term is determined and the term with the lowest statistic will be eliminated if it is lower than the predefined value F_{out}, so

$$F_0 = \min_j \frac{SS_R\left(\hat{\boldsymbol{\theta}}_p\right) - SS_R\left(\hat{\boldsymbol{\theta}}_{p-j}\right)}{s^2} < F_{\text{out}} \tag{40}$$

Stepwise Regression As explained, Stepwise Regression is a combination of forward selection and backward elimination. This algorithm can produce more efficient models, for example, the elimination step may find that earlier added terms have become irrelevant because a combination of other terms contains better information about the system. In Fig. 10, a flowchart is displayed describing the phases of the stepwise regression.

1. Model Criteria
The partial F-statistic is used to determine whether parameters are selected or eliminated. The entry and exit criteria are determined, α_{in} and α_{out}. This is done by trial and error. Initially, 0.015 is taken for both α_{in} and α_{out}. For each force and moment component, the Mean Squared Error (MSE) is used to estimate the entry and exit criteria. The selection criteria used can be found in table 7.

	α_{in}	α_{out}
C_X	$0.6 \cdot 10^{-5}$	$1.5 \cdot 10^{-4}$
C_Y	$0.11 \cdot 10^{-3}$	$1.5 \cdot 10^{-4}$
C_Z	$0.1 \cdot 10^{-3}$	$1 \cdot 10^{-5}$
C_l	$0.3 \cdot 10^{-4}$	$1.5 \cdot 10^{-4}$
C_m	$0.5 \cdot 10^{-6}$	$1.5 \cdot 10^{-3}$
C_n	$2.5 \cdot 10^{-5}$	$1.5 \cdot 10^{-3}$

Table 7. Selection criteria

2. Candidate Regressors
The basic regressors are the states and inputs described in eqs. (31) and (34). Each of the candidate regressors for each force and moment coefficient are carefully selected using comparable models[12]. Higher order terms are products between each of the states and inputs. The candidates are selected to go up to fourth-order regressors. This is in order to achieve a relatively high approximation power and at the same time have a simple model with a limited amount of terms, and later it is found that higher order terms do not significantly add to the performance. The candidates for each force and moment coefficient are:

$$\sum x_k^i x_l^j \quad \text{where} \quad i + j = n \quad n = 1, ..., n \tag{41}$$

Here n is the order of the polynomial and x_k and x_l are the regressors namely:

- Longitudinal (C_X, C_Z and C_m):
  - 1, $\hat{u}$, $\hat{q}$, α, δ_e
- Lateral (C_Y, C_l and C_n):
  - 1, $\hat{p}$, $\hat{r}$, β, δ_a, δ_r

In Table 8 the fixed terms can be found. These terms are expected to have a close relation to the output. In addition, these terms are able to provide important information about the stability of the Flying-V.

	Fixed Parameters
C_X	1, $\hat{u}$, δ_e
C_Y	1, β
C_Z	1, α
C_l	1, $\hat{p}$, δ_a
C_m	1, α, δ_e
C_n	1, β, δ_r

Table 8. Fixed parameters

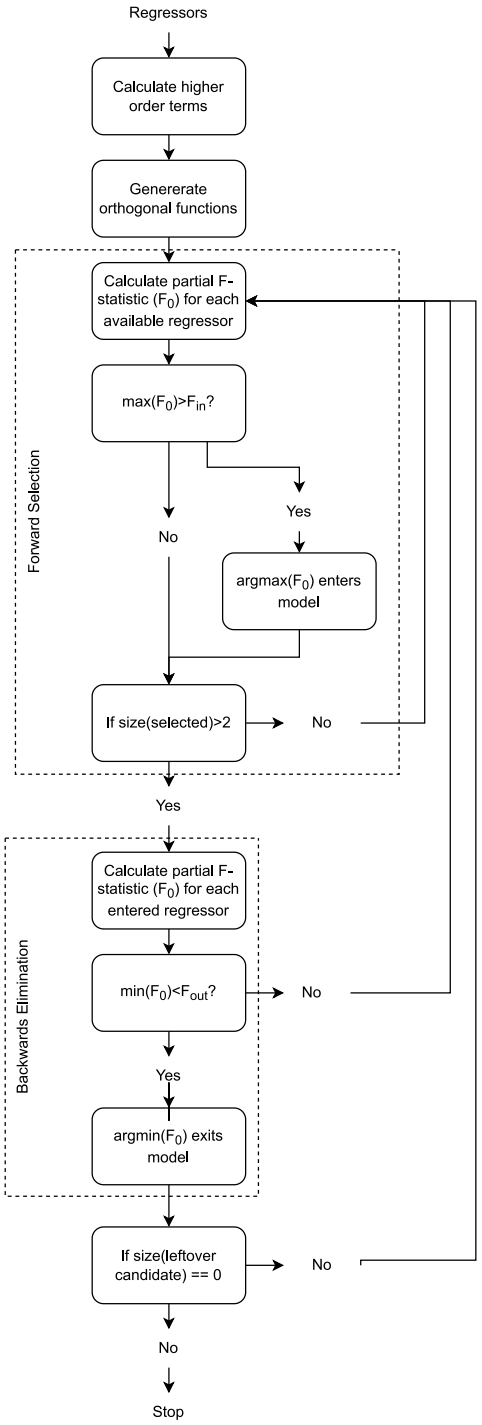

Figure 10. Stepwise regression flowchart

3. Final model structure
The final model structure can be chosen to be the final model that the algorithm will give. In general, this model structure would suffice, because it is the most suitable structure according to the algorithm. However, in this case, the principle of Parsimony is used. Thus a model with similar but lower performance can be chosen over the complex model. This can be done even though the complex model is more precise. To determine whether to choose a less accurate model the Predicted Squared Error [PSE] is applied. This is explained in Eq. 78. This metric compensates for the number of parameters in the model and will give a good estimation if more parameters are needed for better performance. The chosen model structure will be the one with the lowest PSE.

C. Multivariate Orthogonal functions
To improve the selection of, especially, higher order regressors, multivariate orthogonal functions are used. This is a method to uncorrelate regressors so the unique behaviours of each regressor is isolated[13]. For a stepwise regression, orthogonalisation can be performed after each selection or elimination step. The regressors will then be orthogonalised with respect to the, at that point, estimated model structure. However, for this analysis the multivariate orthogonal functions will be generated before the stepwise regression to improve on simplicity. These functions are generated using a Gram-Schmidt orthogonalisation procedure.

The goal is to generate orthogonal regressors which satisfies

$$p_i^T p_j = 0 \tag{42}$$

The orthogonalisation is started by choosing the first orthogonal polynomial. In this case, this is a vector containing only the number one, so $p_0 = 1$. The next regressors is calculated using

$$p_j = \xi_j - \sum_{k=0}^{j-1} \gamma_{kj} p_k \quad j = 1, 2, ..., n \quad \text{and} \quad k = 0, 1, ..., j-1 \tag{43}$$

Where

$$\gamma_{kj} = \frac{p_k^T \xi_j}{p_k^T p_k} \tag{44}$$

In Eq. 43, ξ_j, is an original independent variable. The order in which these are orthogonalised does not matter. The process is repeated until all independent variables are orthogonalised.

The relationship between X, the matrix with columns ξ_j, and P, with matrix columns p_j, is

$$X = PG \tag{45}$$

Here

$$G = \begin{bmatrix} 1 & \gamma_{01} & \gamma_{02} & \cdots & \gamma_{0n} \\ 0 & 1 & \gamma_{12} & \cdots & \gamma_{1n} \\ 0 & 0 & 1 & \cdots & \gamma_{2n} \\ \vdots & \vdots & \vdots & \vdots & \vdots \\ 0 & 0 & 0 & \cdots & 1 \end{bmatrix} \tag{46}$$

After performing the stepwise regression the output model is

$$\hat{y} = P\hat{a} \tag{47}$$

The final model structure can be extracted using the columns of G^{-1} corresponding to the selected orthogonal functions.

A verification of the method explained can be found in section X.

IV. Results and Discussion

The results are presented in this chapter. First the results of the model structure determination performed by the stepwise regression algorithm are revealed. Second, the estimated models are presented. Third, the flight and the wind tunnel model are compared to each other.

A. Model Structure

The stepwise regression algorithm, as explained in subsection III.B, was provided with regressors up to the third order. It was iteratively determined which regressors provide the most information to reconstruct an aerodynamic model of the Flying-V. For all six degrees of freedom, the regression converges to a model structure where the algorithm could not find terms which would improve the performance. This can be observed in section XII. Eventually, the model structure with the lowest MSE was chosen. The model structures can be found in eqs. (48) to (53) and the estimated parameters in table 9. The influence of each model term on the MSE performance is displayed in fig. 11. In these figures, it is clear that certain terms have a small influence on the performance of the models. For both C_Y and C_n, β gives a relatively small improvement. This regressor was manually selected to be in the model, since it can give information on the stability of the Flying-V. The small influence of β in the model indicates that the Flying-V has a low directional stability. From the model structure determination it is already clear that the longitudinal models do not benefit from higher order terms. The algorithm determined that these higher order terms do not significantly improve the fitting capability of the polynomials.

$$C_X = C_{X_0} + C_{X_{\hat{u}}}\hat{u} + C_{X_{\delta_e}}\delta_e + C_{X_\alpha}\alpha + C_{X_{\hat{q}}}\hat{q} + C_{X_{\hat{q}\alpha}}\hat{q}\alpha \tag{48}$$

$$\begin{aligned} C_Y = {} & C_{Y_0} + C_{Y_\beta}\beta + C_{Y_{\hat{p}}}\hat{p} + C_{Y_{\hat{p}\delta_a}}\hat{p}\delta_a + C_{Y_{\delta_a}}\delta_a + C_{Y_{\hat{r}^2}}\hat{r}^2 + C_{Y_{\hat{r}\beta}}\hat{r}\beta \\ & + C_{Y_{\hat{p}\hat{r}}}\hat{p}\hat{r} + C_{Y_{\hat{p}\delta_r^2}}\hat{p}\delta_r^2 + C_{Y_{\hat{r}\delta_a\delta_r}}\hat{r}\delta_a\delta_r + C_{Y_{\beta^3}}\beta^3 \end{aligned} \tag{49}$$

$$C_Z = C_{Z_0} + C_{Z_\alpha}\alpha + C_{Z_{\hat{u}}}\hat{u} + C_{Z_{\hat{q}}}\hat{q} \tag{50}$$

$$\begin{aligned} C_l = {} & C_{l_0} + C_{l_{\hat{p}}}\hat{p} + C_{l_{\delta_a}}\delta_a + C_{l_{\hat{r}}}\hat{r} + C_{l_\beta}\beta \\ & + C_{l_{\hat{r}^2}}\hat{r}^2 + C_{l_{\hat{r}\delta_a}}\hat{r}\delta_a + C_{l_{\hat{p}\delta_a}}\hat{p}\delta_a \end{aligned} \tag{51}$$

$$C_m = C_{m_0} + C_{m_\alpha}\alpha + C_{m_{\delta_e}}\delta_e + C_{m_{\hat{q}}}\hat{q} + C_{m_{\hat{u}}}\hat{u} \tag{52}$$

$$\begin{aligned} C_n = {} & C_{n_0} + C_{n_\beta}\beta + C_{n_{\delta_r}}\delta_r + C_{n_{\hat{p}}}\hat{p} \\ & + C_{n_{\hat{p}\delta_a}}\hat{p}\delta_a + C_{n_{\delta_a}}\delta_a + C_{n_{\hat{r}\beta}}\hat{r}\beta \end{aligned} \tag{53}$$

B. Flying-V Model Performance

In table 10 the quantitative performance metrics can be found. The R^2 is measured compared to the training set and for the MSE and Relative RMSE (RRMSE), the models are compared to a separate validation data set. This table is also a comparison between a first-order model and the current second-order model. Looking at table 10, it becomes clear that C_Y and C_n greatly benefit from a higher order model. Looking at the fitting parameter R^2, C_m is exceptionally low compared to the other. This is due to a shortage of information provided by the available regressors. These did not manage to capture very specific behaviour in C_m.

Comparing the performance of each component to each other, it is clear that the longitudinal models manage to replicate the behaviour of the Flying-V notably better. Multiple factors can be responsible for this behaviour. First of all, more identification manoeuvres, like 3-2-1-1 and doublets, were performed by elevator input. Moreover, generally, the larger pilot inputs were the elevator inputs. The inputs on the aileron and rudder were kept conservative by the pilot because a catastrophic failure cannot be afforded. So controllability was the main consideration when executing the flight tests, as was mentioned earlier. In addition, since the flights were performed outside, external factors for example wind can influence the aircraft's responses.

A time series rudder doublet response can be found in fig. 12. This input resulted in a dutch roll like motion. The lateral models manage to replicate the system behaviour well. The longitudinal components are influenced by the change in rudder deflection, as was found by [7]. These motions do not achieve similar accuracy as for the lateral response. C_X, C_Z and C_m do not manage to replicate the higher amplitudes witnessed in the measured set. For the 3-2-1-1 elevator input and response displayed in Fig. 13. The models manage to approximate the response of the elevator input better than the rudder input. This confirms that longitudinal motions are better modelled than the lateral motions.

		Value	MSE Change		Parameter	Value	MSE Change
C_X	C_{X_0}	$5.584 \cdot 10^{-1}$	$-1.6581 \cdot 10^{-4}$	C_l	C_{l_0}	$-2.003 \cdot 10^{-5}$	$-1.408 \cdot 10^{-9}$
	$C_{X_{\hat{u}}}$	$-6.192 \cdot 10^{-1}$	$-2.3401 \cdot 10^{-4}$		$C_{l_{\hat{p}}}$	$1.062 \cdot 10^{-2}$	$-1.037 \cdot 10^{-8}$
	$C_{X_{\delta_e}}$	$4.030 \cdot 10^{-2}$	$-2.0290 \cdot 10^{-8}$		$C_{l_{\delta_a}}$	$9.090 \cdot 10^{-3}$	$-2.497 \cdot 10^{-9}$
	$C_{X_{\hat{q}}}$	$-4.823 \cdot 10^{-1}$	$-1.2110 \cdot 10^{-6}$		$C_{l_{\hat{r}}}$	$1.310 \cdot 10^{-1}$	$-5.810 \cdot 10^{-7}$
	C_{X_α}	$3.174 \cdot 10^{-1}$	$-2.8236 \cdot 10^{-5}$		C_{l_β}	$-4.146 \cdot 10^{-3}$	$-1.711 \cdot 10^{-7}$
	$C_{X_{\hat{q}\alpha}}$	6.971	$-3.0441 \cdot 10^{-6}$		$C_{l_{\hat{r}^2}}$	-2.708	$-9.683 \cdot 10^{-8}$
					$C_{l_{\hat{r}\delta_a}}$	4.466	$-1.585 \cdot 10^{-7}$
					$C_{l_{\hat{p}\delta_a}}$	$-7.562 \cdot 10^{-1}$	$-2.075 \cdot 10^{-8}$
C_Y	C_{Y_0}	$1.272 \cdot 10^{-3}$	$-2.6820 \cdot 10^{-6}$	C_m	C_{m_0}	$-5.296 \cdot 10^{-2}$	$-2.023 \cdot 10^{-8}$
	C_{Y_β}	$-1.803 \cdot 10^{-2}$	$-5.9581 \cdot 10^{-8}$		C_{m_α}	$-1.344 \cdot 10^{-1}$	$-4.452 \cdot 10^{-6}$
	$C_{Y_{\hat{p}}}$	$3.693 \cdot 10^{-1}$	$-1.5854 \cdot 10^{-5}$		$C_{m_{\delta_e}}$	$-1.023 \cdot 10^{-1}$	$-2.104 \cdot 10^{-5}$
	$C_{Y_{\delta_a}}$	$1.626 \cdot 10^{-1}$	$-8.6718 \cdot 10^{-7}$		$C_{m_{\hat{q}}}$	$2.891 \cdot 10^{-1}$	$-8.889 \cdot 10^{-7}$
	$C_{Y_{\hat{p}\delta_a}}$	$1.201 \cdot 10^{1}$	$-1.0927 \cdot 10^{-5}$		$C_{m_{\hat{u}}}$	$6.823 \cdot 10^{-2}$	$-2.896 \cdot 10^{-8}$
	$C_{Y_{\hat{r}^2}}$	$-1.279 \cdot 10^{1}$	$-9.5546 \cdot 10^{-7}$				
	$C_{Y_{\hat{r}\beta}}$	1.195	$-9.1205 \cdot 10^{-7}$				
	$C_{Y_{\hat{p}\hat{r}}}$	-8.432	$-2.5832 \cdot 10^{-6}$				
	$C_{Y_{\hat{p}\delta_r^2}}$	3.989	$-8.0889 \cdot 10^{-7}$				
	$C_{Y_{\hat{r}\delta_a\delta_r}}$	$-2.325 \cdot 10^{2}$	$-6.6327 \cdot 10^{-7}$				
	$C_{Y_{\beta^3}}$	$-7.656 \cdot 10^{-3}$	$-1.0383 \cdot 10^{-9}$				
C_Z	C_{Z_0}	-2.970	$-7.3218 \cdot 10^{-2}$	C_n	C_{n_0}	$-3.138 \cdot 10^{-4}$	$-1.0368 \cdot 10^{-9}$
	C_{Z_α}	-1.854	$-6.852 \cdot 10^{-3}$		C_{n_β}	$3.024 \cdot 10^{-3}$	$-1.0725 \cdot 10^{-11}$
	$C_{Z_{\hat{u}}}$	2.970	$-5.949 \cdot 10^{-5}$		$C_{n_{\delta_r}}$	$4.501 \cdot 10^{-4}$	$-8.440 \cdot 10^{-8}$
	$C_{Z_{\hat{q}}}$	$-4.250 \cdot 10^{-1}$	$-2.459 \cdot 10^{-6}$		$C_{n_{\hat{p}}}$	$-7.048 \cdot 10^{-2}$	$-5.791 \cdot 10^{-7}$
					$C_{n_{\hat{p}\delta_a}}$	-2.508	$-2.779 \cdot 10^{-7}$
					$C_{n_{\delta_a}}$	$-1.396 \cdot 10^{-2}$	$-9.712 \cdot 10^{-9}$
					$C_{n_{\hat{r}\beta}}$	$-2.576 \cdot 10^{-1}$	$-6.777 \cdot 10^{-8}$

Table 9. Flying-V model parameters and the improvement of MSE for each parameter

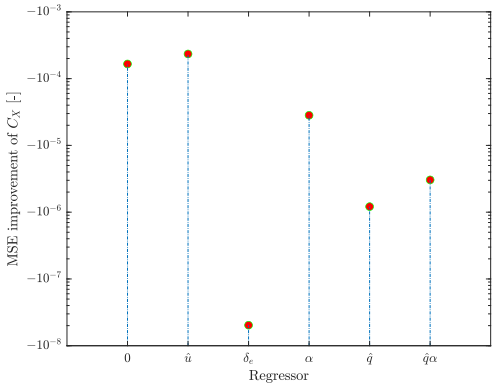

(a) C_X

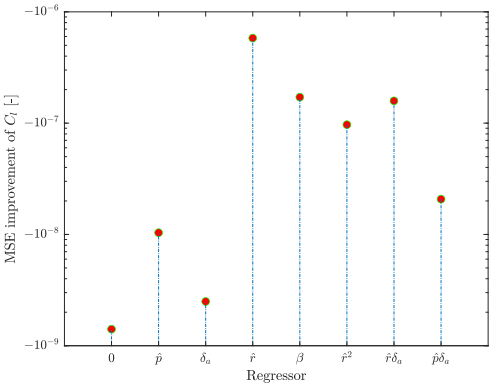

(b) C_l

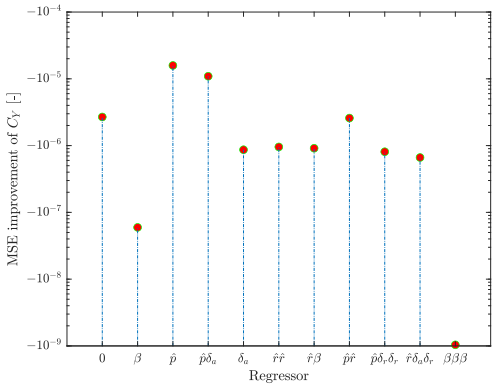

(c) C_Y

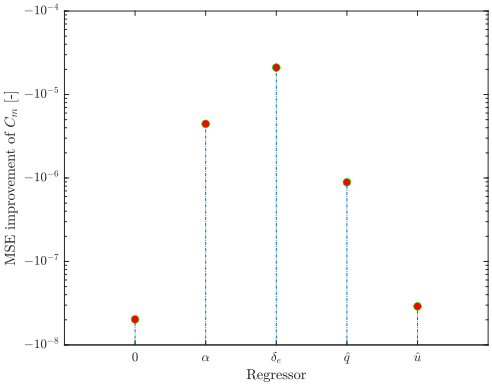

(d) C_m

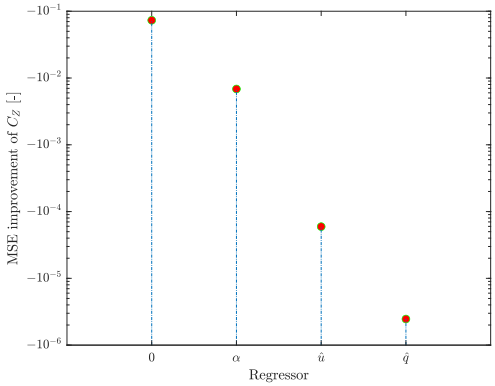

(e) C_Z

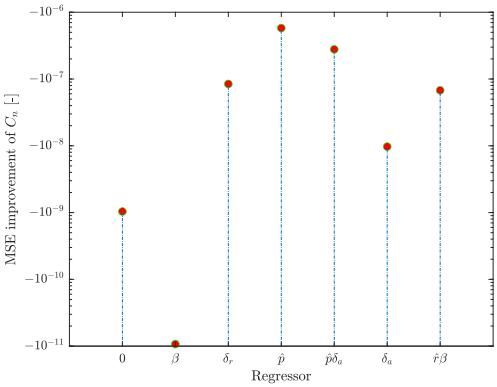

(f) C_n

Figure 11. MSE change for each parameter

	Current (3^{rd} order) model			First order		
	R^2	MSE	RRMSE	R^2	MSE	RRMSE
C_X	0.88	$1.390 \cdot 10^{-4}$	14.1 %	0.87	$1.663 \cdot 10^{-4}$	15.5 %
C_Y	0.26	$8.125 \cdot 10^{-5}$	13.3 %	0.16	$9.3545 \cdot 10^{-5}$	14.3 %
C_Z	0.85	$3.289 \cdot 10^{-3}$	12.9 %	0.85	$3.289 \cdot 10^{-3}$	12.9 %
C_l	0.15	$4.284 \cdot 10^{-6}$	13.9 %	0.12	$4.296 \cdot 10^{-6}$	13.9 %
C_m	0.40	$2.324 \cdot 10^{-5}$	12.7 %	0.40	$2.324 \cdot 10^{-5}$	12.7 %
C_n	0.38	$1.262 \cdot 10^{-6}$	12.9 %	0.28	$1.569 \cdot 10^{-6}$	14.4 %

Table 10. Model fitting performance, 3rd order compared to 1st order

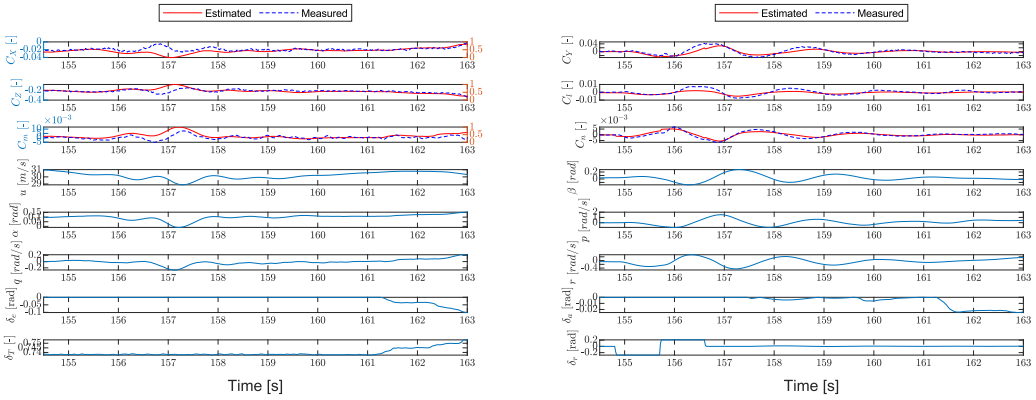

(a) Longitudinal **(b) Lateral**

Figure 12. Rudder doublet

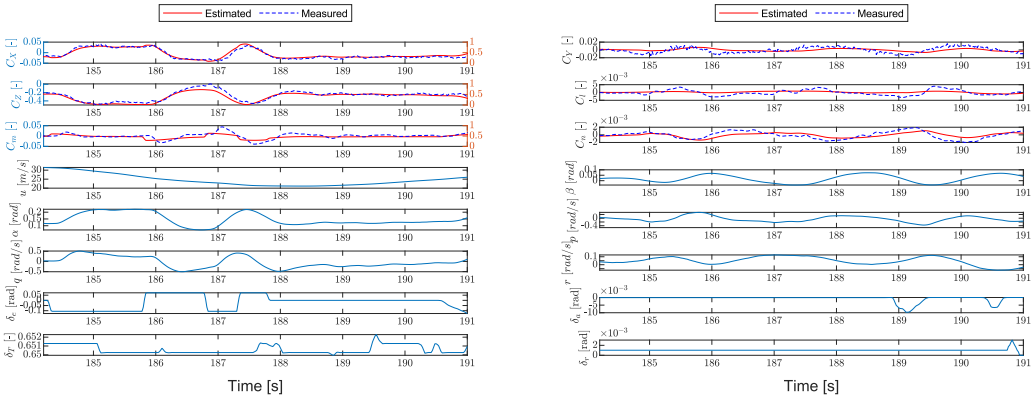

(a) Longitudinal **(b) Lateral**

Figure 13. Elevator 3-2-1-1

C. Comparison to Wind Tunnel Model

In this section, a comparison is made between the flight model and the earlier performed wind tunnel model [9].

Unfortunately, an accurate analysis of the time responses, as was done in the previous section, could not be performed. This is because the wind tunnel tests were performed in a controlled environment where inputs are carefully managed. When real flight data is applied to these models extreme outputs are observed. This makes it difficult to extract meaningful conclusions from such a comparison.

Instead, an analysis is conducted by comparing the relationship between the models that resulted from the wind tunnel tests and flight tests $C_X - \alpha$, $C_Z - \alpha$ and $C_m - \alpha$, see Fig. 14. When comparing these two models it is important to take into account that the wind tunnel experiment was performed with a half-wing model and no engines. The absence of the engines can explain the gap observed for C_X. Logically, the addition of engines should decrease C_X since the drag, C_D, should increase. This is supported by fig. 15, where this increase in drag can clearly be identified in the $C_D - \alpha$ and $C_D - C_L$ plots. This gap in C_X may give an indication of the effect of the addition of the engines, $\Delta C_{X_{engines}}$. By taking the average difference between the flight model and wind tunnel average it is found that $\Delta C_{X_{engines}} = 0.0183$. However, previous research on the effect of adding the engines to the Flying-V[6] found a smaller engine penalty as can be seen in fig. 15. This result aids the conclusion of the previous section, that an improved engine model is needed to get a better estimate of C_X.

C_Z only has a small deviation from the wind tunnel results, similar to C_L. This is likely also due to interference with the engines.

Moreover, the difference of C_m is fairly large. This large difference cannot only be explained by the engine integration. It is suspected that this difference is due to a shortage of excitations contained in the training data set. As explained in the previous section, the stepwise regression algorithm struggled to get a well-fitting model for C_m. This indicates that certain information is missing from the available regressors. There is a possibility for the wind tunnel model to have captured this information.

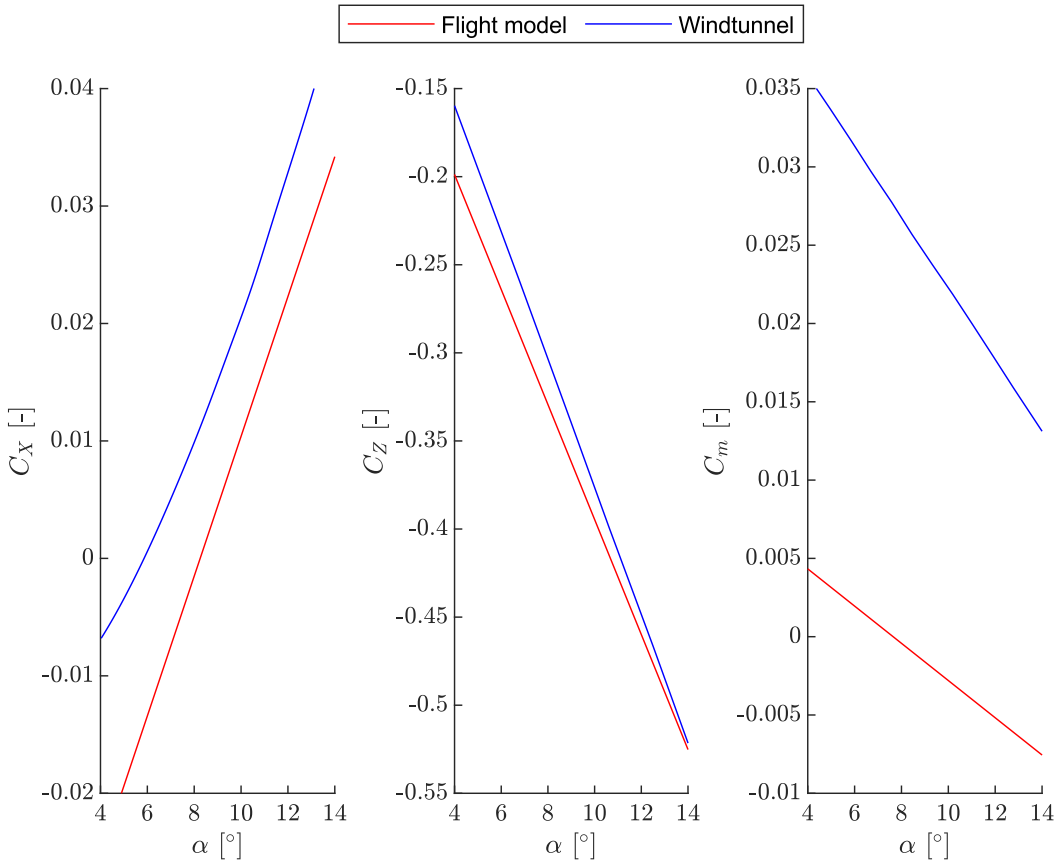

Figure 14. C_X, C_Z **and** C_m **comparison between flight model and wind tunnel model**

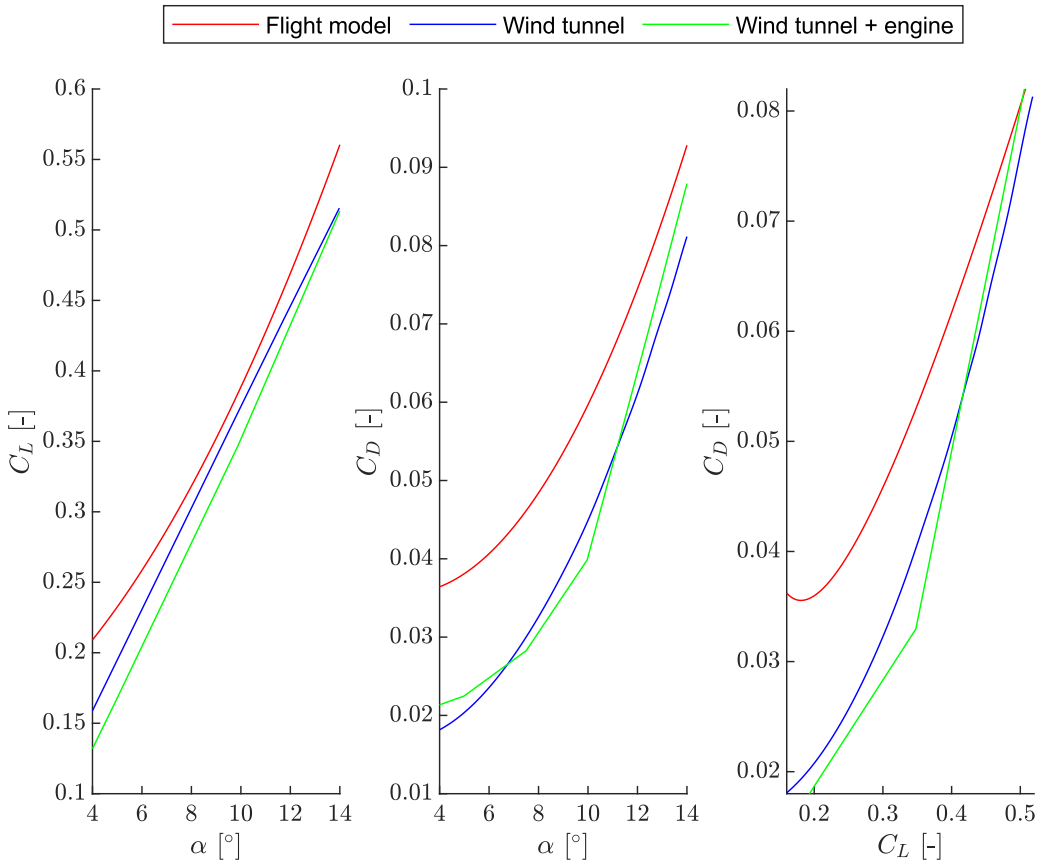

Figure 15. $C_L - \alpha$ $C_D - \alpha$ **and** $C_D - C_L$ **comparison between flight model, wind tunnel model[9] and wind tunnel result including engine[6]**

V. Conclusion

A stepwise regression is used to determine a model structure for an aerodynamic model of a 4.6% scaled Flying-V using flight data. The compact polynomials, with up to second order terms, manage to simulate the behaviour of the novel aircraft reasonably well. All six degrees of freedom polynomials manage to replicate the responses of typical identification methods, for example the doublet and 3-2-1-1 manoeuvres. Compared to the longitudinal polynomials, the lateral ones did use more parameters. This indicates that the lateral motions are more complex than the longitudinal ones. An interaction between longitudinal and lateral states are also found. Especially, rudder inputs generated a delayed longitudinal response. The rudder deflection interacts with the lift generated by the wing, as was also found during the wind tunnel experiments. This influence explains the delayed longitudinal response.

When comparing the flight model to the previously estimated wind tunnel models, it becomes clear that the available engine model does not suffice for this in-flight use case. Especially C_X, and consequently C_D, suffer from the limited knowledge of the flight engine performance. Moreover, a large deviation was also found for C_m. This was partly due to the interaction with the engines. However, it is likely that the available data did not contain the information to fully evaluate the extent of C_m.

Altogether, taking the previously mentioned conditions into account, the presented models will give a realistic representation of the behaviour of the Flying-V. In conclusion, using the presented method, improved models will be able to be estimated when more data becomes available.

VI. Recommendations

Even though in the presented work a suitable aerodynamic model was found, the process of getting to the result gave rise to new questions and revealed more opportunities for future work as for instance.

- The currently available engine model does not manage to model the thrust at the evaluated flight states. For example currently the thrust is not influenced by the high angle of attack motions according to the model.
- Similarly, more data from a larger variety of identification manoeuvres would greatly enrich the available information for future iterations of the currently discussed aerodynamic model.
- It was also found that there is a possible interaction between longitudinal and lateral states. It is expected that this is from an influence between the rudder and the wing. However, more knowledge of these interactions will result in improved future models of the Flying-V and a better understanding of the implications of this phenomena.
- The data set used for this analysis is fairly conservative when it comes to excitations. For future test flights it is recommended to perform manoeuvres with larger control surface deflections and aerodynamic angles. To improve the knowledge on, for example, control effectiveness and directional sensitivity.

References

[1] Benad, J., "the Flying V - a New Aircraft Configuration for Commercial Passenger Transport," *Deutscher Luft- und Raumfahrtkongress*, 2015, pp. 1–8. URL `http://www.dglr.de/publikationen/2015/370094.pdf`.

[2] Martinez-Val, R., "Flying Wings. A New Paradigm for Civil Aviation?" *Acta Polytechnica*, Vol. 47, No. 1, 2007. doi: 10.14311/914.

[3] Faggiano, F., Vos, R., Baan, M., and Van Dijk, R., "Aerodynamic design of a flying V aircraft," *17th*

AIAA Aviation Technology, Integration, and Operations Conference, 2017, , No. June, 2017. doi: 10.2514/6.2017-3589.

[4] R.Viet, "Analysis Of The Flight Characteristics Of A Highly Swept Cranced Flying Wing By Means Of An Experimental Test," 2019, p. 142.

[5] Palermo, M., "The Longitudinal Static Stability And Control Characteristics Of A Flying V Scaled Model," 2019, p. 117. URL `https://repository.tudelft.nl/islandora/object/uuid:6286f9e2-c24a-430c-a4fa-9fb67b9558b4?collection=education`.

[6] Empelen, S. A. V., "Engine Integration of the Flying V," 2020.

[7] Johnson, N., "Effect of Winglet Integration and Rudder Deflection on Flying-V Aerodynamic Characteristics," 2021.

[8] Cappuyns, T., Vos, R., and Bender, K., "Handling Qualities of a Flying V Configuration," Ph.D. Thesis, Delft University of Technology, 2019. URL `http://resolver.tudelft.nl/uuid:69b56494-0731-487a-8e57-cec397452002`.

[9] Garcia, A. R., "Aerodynamic Model Identification of the Flying V using Wind Tunnel Data (MSc Thesis)," 2019. URL `https://repository.tudelft.nl/islandora/object/uuid%3A79e01f29-1789-4501-8556-ca2bcf06f3ab?collection=education`.

[10] Gonzalez, R., and Dabove, P., "Performance assessment of an ultra low-cost inertial measurement unit for ground vehicle navigation," *Sensors (Switzerland)*, Vol. 19, No. 18, 2019, pp. 1–14. doi: 10.3390/s19183865.

[11] García, A. R., "Flying V Scaled Model : Systems Report," , 2020.

[12] Mulder, J., Staveren, W. v., Vaart, J. v. d., Weerdt, E. d., Veld, A. i. t., and Mooij, E., "Flight Dynamics - Lecture Notes," *Princeton University Press*, 2013, p. 570. URL `http://app.knovel.com/web/toc.v/cid:kpFD000016/viewerType:toc/root_slug:flight-dynamics/url_slug:kt00UQFX02?b-q=ailerons&b-within-title=true&b-group-by=false&b-search-type=tech-reference&b-sort-on=default`.

[13] Klein, V., and Morelli, E. A., *Aircraft System Identification: Theory and Practice*, 1st ed., American Institute of Aeronautics and Astronotics, Blacksburrg, Virginia, 2006.

[14] van der Linden, C., "DASMAT-Delft University Aircraft Simulation Model and Analysis Tool," , 1996.

[15] Kashyap, R. L., "A Bayesian Comparison of Different Classes of Dynamic Models Using Empirical Data," *IEEE Transactions on Automatic Control*, Vol. 22, No. 5, 1977, pp. 715–727. doi: 10.1109/TAC.1977.1101594.

Appendix

VII. Kalman filter theorem

The Kalman filter is an optimal filter, meaning that it will estimate the minimum covariance error based on the available observations. Using statistical sensor data and a multitude of different sensors, a state estimation problem can be formulated. The linear filter process is set out as.

A. Linear Kalman filter

The linear Kalman filter is based on the assumption that the equations of motion are linear, so the state-space form is:

$$\dot{\boldsymbol{x}} = \boldsymbol{A}\boldsymbol{x} + \boldsymbol{B}\boldsymbol{u} + \boldsymbol{w} \tag{54}$$

Where $\boldsymbol{A}$ are the system dynamics, $\boldsymbol{B}$ the control dynamics and $\boldsymbol{w}$ white noise. The sensor measurements (z) are linearly dependent on the states, so:

$$\boldsymbol{z} = \boldsymbol{H}\boldsymbol{x} + \boldsymbol{v} \tag{55}$$

Where H is the measurement matrix, and v is white measurement noise. Both eqs. (54) and (55) need to be discretised to be able to use the Kalman filter. The discretised versions are:

$$\underline{x}_{k+1} = \Phi_{k+1,k}\underline{x}_k + \Psi_{k+1,k}\underline{u}_k + \Gamma_{k+1,k}\underline{w}_{d,k} \tag{56}$$

$$\underline{z}_{k+1} = H_{k+1}\underline{x}_{k+1} + D_{k+1}\underline{u}_{k+1} + \underline{v}_{k+1} \tag{57}$$

The filter itself is set up in the following recursive steps:
1) One step ahead measurement prediction
2) One step ahead covariance prediction
3) Determine Kalman gain
4) Measurement update
5) Covariance matrix of state estimation error

Before these steps two initial conditions are determined:

$$\hat{x}(0|0) = \overline{x}_0 \tag{58}$$

$$\boldsymbol{P}(0|0) = \boldsymbol{P}_0 \tag{59}$$

Where $\hat{x}$ is the optimal estimate of the state and $\boldsymbol{P}$ is the covariance matrix. The the Kalman filter steps are defined as follows[13].

- One-step ahead measurement prediction:

$$\underline{\hat{x}}_{k+1,k} = \Phi_{k+1,k}\underline{\hat{x}}_{k,k} + \Phi_{k+1,k}\underline{u}_k; \quad \underline{\hat{x}}_{0,0} = \underline{\hat{x}}_0 \tag{60}$$

$$\tag{61}$$

  Where $\underline{\hat{x}}_{k+1,k}$ is the state prediction, $\underline{\hat{x}}_{k,k}$ the current state.

- One-step ahead covariance prediction:

$$P_{k+1,k} = \Phi_{k+1,k}P_{k,k}\Phi^T_{k+1,k} + \Gamma_{k+1,k}Q_{d,k}\Gamma^T_{k+1,k}; \quad P_{0,0} = P_0 \tag{62}$$

Where $P_{k+1,k}$ is the covariance prediction and $P_{k,k}$ the current covariance matrix. $Q_{d,k}$ is the white noise characteristic, defined as $E\left\{\underline{w}_{d,i}\underline{w}_{d,j}^T\right\} = Q_{d,i}$.

- Determine Kalman gain (K_{k+1}):

$$K_{k+1} = P_{k+1,k}H_{k+1}^T(H_{k+1}P_{k+1,k}H_{k+1}^T + R_{k+1})^{-1} \tag{63}$$

Where R_{k+1} is the sensor noise covariance defined as: $E\underline{v}_i\underline{v}_j^t = R_i$.

- Measurement update:

$$\hat{\underline{x}}_{k+1,k+1} = \hat{x}_{k+1,k} + K_{k+1}\left(\underline{z}_{k+1} - H_{k+1}\hat{x}_{k+1,k}\right) \tag{64}$$

Where $x_{k+1,k+1}$ is the optimal state estimate.

- Covariance matrix of state estimation error:

$$P_{k+1,k+1} = \left(I - K_{k+1}H_{k+1}\right)P_{k+1,k} \tag{65}$$

$P_{k+1,k+1}$ is the optimal covariance matrix

B. Non-linear Kalman filter

In addition to the linear Kalman filter, several different other Kalman filters exist. The most common non-linear Kalman filter is the Extended Kalman filter(EKF).

C. Extended Kalman filter

Contrary to the linear Kalman filter, in the EKF the state is estimated using perturbations. Which results two extra steps. The non-linear equations of motion are in this case:

$$\dot{\underline{x}}(t) = f(\underline{x}(t), \underline{u}(t), t) + G(\underline{x}(t), t)\underline{w}(t) \tag{66}$$

And the observation equation:

$$\underline{z}(t) = h(\underline{x}(t), \underline{u}(t), t) \tag{67}$$

The perturbation equations derived from Eq. 66 and Eq. 67 are:

$$\delta\dot{\underline{x}}(t) = F_x(\underline{x}, \underline{u}(t))\delta\underline{x}(t) + G(\underline{x}(t), t)\underline{w}(t) \tag{68}$$

$$\delta\underline{z}(t) = H_x(\underline{x}(t), \underline{u}(t), t)\delta\underline{x}(t) \tag{69}$$

It is assumed that $f(\underline{x}(t), \underline{u}(t), t)$ and $h(\underline{x}(t), \underline{u}(t), t)$ are continuous and differentiable with respect to $\underline{x}$ and $\underline{u}$. The addition of the EKF compared to the linear Kalman Filter, is that the nonlinear state and observation equations will be linearised about the nominal values of $\underline{x}^*(t)$ and $\underline{u}^*(t)$. This is done by calculating the Jacobian of eqs. (66) and (67), which results in the perturbation equations eqs. (68) and (69). The Jacobians, $F_x(\underline{x}, \underline{u}(t))$ and $H_x(\underline{x}(t), \underline{u}(t), t)$ will be discretised. The remainder of the EKF is the same as the linear Kalman filter. The steps are set out as follows, the extra steps with respect to the linear Kalman filter are marked in bolt.

1) One-step ahead prediction:

$$\underline{\hat{x}}_{k+1,k} = \underline{\hat{x}}_{k,k} + \int_{t_k}^{t_{k+1}} f\left(\underline{\hat{x}}_{k,k}, \underline{u}_k^*, t\right) dt \tag{70}$$

2) **Calculate Jacobians:**

$$F_x\left(\underline{x}^*(t), \underline{u}^*(t), t\right) = \frac{\partial}{\partial \underline{x}} f(\underline{x}(t), \underline{u}(t), t)$$

and

$$H_x\left(\underline{x}^*(t), \underline{u}^*(t), t\right) = \frac{\partial}{\partial \underline{x}} h(\underline{x}(t), \underline{u}(t), t)$$

3) **Discretise the Jacobians**

4) Covariance matrix of state prediction error:

$$P_{k+1,k}\left(\underline{x}^*(t), \underline{u}^*(t), t\right) = \Phi_{k+1,k}\left(\underline{x}^*(t), \underline{u}^*(t), t\right) P_{k,k} \Phi_{k+1,k}^T\left(\underline{x}^*(t), \underline{u}^*(t), t\right) \tag{71}$$

$$+\Gamma_{k+1,k}\left(\underline{x}^*(t), \underline{u}^*(t), t\right) Q_{d,k}\left(\underline{x}^*(t), \underline{u}^*(t), t\right) \Gamma_{k+1,k}^T\left(\underline{x}^*(t), \underline{u}^*(t), t\right) \tag{72}$$

5) Calculate Kalman gain:

$$K_{k+1}\left(\underline{x}^*(t), \underline{u}^*(t), t\right) = P_{k+1,k}\left(\underline{x}^*(t), \underline{u}^*(t), t\right) H_x^T\left(\underline{x}^*(t), \underline{u}^*(t), t\right) \tag{73}$$

$$\left[H_x\left(\underline{x}^*(t), \underline{u}^*(t), t\right) P_{k+1,k}\left(\underline{x}^*(t), \underline{u}^*(t), t\right) H_x^T\left(\underline{x}^*(t), \underline{u}^*(t), t\right) + R_{k+1}\right]^{-1} \tag{74}$$

6) Measurement update:

$$\underline{\hat{x}}_{k+1,k+1} = \underline{\hat{x}}_{k+1,k} + K_{k+1}\left(\underline{x}^*(t), \underline{u}^*(t), t\right)\left[\underline{z}_{k+1} - \underline{h}\left(\underline{\hat{x}}_{k+1,k}, \underline{u}_{k+1}^*\right)\right] \tag{75}$$

7) Covariance matrix of state estimation error:

$$\begin{aligned} &P_{k+1,k+1}\left(\underline{x}^*(t), \underline{u}^*(t), t\right) = \\ &\left[I_n - K_{k+1}\left(\underline{x}^*(t), \underline{u}^*(t), t\right) H_x\left(\underline{x}^*(t), \underline{u}^*(t), t\right)\right] P_{k+1,k}\left(\underline{x}^*(t), \underline{u}^*(t), t\right) \end{aligned} \tag{76}$$

VIII. Flight data

In this appendix figures containing the measured flight data captured for each test flight can be found. These figures also include the results of the Iterated Extended Kalman Filter.

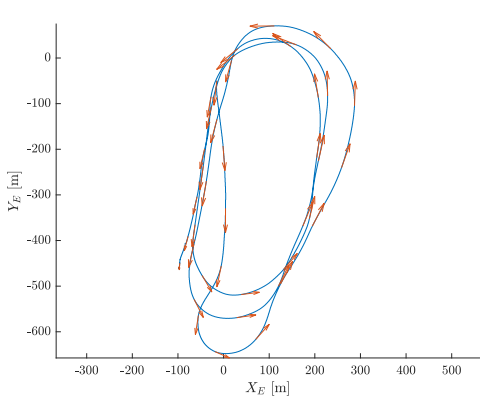

(a) X-Y position

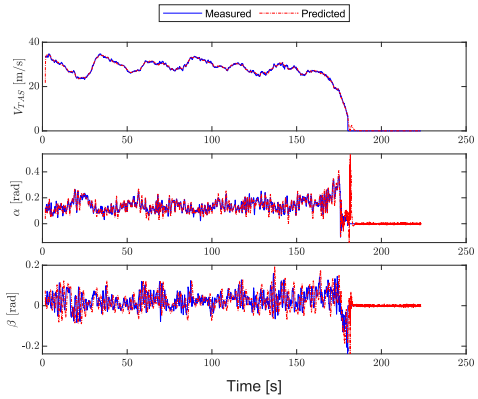

(b) V_{TAS}, α and β

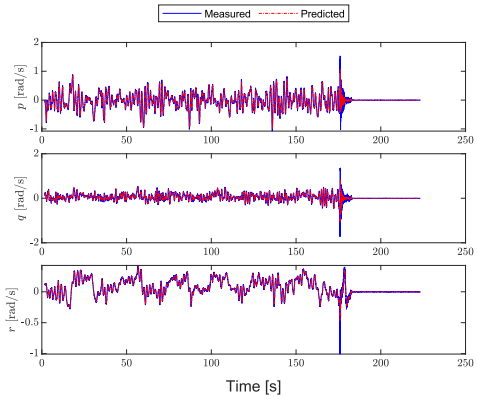

(c) p, q and r

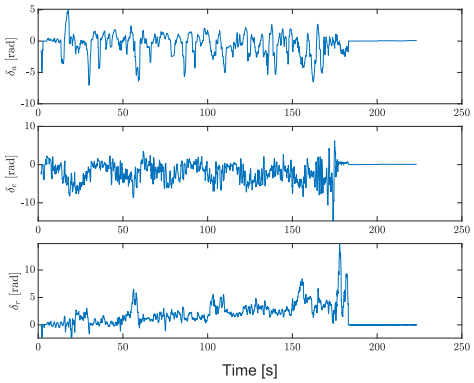

(d) δ_a, δ_e and δ_r

Figure 16. Set 1

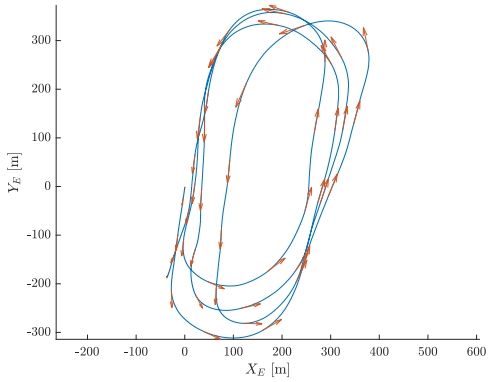

(a) X-Y position

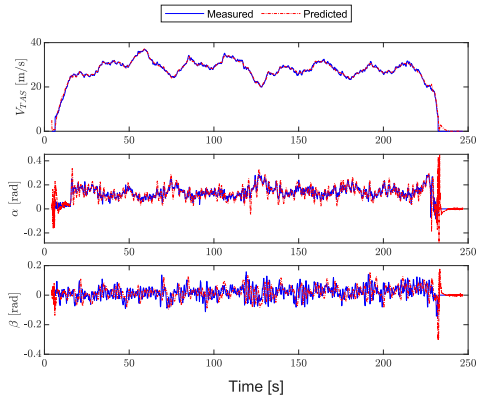

(b) V_{TAS}, α and β

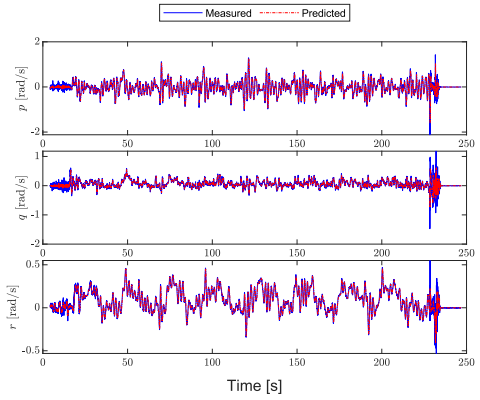

(c) p, q and r

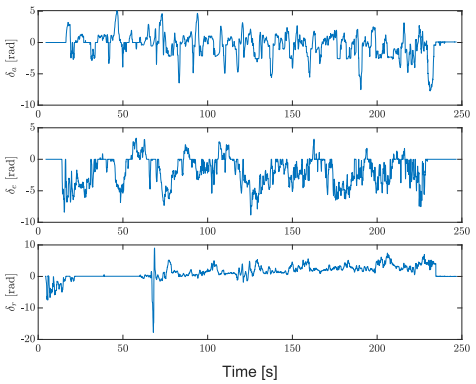

(d) δ_a, δ_e and δ_r

Figure 17. Set 2

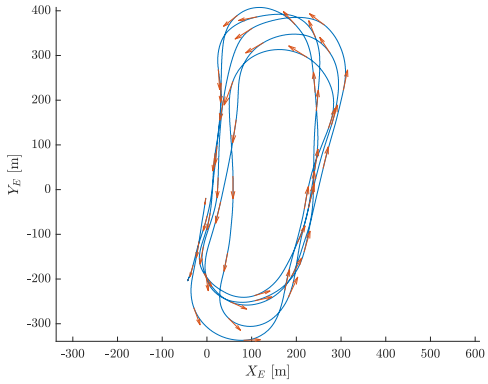

(a) X-Y position

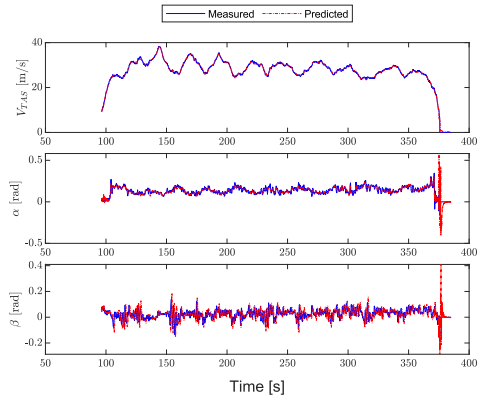

(b) V_{TAS}, α and β

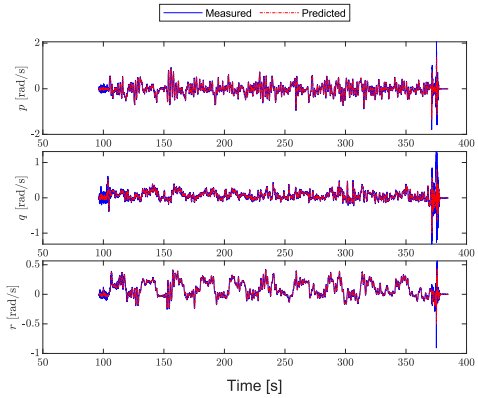

(c) p, q and r

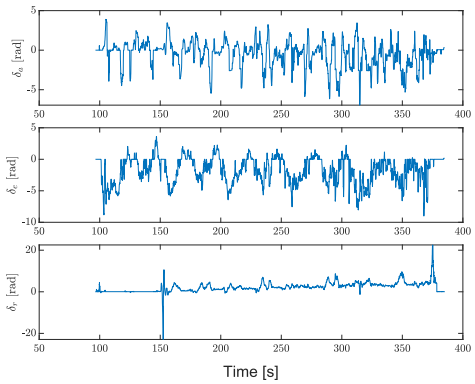

(d) δ_a, δ_e and δ_r

Figure 18. Set 3

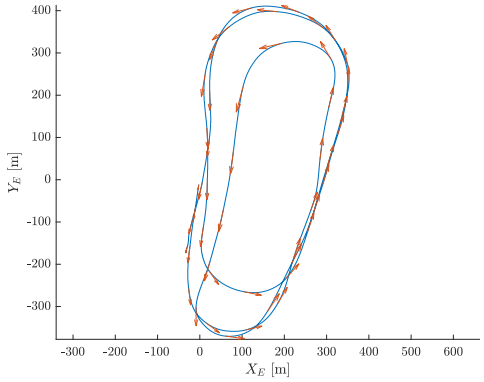

(a) X-Y position

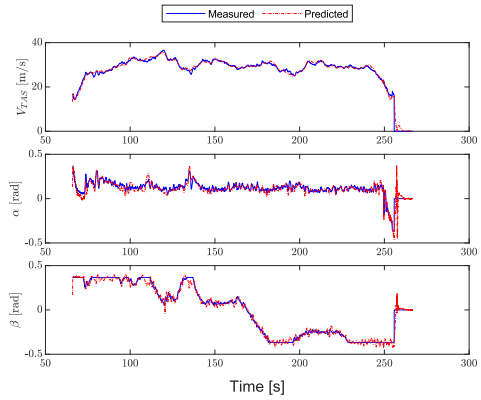

(b) V_{TAS}, α and β

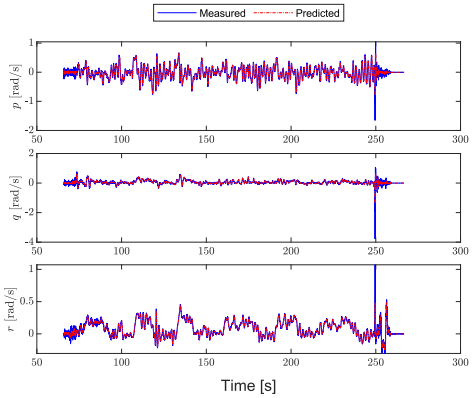

(c) p, q and r

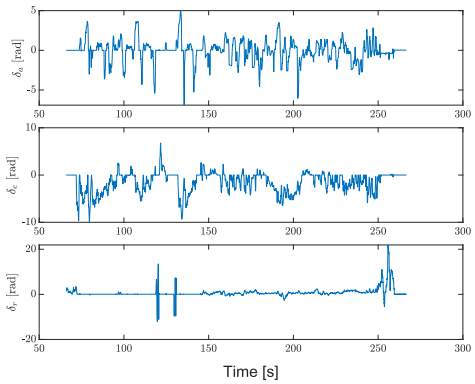

(d) δ_a, δ_e and δ_r

Figure 19. Set 4

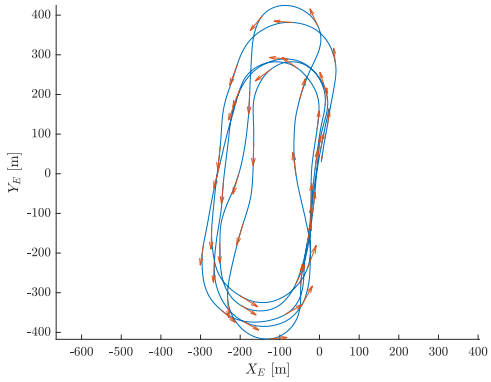

(a) X-Y position

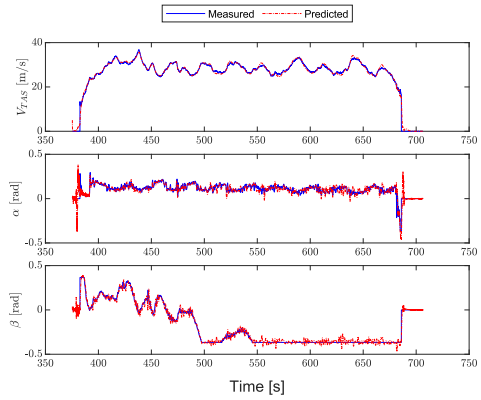

(b) V_{TAS}, α and β

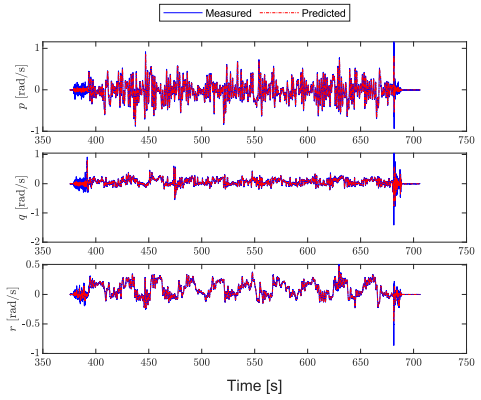

(c) p, q and r

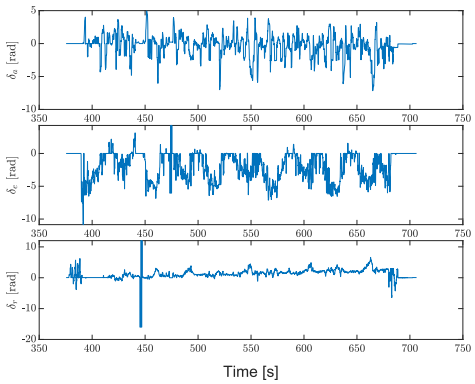

(d) δ_a, δ_e and δ_r

Figure 20. Set 5

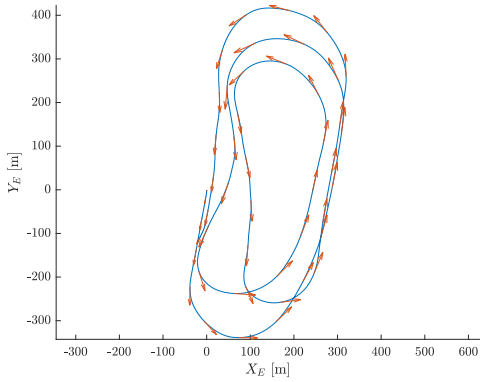

(a) X-Y position

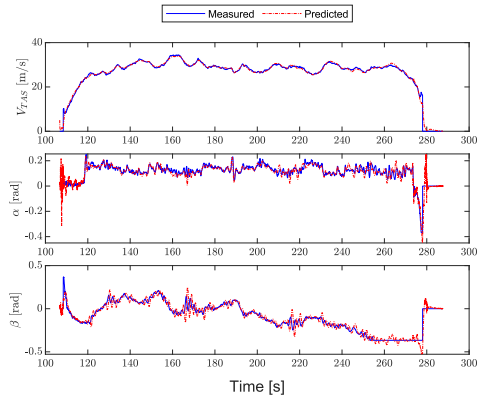

(b) V_{TAS}, α and β

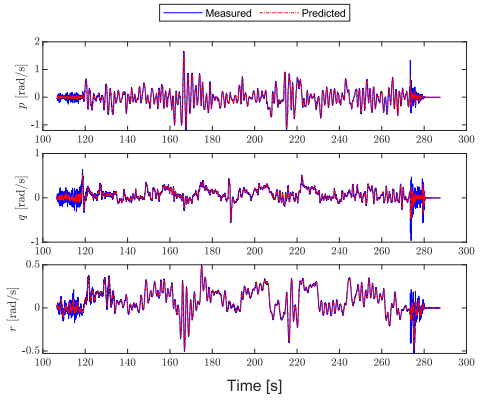

(c) p, q and r

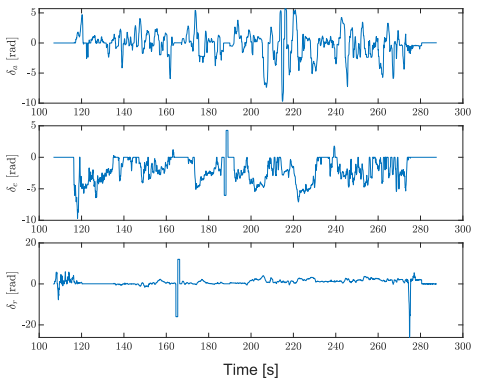

(d) δ_a, δ_e and δ_r

Figure 21. Set 6

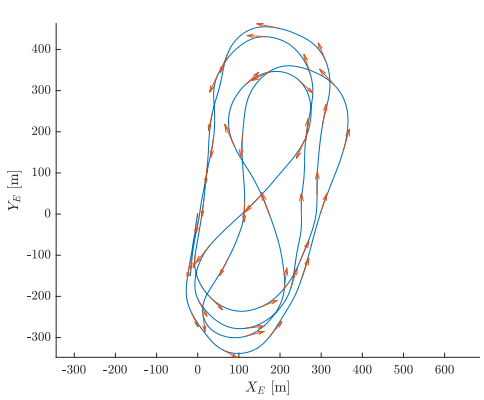

(a) X-Y position

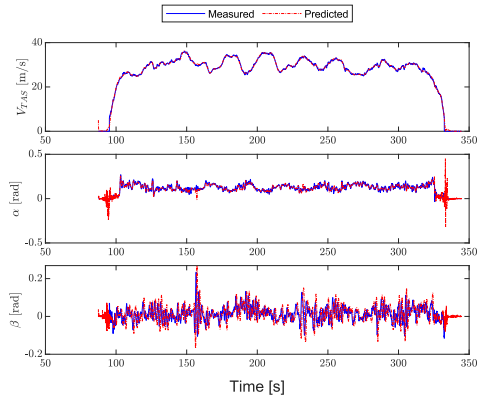

(b) V_{TAS}, α and β

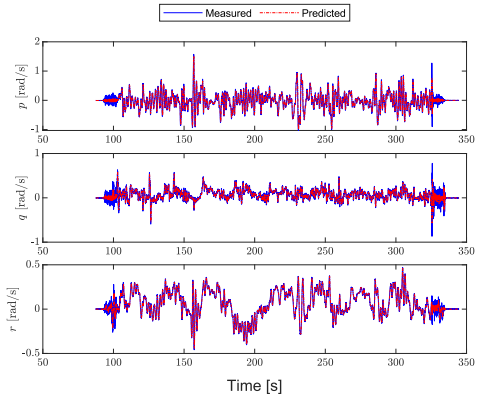

(c) p, q and r

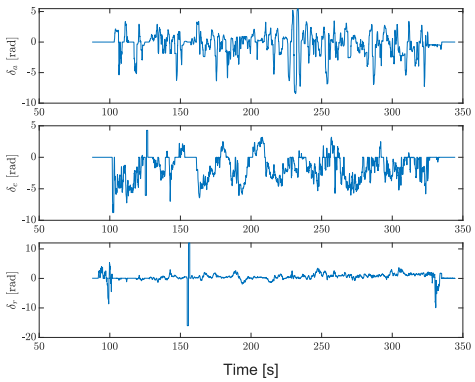

(d) δ_a, δ_e and δ_r

Figure 22. Set 7

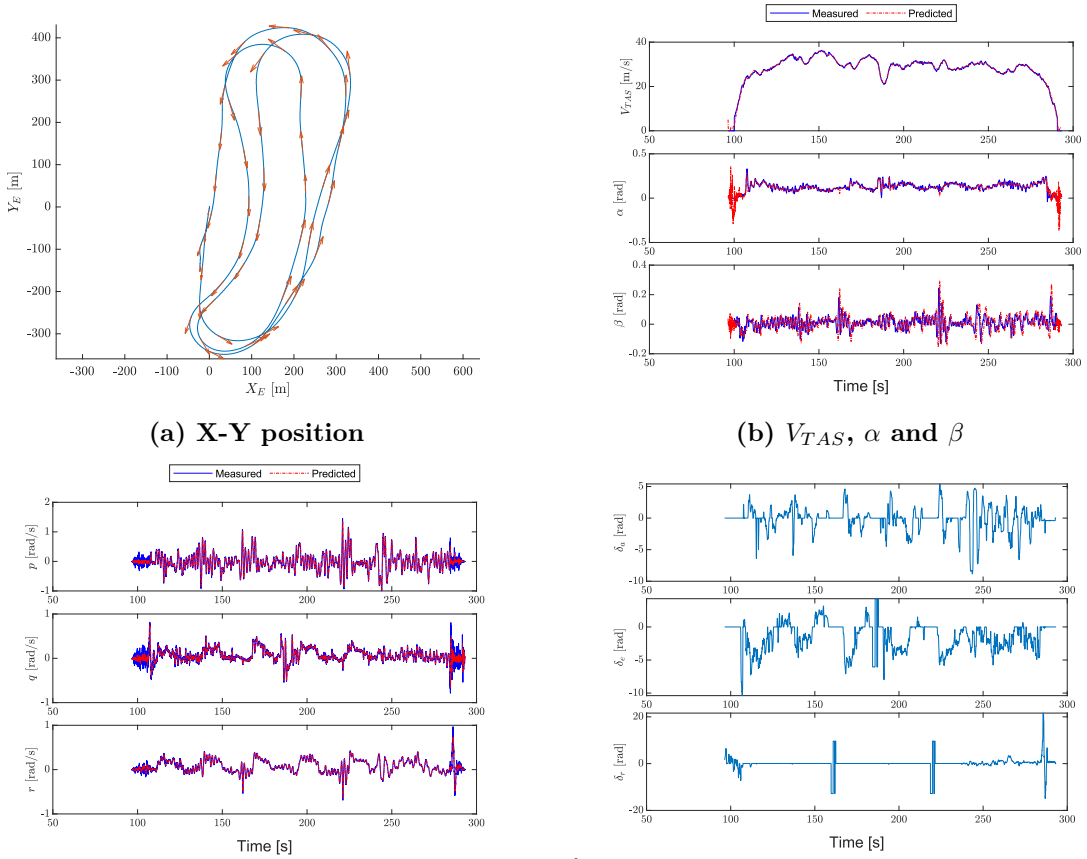

(a) X-Y position

(b) V_{TAS}, α and β

(c) p, q and r

(d) δ_a, δ_e and δ_r

Figure 23. Set 8

IX. Flowcharts

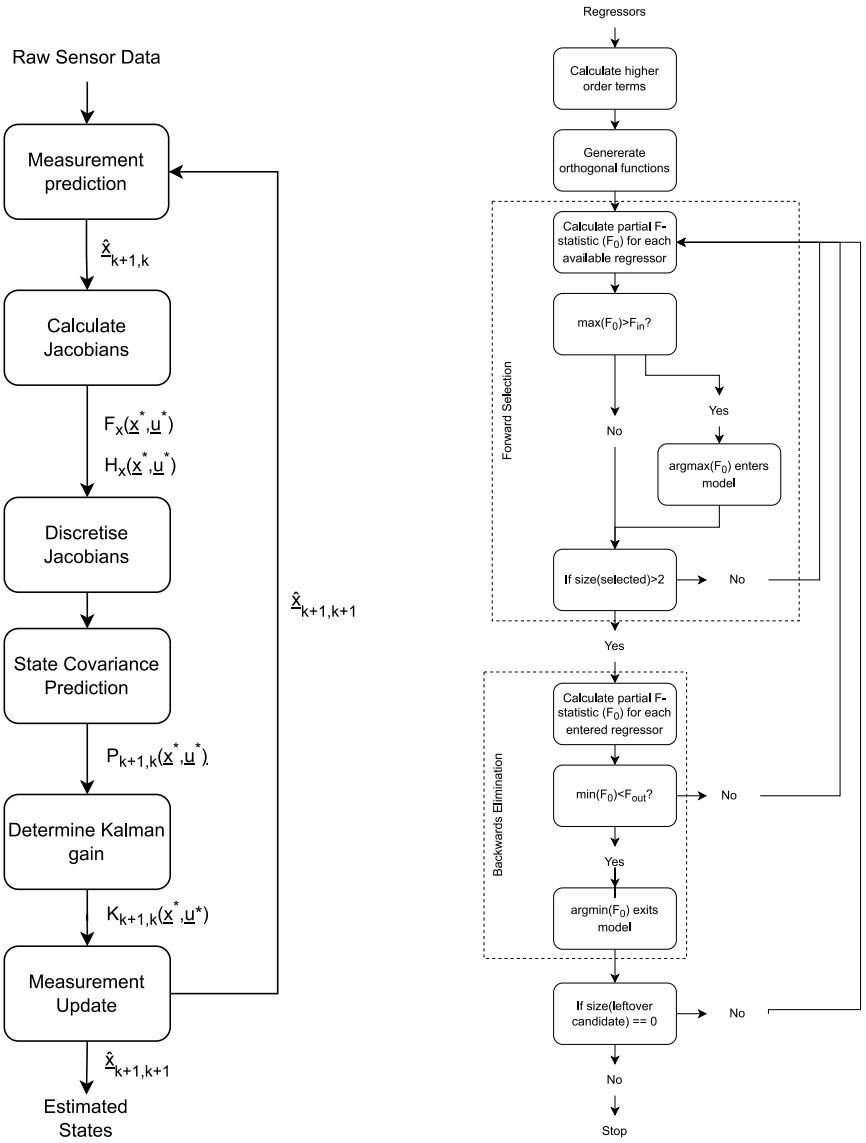

(a) IEKF flowchart **(b) Stepwise regression flowchart**

Figure 24. Comparison between in-flight and wind tunnel

X. Verification

The model determination algorithm is verified using multiple identification control inputs to a known Cessna Citation-II DASMAT model [14]. The stepwise regression algorithm is then used to estimate a model, which can be compared to the results of the truth model. Looking at figs. 25c and 25d, it can be seen that the model manages to estimate the system. At large inputs, the model deviates from the original. This is likely due to the small amount of training data. In addition, the DASMAT model is an non-linear table based model. Different flight conditions may give different model parameters. In order to get a better estimate, more varying inputs which stretch to the edges of the flight envelope should be given. This difference in estimation between the longitudinal and lateral motions highlights that the estimation method is only as good as the provided.

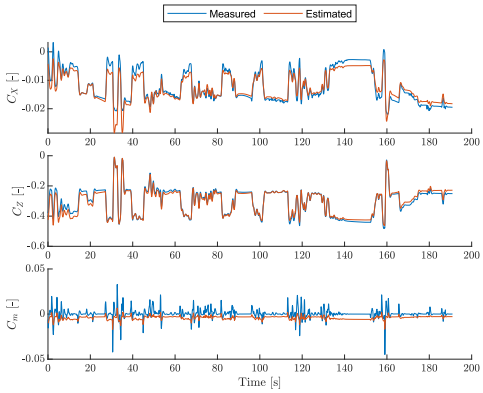

(a) C_X, C_Z, C_m

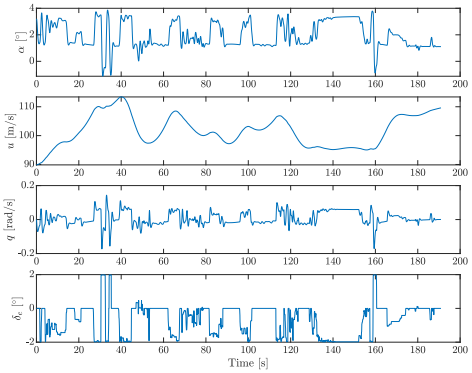

(b) Longitudinal inputs

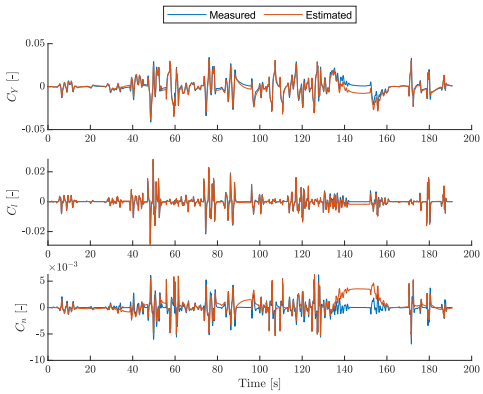

(c) C_Y, C_l, C_n

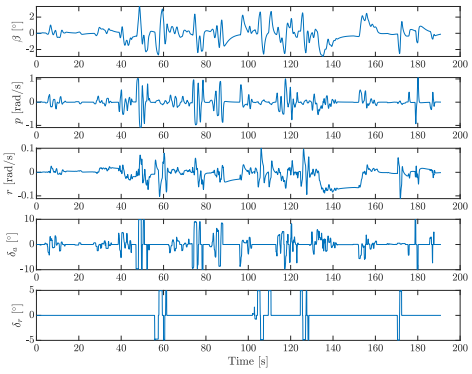

(d) Lateral inputs

Figure 25. Estimation results and model inputs

XI. Model Performance

A good model is not only defined by how well it can approximate the system, the usability is also an important aspect. That means a model needs to be good enough to estimate a system, but also easy enough to be used by the users. The principle of Parsimony[15] is taken into account to select the most suitable model, this principle states states:

"Given two models fitted to the same data with nearly equal residual variances, choose

the model with the fewest parameters."

To test the model on both performance and usability the following accuracy and fitting performance metrics are used:

- Mean Squared Error (MSE)
  - Judges overal fitting performance of the model
  - Defined as:

$$MSE = \frac{1}{N}\sum_{i=1}^{N} v(i)^2 \tag{77}$$

- Predicted Squared Error (PSE)
  - Similar to MSE, but corrected for the amount of model terms
  - Defined as:

$$PSE = \underbrace{\frac{1}{N}\sum_{i=1}^{N} v(i)^2}_{\text{MSE}} + 2\sigma_{max}^2 \frac{n}{N} \tag{78}$$

- Coefficient of determination (R^2)
  - Assesses the overall fit of the model
  - Defined as:

$$R^2 = \frac{SS_R}{SS_T} = 1 - \frac{SS_E}{SS_T} = \frac{\hat{\boldsymbol{\theta}}\boldsymbol{X}^T\boldsymbol{z} - N\bar{z}^2}{z^T z - N\bar{z}^2} \quad \text{where} \quad 0 \leq R^2 \leq 1 \tag{79}$$

- F statistic (F_0)
  - Can be used to find the optimal amount of parameters, since a large amount of parameters will decrease the performance
  - Defined as:

$$F_0 = \frac{SS_R/n}{SS_E/(N-p)} = \frac{\hat{\boldsymbol{\theta}}\boldsymbol{X}^T\boldsymbol{z} - N\bar{z}^2}{ns^2} = \frac{(N-p)}{p-1}\frac{R^2}{1-R^2} \tag{80}$$

XII. Model Fitting Performance

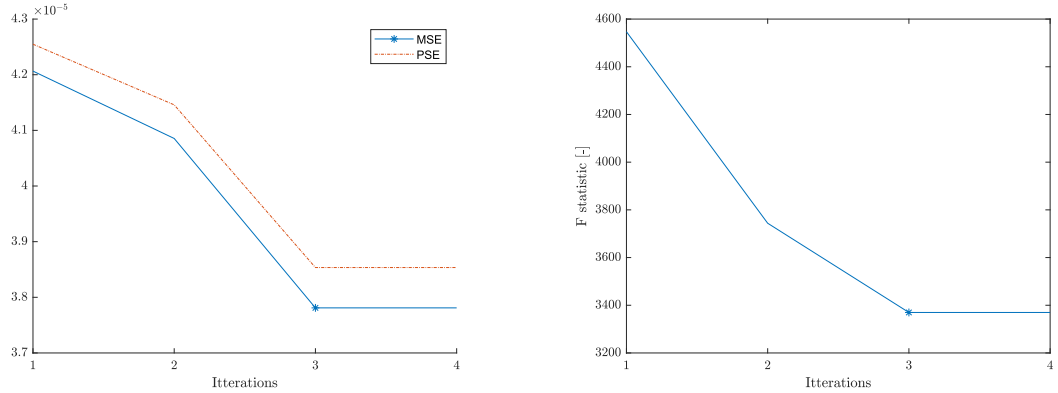

(a) MSE and PSE (b) F-Statistic

Figure 26. MSE, PSE and RMSE of C_X. The star indicates the itteration step for the final model

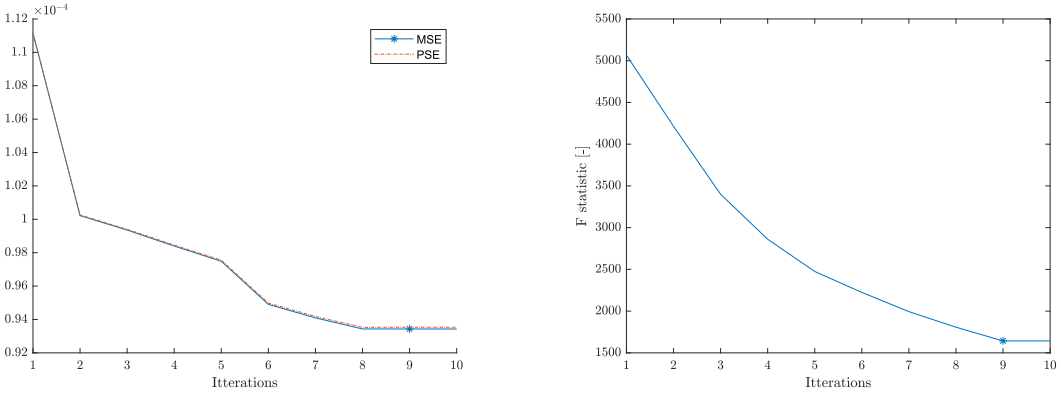

(a) MSE and PSE (b) F-Statistic

Figure 27. MSE, PSE and RMSE of C_Y. The star indicates the itteration step for the final model

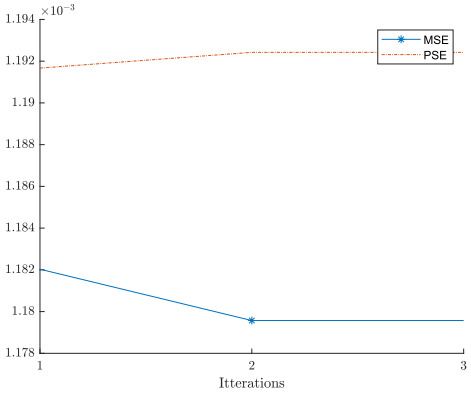

(a) MSE and PSE

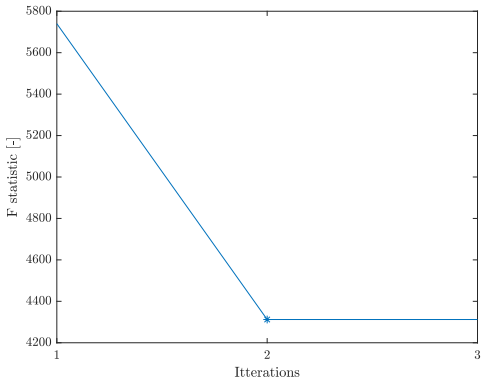

(b) F-Statistic

Figure 28. MSE, PSE and RMSE of C_Z. The star indicates the itteration step for the final model

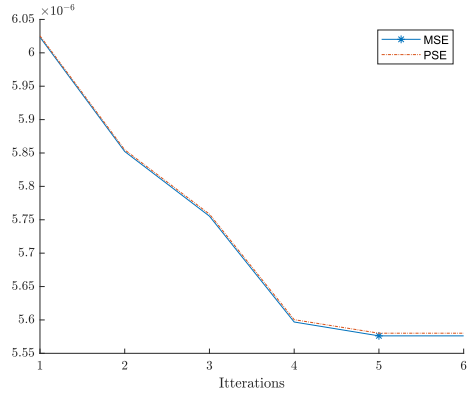

(a) MSE and PSE

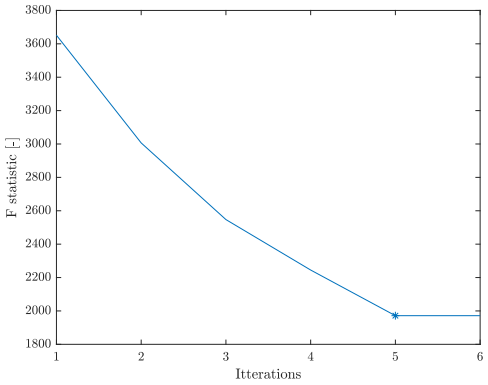

(b) F-Statistic

Figure 29. MSE, PSE and RMSE of C_l. The star indicates the itteration step for the final model

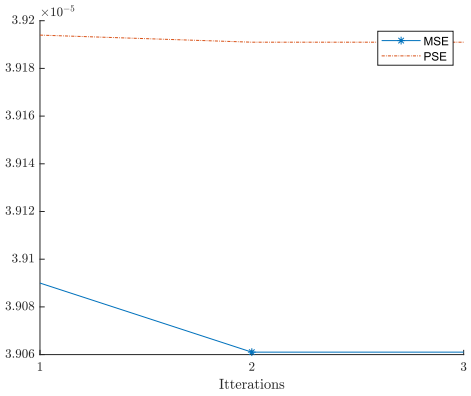

(a) MSE and PSE

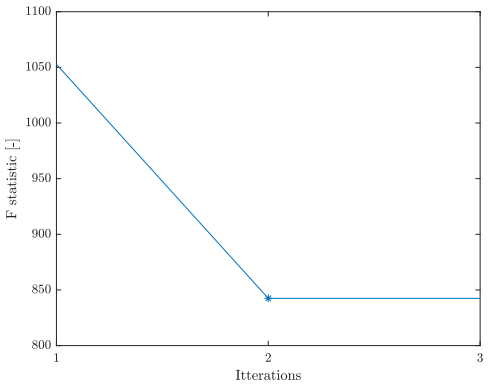

(b) F-Statistic

Figure 30. MSE, PSE and RMSE of C_m. The star indicates the itteration step for the final model

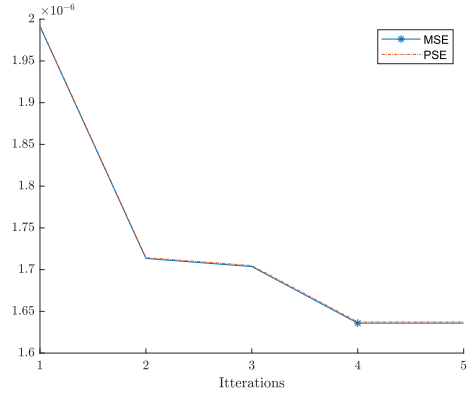

(a) MSE and PSE

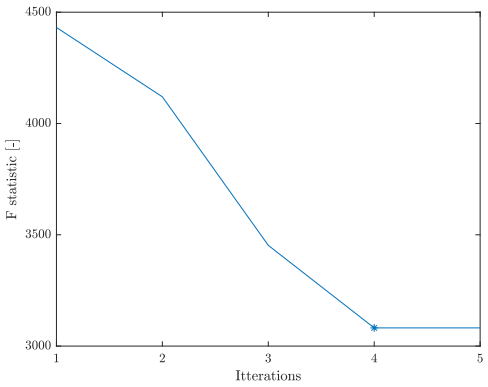

(b) F-Statistic

Figure 31. MSE, PSE and RMSE of C_n. The star indicates the itteration step for the final model

XIII. Fit over full data sets

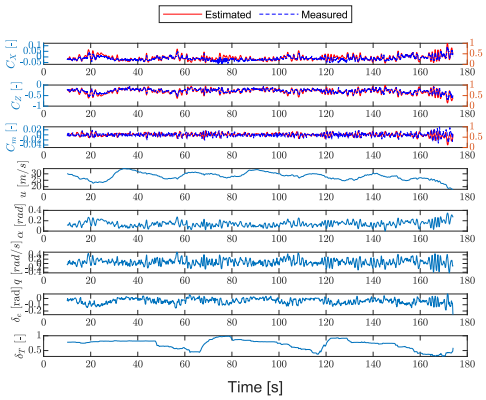

(a) Longitudinal

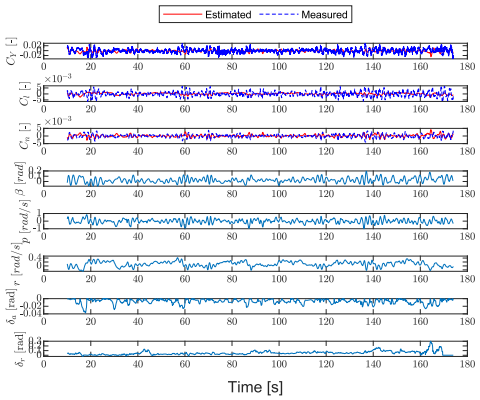

(b) Lateral

Figure 32. Flight 1 comparison between flight data and model, including regressors.

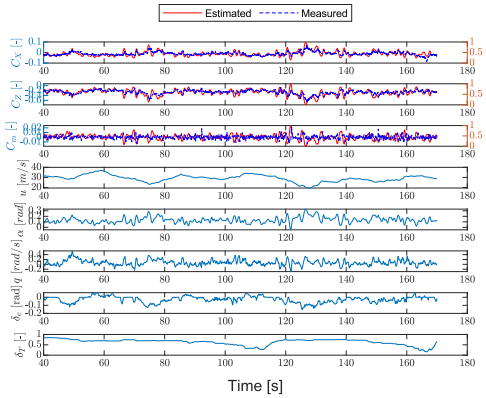

(a) Longitudinal

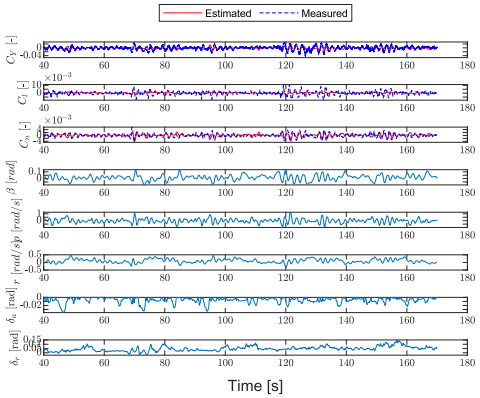

(b) Lateral

Figure 33. Flight 2 comparison between flight data and model, including regressors.

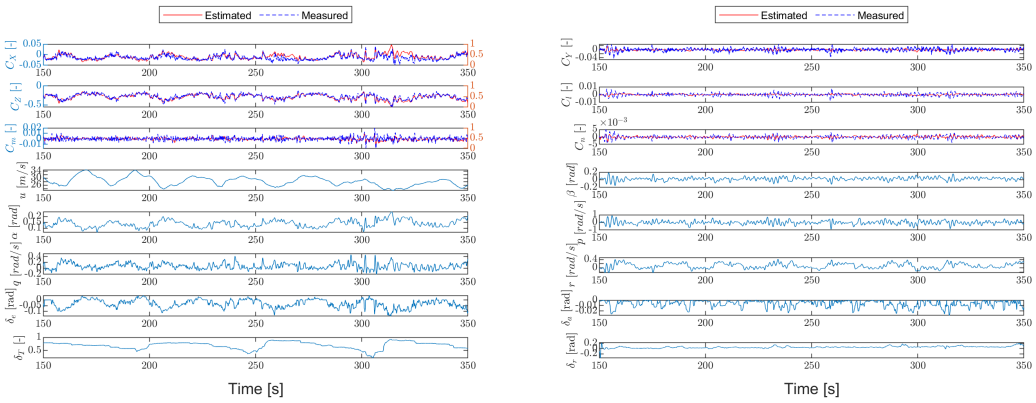

(a) Longitudinal (b) Lateral

Figure 34. Flight 3 comparison between flight data and model, including regressors.

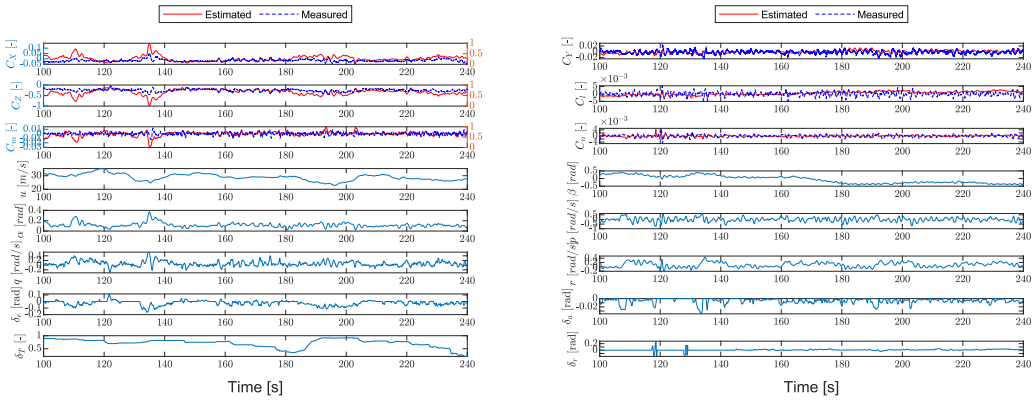

(a) Longitudinal (b) Lateral

Figure 35. Flight 4 comparison between flight data and model, including regressors.

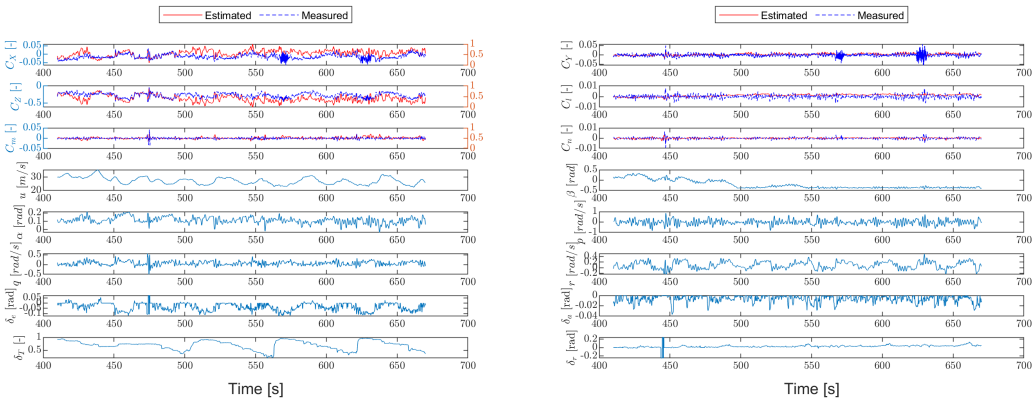

(a) Longitudinal (b) Lateral

Figure 36. Flight 5 comparison between flight data and model, including regressors.

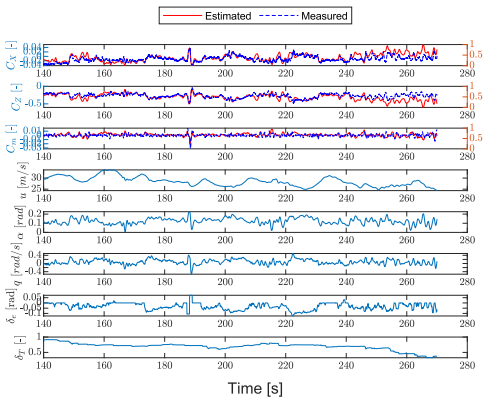

(a) Longitudinal

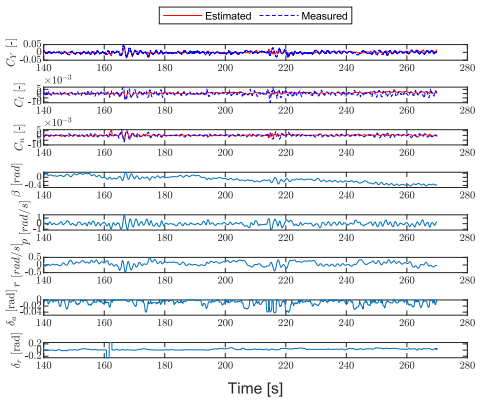

(b) Lateral

Figure 37. Flight 6 comparison between flight data and model, including regressors.

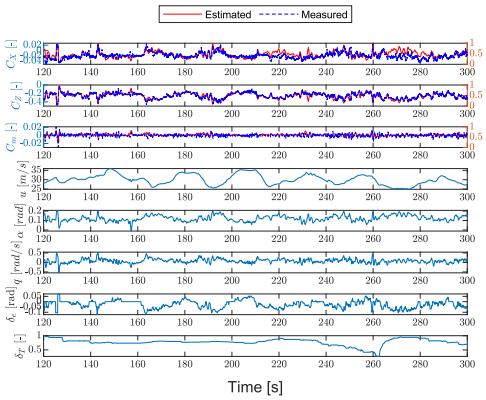

(a) Longitudinal

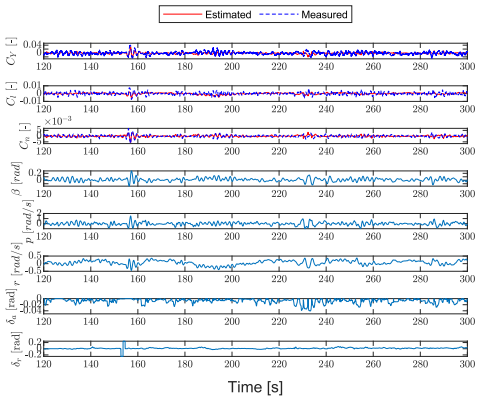

(b) Lateral

Figure 38. Flight 7 comparison between flight data and model, including regressors.

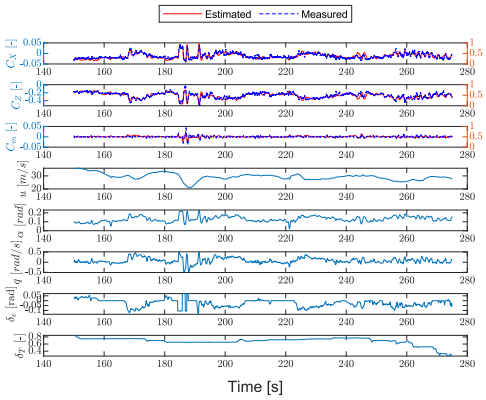

(a) Longitudinal

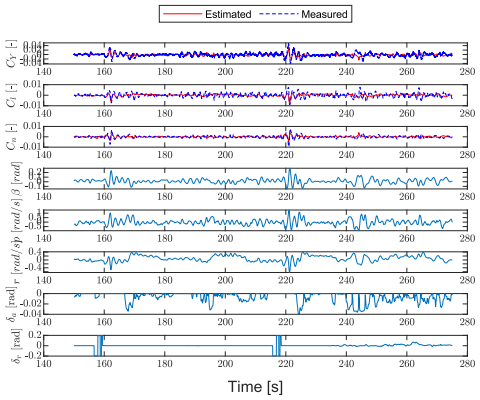

(b) Lateral

Figure 39. Flight 8 comparison between flight data and model, including regressors.

III

LITERATURE SURVEY

10 Introduction

From the iconic Douglas DC3 to the state of the art Airbus A350, for the past ninety years, air transportation has been reliant on aircraft with a tube and wing layout. To improve fuel efficiency, the Flying-V was proposed by Benad [2015], which breaks with the conventional tube and wing layout. This "flying wing" configuration where, passengers and cargo will be placed inside the wing offers multiple advantages, as found by Martinez-Val [2007], like reduced fuel consumption and noise levels at take-off and landing. Studies have shown an aerodynamic efficiency increase of 25% compared to an Airbus A350[Faggiano et al., 2017]. Because of the incredible efficiency improvement interest has been shown by industry[2] and the TU Delft, where the project was picked up to continue development. Here more aerodynamic analysis and optimisations were performed [Faggiano et al., 2017; R.Viet, 2019; Palermo, 2019; Empelen, 2020; Johnson, 2021]. In addition, preliminary aerodynamic models have also been developed. Cappuyns et al. [2019] made an initial model using computational methods. Later Garcia [2019], continued by developing a model using wind tunnel data.

This literature study is focused on researching the possibilities of using in-flight experimental data of a 4.6% scaled Flying-V model to estimate an aerodynamic model. To aid this process, the following research questions are formulated:

- Which methods are most suitable for aerodynamic system identification of the Flying-V using experimental flight data?
- What new information on handling and stability of the Flying-V can be gathered compared to the wind tunnel models?

To answer these questions the report is set up as follows. In chapter 11 the background of the project and previous work done on it is treated. Followed by an elaborate chapter on the basics of system identification and methods that can be used for it in chapter 12. And finally, system identification performed on the Flying-V and the layout of the aircraft can be found in chapter 13.

[2] https://news.klm.com/klm-and-tu-delft-present-successful-first-flight-flying-v/ [visited 9-9-2021]

11 | Background

11.1. Flying-V Project

The Flying-V was first proposed in 2015 by Benad [2015]. This revolutionary new aircraft is comparable to an Airbus A350-900, however initial simulations have shown that the new shape is estimated to have a 10% higher L/D and a 2% lower empty weight. Moreover, in the design, the engines are mounted on top of the aircraft, reducing the noise level compared the reference aircraft.

At the TU Delft the research into the advantages of the Flying-V was continued. Faggiano et al. [2017] performed an optimisation at the cruise condition of Mach 0.85, lift coefficient (C_L) of 0.26 and an altitude of 13,000m. A key adjustment made to the design was to increase the outer wing sweep from 15° to 30° to reduce high local Mach numbers on the wing and improve the lift distribution. To extend, this also improved the L/D ratio from 22.8 to 23.5. Finally, this newly optimised design was compared to the NASA Common Research Model. With an L/D of 18.9, it was found that the Flying-V is 25% more efficient than the reference model.

After the aerodynamic optimisation, the flight characteristics were analysed by R.Viet [2019]. Experiments were conducted on a 4.6% scaled model in the Open Jet Facility at the Delft University of Technology. Using balance measurements it was shown that at untrimmed configuration the wind tunnel model has a maximum lift coefficient of 1.09 at 41 degrees angle of attack. The same measurements concluded that the stability derivative of the pitching moment is negative up to an angle of attack of 20°, measured at the quarter mean aerodynamic chord. The opportunity was also taken to investigate trimmed flight. It was found that due to trim limitations the centre of gravity location is limited between 1.345 and 1.425 meters behind the nose. An optimal centre of gravity location of 1.365 meters behind the nose was found when approach was taken into account. At this trimmed condition, the stall speed was found to be at $14.8 m/s$ at an angle of attack of 28.5°.

Continuing with experimenting in the wind tunnel, the static stability and control characteristics were researched by Palermo [2019]. At an angle of attack range from −10° to 35° deep-stall characteristics were not observed, meaning that at least within this range control surfaces will stay effective. It was found that the optimal centre of gravity position for a maximised lift coefficients at a position of 1.336 meters from the nose. The maximum lift coefficient in clean configuration at horizontal steady flight is 0.7. It is concluded that statically stable flight can be achieved with a maximum lift coefficient of 0.7 at the most forward centre of gravity location of 1.33 meters and 0.6 with the centre of gravity at the most aft location of 1.39 meters from the nose.

Another wind tunnel research discussed in this paper is performed by Garcia [2019]. Here a model identification was performed using the gathered wind tunnel data of the Flying-V model. It was found that in general global polynomials, where the model structure was determined using a Modified Stepwise Regression, achieve appropriate prediction performance. Deficiencies were found due to the large range of measured angle of attack. Therefore, splines were used to estimate a continuous model with a better fit. Unfortunately, it was not possible to compare these results with other Flying-V model data, since these were not available at the time. The estimated models did provide the possibility to determine thrust and control surfaces settings required for level flight at different airspeeds and flight angles. It also included the centre of gravity range that needs to be maintained to ensure controllable of the aircraft in the most probable flight conditions.

The previous wind tunnel experiments did not include any engines on the scaled model. Empelen [2020] investigated the effects on the performance when engines are integrated. It was found that this integration generates additional lift due to jet inference. However, an increase in drag has also been observed. Moreover, C_{m_α} gets influenced by the addition. Between 5° and 12.5° C_{m_α} is decreased, while it increases between 12.5° and 22.5°. For the trim, it was observed that the deflection will be less than ±2.5° due to

engine interference.

Finally, the winglets were added to the wind tunnel model. Johnson [2021] performed an analysis on the effects of a winglet and rudder deflection since these are integrated into the winglets. For angels below 10° it was found that the lift coefficient slightly increases with about 0.0035 and for higher angels decreases by about 0.016. The drag coefficient increases by about 0.004 for angels below 28°. In addition, a winglet also reduces the maximum untrimmed L/D ratio from 14.4 to 12.3 at 10° angle of attack and increases the pitching moment. The rudder deflections have also been found to reduce the lift coefficient, with a maximum of 0.0024.

11.2. FLYING-V LAYOUT

The layout of the Flying-V is presented in this section. In Table 11.1 the important physical parameters of the Flying-V can be found and in figs. 11.1a to 11.1d multiple views of the Flying-V are presented[3].

Table 11.1: Design parameters of the full scale Flying-V [Cappuyns et al., 2019]

Parameter	Value	Unit
Length	55	[m]
Wingspan	65	[m]
Height	17	[m]
Pax	314	[−]
Fuel capacity	140.000	[l]
Cargo Capacity	160	[m^3]
Design Mach number	0.85	[−]
Cruise altitude	43,000	[ft]

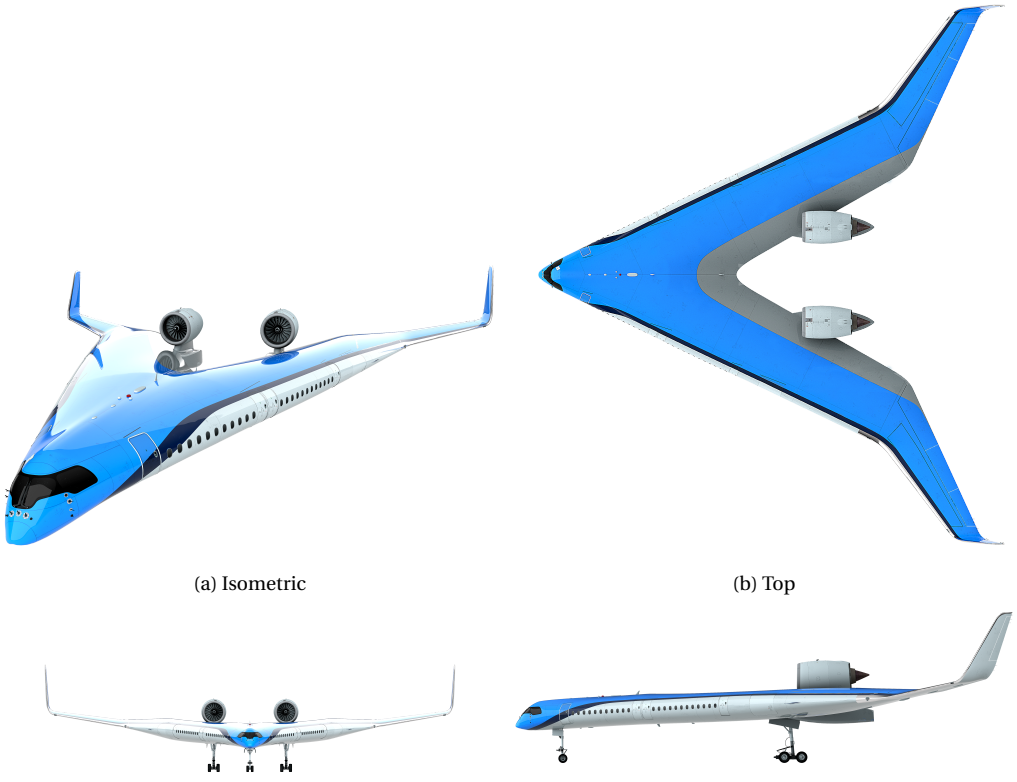

(a) Isometric

(b) Top

(c) Front

(d) Left

Figure 11.1: Renderings of the Flying-V

[3] https://www.tudelft.nl/en/ae/flying-v/

12 | Aircraft model identification

Since the early years of science human try to develop models to approximate and predict the behaviour of systems[Klein and Morelli, 2006], this has developed into the field of system identification. Scientists observe the input and output behaviour of systems and identify mathematical models that can approximate certain behaviours of the system. This process can be applied to a wide variety of fields, from chemistry to meteorology and engineering, they all rely on a form of system identification to study system behaviour[Ljung, 2017]. Aircraft system identification is one important aspect of aircraft development. The mathematical models are needed to analyse system behaviour, develop controllers and build simulators. In this chapter a definition of system identification is explained in section 12.1, after that, in section 12.2, the definitions of the important frames of reference are given. Followed by the equations of motion in section 12.3. Then the steps of parameter estimation and different methods are discussed in section 12.4. Measures of performance are given in section 12.5. Then the effects of scaling aircrafts are briefly elaborated on in section 12.6. And finally, in section 12.7, manoeuvres are discussed which optimise the identification process.

12.1. System identification

As explained by Klein and Morelli [2006], system identification is one of the following three main problems in aircraft dynamics and control:

1. Simulation: given input **u** and system **S**, find output **y**
2. Control: given system **S** and output **y**, find input **u**
3. System identification: given input **u** and output **y**, find system **S**

For aircraft system identification most commonly the inputs are often controller inputs, like ailerons, elevator, rudder and thrust or external inputs like gusts, i.e. the forces and moments acting on the aircraft. The outputs are the vehicle attitudes or change in attitude. The data can be gathered using in-flight testing or, when the aircraft is still in early developing stages the data can be obtained during wind tunnel testing[García et al., 2020].

12.1.1. Mathematical Modelling

Depending on the system, the prior knowledge and available tools, the eventual mathematical model that represents the system can take different forms. Therefore it is important to know which system will be identified, what the operational conditions are and data can be gathered.

Classification of Identification Problem

The available data and knowledge of the system direct the category of the identification problem, according to Laban [1994]. The problems can be classified into three categories:

1. General system identification problem
    - When prior knowledge about the of the system and possible model is scarce, it can be regarded as a general system identification problem. These models purely rely on input-output relations. Therefore, the model itself does not hold any information about the physics of the system. These models are therefore also referred to as "black-box" models, as the user will not be able to extract any meaningful relationships from the model. The main strength of this method is that it can be used to model any system with a quantifiable input and output. However, the main limitation is that the result of the black box model is generally only valid within the range it has been trained in.
2. State-parameter estimation problem

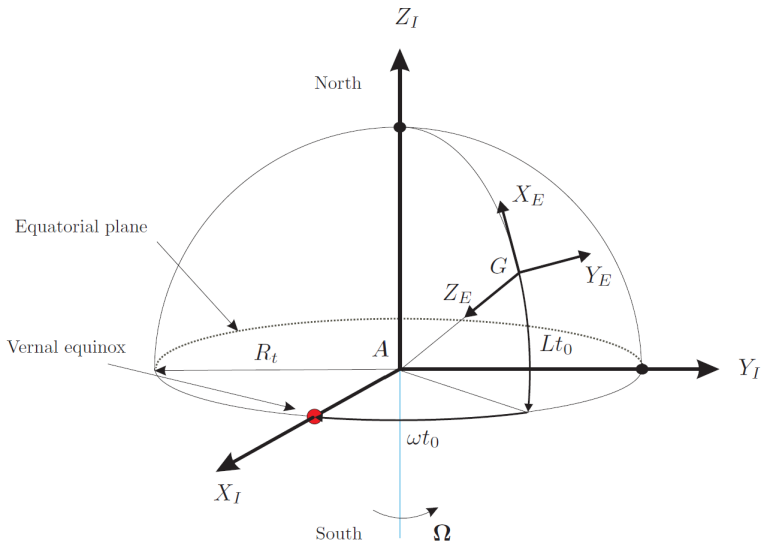

Figure 12.1: Vehicle carried normal Earth reference frame, with a spherical earth [Mulder et al., 2013].

- In the case that a model structure is known, but the states and parameters of this model are still unknown it is a state-parameter estimation problem. This model can be determined by performing a theoretical analysis of the system. The states can be determined indirectly using a combination of different sensors and knowledge of the system and its environment. Using the model and states, the parameters of the model can be estimated. This kind of problem is very common for aircraft aerodynamic system identification. Models that can represent aircraft behaviour have already been developed, [Klein and Morelli, 2006]. To fit these models to different types of aircraft measured states will be used to estimate the model parameters.

3. Parameter estimation problem

   - When the states of the system and the model structure are known, the problem can be reduced to a parameter estimation problem. The only task required is the estimation of the model parameters. For example as is done by Garcia [2019].

12.2. FRAMES OF REFERENCE

Before any kind of dynamic system modelling can be performed, it is necessary to first consider the frames of reference. A reference frames are needed to eventually derive a physical model and define the sign conventions. The three reference frames used in this research will be the Body-fixed reference frame (F_b) and the Aerodynamic reference frame (F_a). They are discussed in subsection 12.2.2 and subsection 12.2.3, respectively.

12.2.1. VEHICLE CARRIED NORMAL EARTH REFERENCE FRAME, F_E

A drawing of the Vehicle carried normal Earth reference frame can be found in Figure 12.1. The origin of this frame is at the centre of gravity of the aircraft. Tangent to the Earth surface is the $X_E Y_E$ plane. The X_E-axis points towards the north and perpendicular towards the right is the Y_E-axis. In this case it is assumed that the earth is spherical, so the Z_E-axis points, parallel with the gravitational attraction vector g_r, to the centre of the earth, as can be seen in Figure 12.1 [Mulder et al., 2013].

12.2.2. BODY-FIXED REFERENCE FRAME, F_b

The body-fixed reference frame, depicted in Figure 12.2, is a right handed orthogonal coordinate system. The origin is located at the centre of mass, and remains fixed independent of the aircraft motion. The X_b-axis points forward and coincides with the symmetry plain of the aircraft. Similarly, the Z_b-axis coincides with the symmetry plain of the aircraft, but points downwards. The Y_b-axis points to the right, perpendicular to the symmetry plain [Mulder et al., 2013].

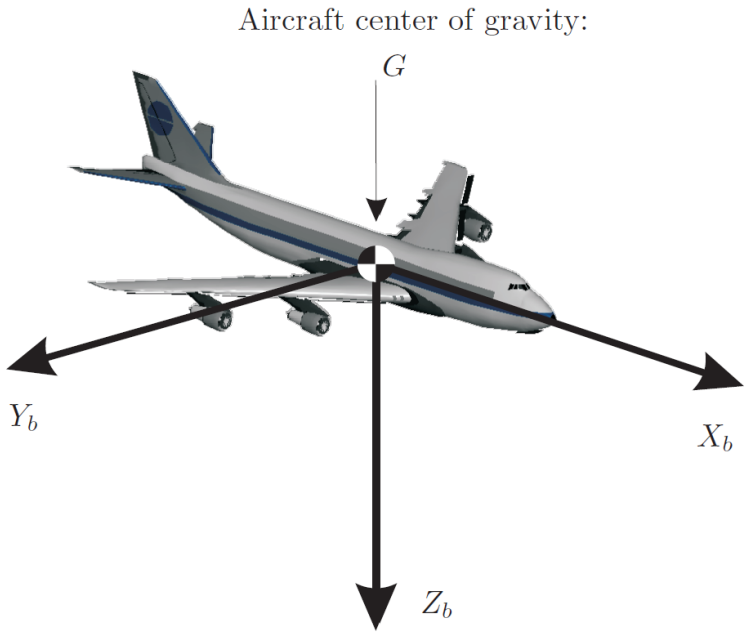

Figure 12.2: Body-fixed reference frame [Mulder et al., 2013]

12.2.3. AERODYNAMIC REFERENCE FRAME, F_a

The aerodynamic reference frame is coupled to the aerodynamic velocity of the vehicle. The origin and sign conventions are the same as the body-fixed reference frame. However, contrary to the former, the direction of the X_a-axis is not dependent on the symmetry plane. The X_a-axis is is in the direction of the velocity vector $\boldsymbol{V}_a$. The Z_a-axis is on the symmetry plain of the aircraft. The Y_a is perpendicular to the X_aZ_a plane. The velocity vector $\boldsymbol{V}_a$ is defined as:

$$\boldsymbol{V}_a = \begin{bmatrix} u_a^a \\ v_a^a \\ w_a^a \end{bmatrix} = \begin{bmatrix} V_a \\ 0 \\ 0 \end{bmatrix} \tag{12.1}$$

Expressing the aerodynamic velocity vector in the body-fixed reference frame yields:

$$\boldsymbol{V}_a^b = \begin{bmatrix} u_a^b \\ v_a^b \\ w_a^b \end{bmatrix} = \begin{bmatrix} u \\ v \\ w \end{bmatrix} \tag{12.2}$$

Figure 12.3, depicts the relationship between the aerodynamic reference frame and the body-fixed reference frame. Here α_a is the aerodynamic angle of attack and β_a the aerodynamic angle of sideslip [Mulder et al., 2013].

12.2.4. TRANSFORMATION BETWEEN REFERENCE FRAMES

In order to relate the three different reference frames to each other they have to be transformed [Mulder et al., 2013]. The transformation is as follows:

FROM F_E TO F_b

Three consecutive rotations need to be performed, therefore two intermediate reference frames are defined. The steps are:

- $F_E \rightarrow F_{E'} \rightarrow F_{E''} \rightarrow F_b$

The rotations are:

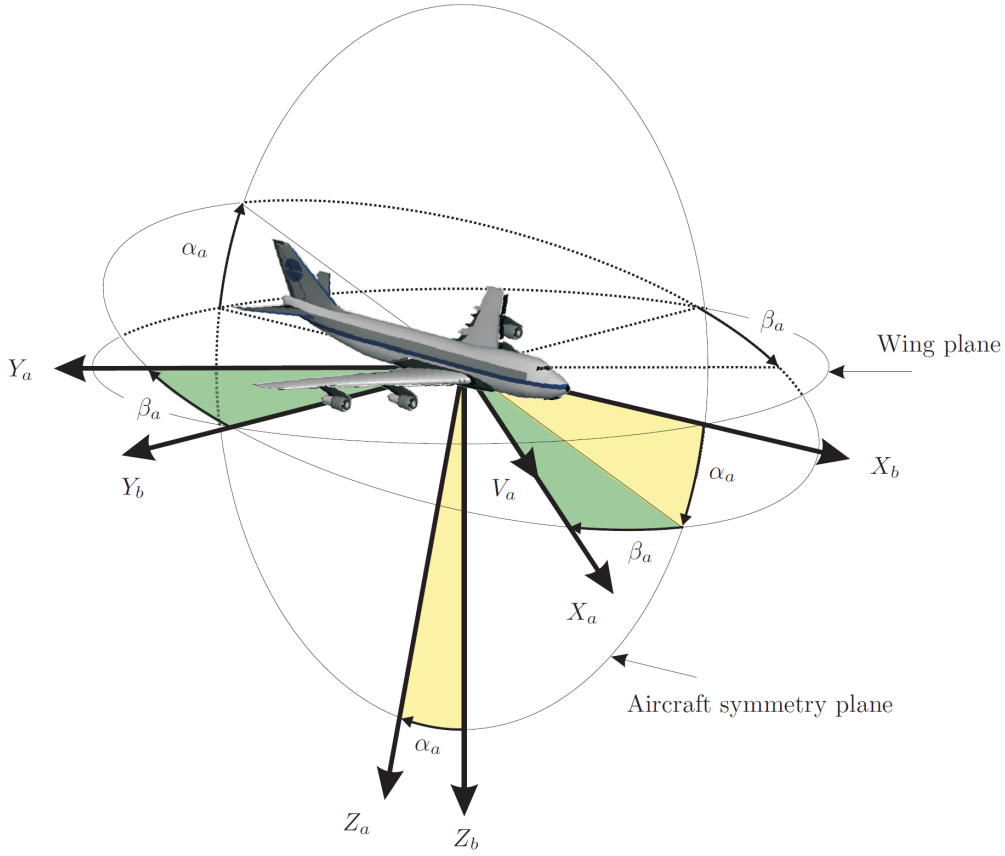

Figure 12.3: Relation between aerodynamic and body-fixed reference frame [Mulder et al., 2013].

- Rotation yaw angle ψ about Z_E-axis.
- Rotation pitch angle θ about $Y_{E'}$-axis.
- Rotation roll angle ϕ about the $X_{E''}$-axis.

This results to the following transformation matrix:

$$\mathbb{T}_{bE} = \begin{bmatrix} 1 & 0 & 0 \\ 0 & cos(\phi) & sin(\phi) \\ 0 & -sin(\phi) & cos(\phi) \end{bmatrix} \begin{bmatrix} cos(\theta) & 0 & -sin(\theta) \\ 0 & 1 & 0 \\ sin(\theta) & 0 & cos(\theta) \end{bmatrix} \begin{bmatrix} cos(\psi) & sin(\psi) & 0 \\ -sin(\psi) & cos(\psi) & 0 \\ 0 & 0 & 1 \end{bmatrix} \tag{12.3}$$

FROM F_E TO F_a

Similar to the previous transformation, two intermediate frames are defined. The transformation sequence is:

- $F_E \rightarrow F_{E'} \rightarrow F_{E''} \rightarrow F_a$

The three steps are:

- Rotation χ_a aerodynamic heading angle about the Z_E-axis.
- Rotation λ_a aerodynamic flight-path angle about the $Y_{E'}$-axis.
- Rotation μ_a aerodynamic bank angle about the X_a-axis.

This results in the following transformation matrix:

$$\mathbb{T}_{aE} = \begin{bmatrix} 1 & 0 & 0 \\ 0 & cos(\mu_a) & -sin(\mu_a) \\ 0 & sin(\mu_a) & cos(\mu_a) \end{bmatrix} \begin{bmatrix} cos(\lambda_a) & 0 & -sin(\lambda_a) \\ 0 & 1 & 0 \\ sin(\lambda_a) & 0 & cos(\lambda_a) \end{bmatrix} \begin{bmatrix} cos(\chi_a) & sin(\chi_a) & 0 \\ -sin(\chi_a) & cos(\chi_a) & 0 \\ 0 & 0 & 1 \end{bmatrix} \tag{12.4}$$

12.2.5. FROM F_b TO F_a

In contrast to the previous two transformations, this transformation only has two steps and therefore only needs on intermediate reference frame to be defined. The transformation steps are:

- $F_b \rightarrow F_{b'} \rightarrow F_a$

The rotation sequences are:

- Rotation $-\alpha_a$ aerodynamic angle of attack about the Y_b-axis.
- Rotation β_a aerodynamic sideslip angle about the $Z_{b'}$-axis.

Which results in the following transformation matrix:

$$\mathbb{T}_{ab} = \begin{bmatrix} cos(\beta_a) & sin(\beta_a) & 0 \\ -sin(\beta_a) & cos(\beta_a) & 0 \\ 0 & 0 & 1 \end{bmatrix} \begin{bmatrix} cos(\alpha_a) & 0 & sin(\alpha_a) \\ 0 & 1 & 0 \\ -sin(\alpha_a) & 0 & cos(\alpha_a) \end{bmatrix} \tag{12.5}$$

12.3. EQUATIONS OF MOTION

In order to mathematically describe the motion of the aircraft, the Equations of Motion(EoM) are constructed. The EoM consist of:

- Force and Moment equations
- Kinematic equations
- Wind-axis force equations

First, some assumptions are made in subsection 12.3.1. After that the three parts of the EoM are constructed in subsection 12.3.2, subsection 12.3.3 and subsection 12.3.4.

12.3.1. ASSUMPTIONS

To derive the equations of motion the following assumptions have to be made,[Klein and Morelli, 2006]:

- The aircraft is a rigid body with a fixed mass distribution and constant mass.
- The aircraft is symmetric.
- The air is at rest relative to the earth.
- The earth is fixed in inertial space.
- The earth's (local) surface is flat and non-rotating
- Gravity is uniform

12.3.2. FORCE AND MOMENT EQUATIONS

Keeping the assumptions into account the general motion of a rigid aircraft model can be formulated by Newton's second law:

$$\boldsymbol{F} = \frac{d}{dt}(m\boldsymbol{V}) \tag{12.6}$$

$$\boldsymbol{M} = \frac{d}{dt}(\boldsymbol{I\omega}) \tag{12.7}$$

Equation 12.6 describes the resulting force acting on the airplane, $\sum \boldsymbol{F}$. Where m is the airplane mass and $\boldsymbol{V}$ the resulting velocity vector. The resulting moment, $\boldsymbol{M}$, is expressed in Equation 12.7, where $\boldsymbol{I}$ is the mass moment of inertia and $\boldsymbol{\omega}$ the rotational rate vector [Klein and Morelli, 2006]. The components of the vectors are:

$$\boldsymbol{F} = \begin{bmatrix} F_x \\ F_y \\ F_z \end{bmatrix} \quad \boldsymbol{V} = \begin{bmatrix} u \\ v \\ w \end{bmatrix} \tag{12.8}$$

$$\boldsymbol{M} = \begin{bmatrix} M_x \\ M_y \\ M_z \end{bmatrix} \quad \boldsymbol{I} = \begin{bmatrix} I_{xx} & -I_{xy} & -I_{xz} \\ -I_{yx} & I_{yy} & -I_{yz} \\ -I_{zx} & -I_{yz} & I_{zz} \end{bmatrix} \quad \boldsymbol{\omega} \begin{bmatrix} p \\ q \\ r \end{bmatrix} \tag{12.9}$$

Since one of the assumptions is that the aircraft is symmetric all the asymmetric moments of inertia are equal to zero, so

$$\boldsymbol{I} = \begin{bmatrix} I_{xx} & 0 & -I_{xz} \\ 0 & I_{yy} & 0 \\ -I_{zx} & 0 & I_{zz} \end{bmatrix} \tag{12.10}$$

From Equation 12.6 and Equation 12.7, the vector derivatives, $\frac{d}{dt}(m\boldsymbol{V})$ and $\frac{d}{dt}(\boldsymbol{I\omega})$, are expressed as:

$$\frac{d}{dt}(m\boldsymbol{V}) = \frac{d}{dt}(m\boldsymbol{V}) + \boldsymbol{\omega} \times (m\boldsymbol{V}) \tag{12.11}$$

and

$$\frac{d}{dt}(\boldsymbol{I\omega}) = \frac{d}{dt}(\boldsymbol{I\omega}) + \omega \times (\boldsymbol{I\omega}) \tag{12.12}$$

Combining and expanding Equation 12.6 and Equation 12.11 results in:

$$\boldsymbol{F} = \begin{bmatrix} F_x \\ F_y \\ F_z \end{bmatrix} = m \begin{bmatrix} \dot{u} + qw - rv \\ \dot{v} + ru - pq \\ \dot{w} + pv - qu \end{bmatrix} \tag{12.13}$$

Doing the same to Equation 12.7 and Equation 12.11 gives:

$$\boldsymbol{M} = \begin{bmatrix} M_x \\ M_y \\ M_z \end{bmatrix} = \begin{bmatrix} \dot{p}I_x - \dot{r}I_{xz} + qr(I_z - I_y) - qpI_{xz} \\ \dot{q}I_y + pr(I_x - I_z) + (p^2 - r^2)I_{xz} \\ \dot{r}I_z - \dot{p}I_{xz} + pq(I_y - I_x) + qrI_{xz} \end{bmatrix} \tag{12.14}$$

The external forces and moments ($\boldsymbol{F}$ and $\boldsymbol{M}$) acting on the aircraft can be split up into the three main forces:

- Gravity
- Aerodynamics
- Propulsion

GRAVITY

Both the magnitude and direction are assumed to be constant. As stated in subsection 12.2.1, the gravity vector coincides with the Z_E-axis [Klein and Morelli, 2006]. Since the gravity vector originates at the centre of gravity, it will not cause a moment. The gravity vector, $\boldsymbol{F_G^E}$, is defined as:

$$F_G^E = m \begin{bmatrix} 0 \\ 0 \\ g \end{bmatrix} \tag{12.15}$$

Where g is the gravitational constant. Ideally, every influence is expressed in the same reference frame, in this case the body-fixed reference frame, F_b. Transforming the gravity vector to F_b results in:

$$\begin{gathered} \boldsymbol{F_G^b} = \mathbb{T}_{bE} F_G^E \\ \boldsymbol{F_G^b} = m \begin{bmatrix} g_x \\ g_y \\ g_z \end{bmatrix} = \begin{bmatrix} -mg\sin(\theta) \\ g\sin(\phi)\cos(\theta) \\ g\cos(\phi)\cos(\theta) \end{bmatrix} \end{gathered} \tag{12.16}$$

AERODYNAMICS

The airflow around the aircraft creates pressure differences, which generates forces on the body. The resulting aerodynamic force can be expressed in both the body-fixed reference frame($\boldsymbol{F_A^b}$) and the aerodynamic reference frame($F\boldsymbol{F_A^a}$. The two force vectors are defined as:

$$\boldsymbol{F_A^b} = \begin{bmatrix} X^b \\ Y^b \\ Z^b \end{bmatrix} \quad \boldsymbol{F_A^a} = \begin{bmatrix} X^a \\ Y^a \\ Z^a \end{bmatrix}$$

Where X, Y and Z are the forces in each corresponding carthesian axis. Using the transformation matrix from Equation 12.5, $\boldsymbol{F_A^b}$ and $\boldsymbol{F_A^a}$ can be related to eachother resulting in[Mulder et al., 2013]:

$$\begin{gathered} \boldsymbol{F_A^b} = \mathbb{T}\boldsymbol{F_A^a} \\ \begin{bmatrix} X^b \\ Y^b \\ Z^b \end{bmatrix} = \begin{bmatrix} \cos(\beta_a)\cos(\alpha_a) & -\sin(\beta_a)\cos(\alpha_a) & -\sin(\alpha_a) \\ \sin(\beta_a) & \cos(\beta_a) & 0 \\ \cos(\beta_a)\sin(\alpha_a) & -\sin(\beta_a)\sin(\alpha_a) & \cos(\alpha_a) \end{bmatrix} \begin{bmatrix} X^a \\ Y^a \\ Z^a \end{bmatrix} \end{gathered} \tag{12.17}$$

Since the resulting aerodynamic force does generally not act on the centre of gravity, it causes a moment. The resulting aerodynamic moment in F_b and in F_a are defined as:

$$\boldsymbol{M_A^b} = \begin{bmatrix} L^b \\ M^b \\ N^b \end{bmatrix} \quad \boldsymbol{M_A^a} = \begin{bmatrix} L^a \\ M^a \\ N^a \end{bmatrix} \tag{12.18}$$

Where L, M and N are the moments about the x, y and z axis, respectively. The force and moment vectors can also be expressed in non-dimensional coefficients:

$$\boldsymbol{F_A} = \overline{q}S \begin{bmatrix} C_X \\ C_Y \\ C_Z \end{bmatrix} \quad \boldsymbol{M_A} = \overline{q}S \begin{bmatrix} bC_l \\ \overline{c}C_m \\ bC_n \end{bmatrix} \quad With \quad \overline{q} = \frac{1}{2}\rho V^2 \tag{12.19}$$

Where $\overline{q}$ is the dynamic pressure, ρ the air density, V the magnitude of the airspeed, S the wing reference area, b the wingspan, and $\overline{c}$ the mean aerodynamic chord[Klein and Morelli, 2006].

PROPULSION

It is assumed that the thrust provided by the propulsion system acts along the x-axis in F_b[Klein and Morelli, 2006]. The thrust vector is defined as:

$$\boldsymbol{F}_T^b = \begin{bmatrix} T \\ 0 \\ 0 \end{bmatrix}$$

Where T is the magnitude of the thrust. The force vector may not act on the centre of gravity and can therefore cause a moment [Mulder et al., 2013]. The moment vector in F_b is defined as:

$$\boldsymbol{M}_P^b = \begin{bmatrix} M_{P,x}^b \\ M_{P,y}^b \\ M_{P,z}^b \end{bmatrix}$$

In addition, the angular momentum of rotating mass of the propulsion system may induce a moment. Since the thrust is assumed to act along the x-axis, the angular momentum can be described as:

$$\boldsymbol{h}_p = \begin{bmatrix} I_p\Omega_p \\ 0 \\ 0 \end{bmatrix}$$

Where I_p is the moment of inertia of the rotational mass and Ω_p the angular velocity. When the angular velocity is constant, the moment due to the angular momentum is defined as [Klein and Morelli, 2006]:

$$\boldsymbol{M}_T = \frac{d}{dt}(\boldsymbol{h_p}) = \boldsymbol{\omega} \times \boldsymbol{h}_p = \begin{bmatrix} 0 & -r & -q \\ r & 0 & -p \\ -q & p & 0 \end{bmatrix} \begin{bmatrix} I_p\Omega_p \\ 0 \\ 0 \end{bmatrix} = \begin{bmatrix} 0 \\ I_p\Omega_p r \\ -I_p\Omega_p q \end{bmatrix} \tag{12.20}$$

Summarising, adding the external forces and moments together results in:

$$\begin{bmatrix} \dot{u} \\ \dot{v} \\ \dot{w} \end{bmatrix} = \begin{bmatrix} rv - qw + \frac{\overline{q}S}{m}C_X - g\sin(\theta) + \frac{T}{m} \\ pw - ru + \frac{\overline{q}S}{m}C_Y + g\cos(\theta)\sin(\phi) \\ qu - pv + \frac{\overline{q}S}{m}C_z + g\cos(\theta)\cos(\phi) \end{bmatrix} \tag{12.21}$$

and

$$\begin{bmatrix} \dot{p} - \frac{I_{xz}}{I_x}\dot{r} \\ \dot{q} \\ \dot{r} - \frac{I_{xz}}{I_z}\dot{p} \end{bmatrix} = \begin{bmatrix} \frac{\overline{q}Sb}{I_x}C_l - \frac{(I_z - I_y)}{I_x}qr + \frac{I_{xz}}{I_x}qp \\ \frac{\overline{q}S\overline{c}}{I_y}C_m - \frac{(I_x - I_z)}{I_y}pr - \frac{I_{xz}}{I_y}(p^2 - r^2) + \frac{I_p}{I_y}\Omega_p r \\ \frac{\overline{q}Sb}{I_z}C_n - \frac{(I_y - I_x)}{I_z}pq - \frac{I_{xz}}{I_z}qr - \frac{I_p}{I_z}\Omega_p q \end{bmatrix} \tag{12.22}$$

12.3.3. ROTATIONAL KINEMATIC EQUATIONS

The rotational kinematic equations describe the rate of change of the Euler angles of the angular velocity in F_b [Klein and Morelli, 2006]. The derivation is as follows:

$$\begin{bmatrix} p \\ q \\ r \end{bmatrix} = \begin{bmatrix} \dot{\phi} \\ 0 \\ 0 \end{bmatrix} + \begin{bmatrix} 1 & 0 & 0 \\ 0 & \cos(\phi) & \sin(\phi) \\ 0 & -\sin(\phi) & \cos(\phi) \end{bmatrix} \begin{bmatrix} 0 \\ \dot{\theta} \\ 0 \end{bmatrix} + \begin{bmatrix} 1 & 0 & 0 \\ 0 & \cos(\phi) & \sin(\phi) \\ 0 & -\sin(\phi) & \cos(\phi) \end{bmatrix} \begin{bmatrix} \cos(\theta) & 0 & -\sin(\theta) \\ 0 & 1 & 0 \\ \sin(\theta) & 0 & \cos(\theta) \end{bmatrix} \begin{bmatrix} 0 \\ 0 \\ \dot{\psi} \end{bmatrix}$$

$$\begin{bmatrix} p \\ q \\ r \end{bmatrix} = \begin{bmatrix} 1 & 0 & -\sin(\theta) \\ 0 & \cos(\phi) & \sin(\phi)\cos(\theta) \\ 0 & -\sin(\phi) & \cos(\phi)\cos(\theta) \end{bmatrix} \begin{bmatrix} \dot{\phi} \\ \dot{\theta} \\ \dot{\psi} \end{bmatrix} \tag{12.23}$$

Equation 12.3.3 can be rewritten to:

$$\begin{bmatrix} \dot{\phi} \\ \dot{\theta} \\ \dot{\psi} \end{bmatrix} = \begin{bmatrix} p + \tan(\theta)(q\sin(\phi) + r\cos(\phi)) \\ q\cos(\phi) - r\sin(\phi) \\ \frac{q\sin(\phi) + r\cos(\phi)}{\cos(\theta)} \end{bmatrix} \tag{12.24}$$

12.3.4. WIND-AXIS FORCE EQUATIONS

In general, the aerodynamic force and moment coefficients, derived in Equation 12.19, are expressed as functions of α, β and $\frac{V}{a}$, where a is the speed of sound. As can be seen in Figure 12.3, the angle of attack, α, angle as sideslip, β, and airspeed, V, are defined as:

$$\alpha = \arctan(\frac{w}{u}) \tag{12.25}$$

$$\beta = \arcsin(\frac{v}{V}) \tag{12.26}$$

$$V = \sqrt{u^2 + v^2 + w^2} \tag{12.27}$$

Using these the velocity components in F_b can be expressed as:

$$\boldsymbol{V} = \begin{bmatrix} u \\ v \\ w \end{bmatrix} = \begin{bmatrix} V\cos(\alpha)\cos(\beta) \\ V\sin(\beta) \\ V\sin(\alpha)\cos(\beta) \end{bmatrix} \tag{12.28}$$

By differentiating Equation 12.25, Equation 12.26 and Equation 12.27 the following rotational rates can be found:

$$\dot{V} = \frac{1}{V}(u\dot{u} + v\dot{v} + w\dot{w}) \tag{12.29}$$

$$\dot{\alpha} = \left(\frac{u\dot{w} - w\dot{u}}{u^2 + w^2}\right) \tag{12.30}$$

$$\dot{\beta} = \left(\frac{V\dot{v} - v\dot{V}}{V^2}\right)\left[\frac{1}{\sqrt{1-(v/V)^2}}\right] = \frac{(u^2+w^2)\dot{v} - v(u\dot{u} + v\dot{v} + w\dot{w})}{V^2\sqrt{u^2+w2}} \tag{12.31}$$

Substituting Equation 12.28 gives:

$$\dot{V} = -\frac{\bar{q}S}{m}C_{D_W} + \frac{T}{m}\cos(\alpha)\cos(\beta) + g(\cos(\phi)\cos(\theta)\sin(\alpha)\cos(\beta) + \sin(\phi)\cos(\theta)\sin(\beta) - \sin(\theta)\cos(\alpha)\cos(\beta)) \tag{12.32}$$

$$\dot{\alpha} = -\frac{\bar{q}S}{mV\cos(\beta)}C_L + q - \tan(\beta)(p\cos(\alpha) + r\sin(\alpha)) + \frac{g}{V\cos(\beta)}(\cos(\phi)\cos(\theta)\cos(\alpha) + \sin(\theta)\sin(\alpha)) - \frac{T\sin(\alpha)}{mV\cos(\beta)} \tag{12.33}$$

$$\dot{\beta} = \frac{\bar{q}S}{mV}C_{Y_W} + p\sin(\alpha) - r\cos(\alpha) + \frac{g}{V}\cos(\beta)\sin(\phi)\cos(\theta) + \frac{\sin(\beta)}{V}\left(g\cos(\alpha)\sin(\theta) - g\sin(\alpha)\cos(\phi)\cos(\theta) + \frac{T\cos(\alpha)}{m}\right) \tag{12.34}$$

Where

$$C_L = -C_Z\cos(\alpha) + C_X\sin(\alpha) \tag{12.35}$$
$$C_D = -C_X\cos(\alpha) - C_Z\sin(\alpha) \tag{12.36}$$
$$C_{D_W} = C_D\cos(\beta) - C_Y\sin(\beta) \tag{12.37}$$
$$C_{Y_W} = C_Y\cos(\beta) + C_D\sin(\beta) \tag{12.38}$$

12.3.5. COMPLETE SET OF EQUATIONS OF MOTION

The previous discussed eqs. (12.21), (12.22), (12.24) and (12.32) to (12.34) make up the EoM. Now the aircraft motion can be described as

$$\dot{\boldsymbol{x}} = \boldsymbol{f}(\boldsymbol{x}, \boldsymbol{u}) \tag{12.39}$$

where $\boldsymbol{x}$ is the state vector, $\boldsymbol{u}$ the input vector and $\boldsymbol{f}(\boldsymbol{x}, \boldsymbol{u})$ the system model [Klein and Morelli, 2006].

12.3.6. LINEARISED EQUATIONS OF MOTION

Equation 12.39 is a nonlinear first order differential equation. In order to improve usability, the EoM can be linearised. They will be linearised around a given flight condition, meaning that the final results will only be valid for that flight condition [Mulder et al., 2013]. The linearisation will be performed using a Taylor series expansion. Take Equation 12.39, this will be expanded to:

$$\begin{aligned} y = {} & f(x_0, u_0) + \left[f_x(x_0, u_0)\Delta x + f_u(x_0, u_0)\Delta u\right] \\ & + \frac{1}{2!}\left[f_{xx}(x_0, u_0)\Delta x^2 + 2f_{xu}(x_0, u_0)\Delta x\Delta u + f_{uu}(x_0, u_0)\Delta u^2\right] \\ & + \frac{1}{3!}\left[f_{xxx}(x_0, u_0)\Delta x^3 + 3f_{xxu}(x_0, u_0)\Delta x^2\Delta u\right. \\ & + \left. 3f_{xuu}(x_0, u_0)\Delta x\Delta u^2 + f_{uuu}(x_0, u_0)\Delta u^3\right] \\ & + \ldots \end{aligned} \tag{12.40}$$

Where x_0 and u_0 are the given flight condition. Each part of the EoM can be linearised in this manner. Linearising the Equations of Motion yields:

$$X = X_o + X_u\Delta u + X_w\Delta w + X_q q + X_\delta\Delta\delta \tag{12.41}$$
$$Y = Y_o + Y_v\Delta v + Y_p p + Y_r r + Y_\delta\Delta\delta \tag{12.42}$$
$$Z = Z_o + Z_u\Delta u + Z_w\Delta w + Z_{\dot{w}}\Delta\dot{w} + Z_q q + Z_\delta\Delta\delta \tag{12.43}$$
$$L = L_o + L_v\Delta v + L_p p + L_r r + L_\delta\Delta\delta \tag{12.44}$$
$$M = M_o + M_u\Delta u + M_w\Delta w + M_{\dot{w}}\Delta\dot{w} + M_q q + M_\delta\Delta\delta \tag{12.45}$$
$$N = N_o + N_v\Delta v + N_p p + N_r r + N_\delta\Delta\delta \tag{12.46}$$

Where X_i, Y_i, Z_i, L_i, M_i and N_i are the derivatives of the moment or force in the corresponding direction with respect to i [Klein and Morelli, 2006].

12.3.7. NON-DIMENSIONAL MODEL

A non-dimensional model is used to make it it independent of airspeed and air density. The forces and moments will be expressed as non-dimensional coefficients which are dependent on the states, so:

$$C_X = C_X(u, w, q, \delta) \tag{12.47}$$
$$C_Y = C_Y(v, p, r, \delta) \tag{12.48}$$
$$C_Z = C_Z(u, w, \dot{w}, q, \delta) \tag{12.49}$$
$$C_L = C_L(v, q, r, \delta) \tag{12.50}$$
$$C_M = C_M(u, w, \dot{w}, q, \delta) \tag{12.51}$$
$$C_N = C_N(v, p, r, \delta) \tag{12.52}$$

Since u, v and w will be normalised with the pre-set velocity and when it is assumed that only small angles will occur, the velocities can be replaced by aerodynamic angles, since:

$$\alpha \approx \frac{\delta u}{V_0} \quad \beta \approx \frac{\delta v}{V_0} \quad \gamma \approx \frac{\delta w}{V_0}$$

In addition, since small angles are assumed and using eqs. (12.35) and (12.36), $C_X \approx -C_D$ and $C_Z \approx -C_L$. The non-dimensional force and moment equations can be expressed as:

Longitudinal

$$C_L = C_{L_0} + C_{L_V}\frac{\Delta V}{V_0} + C_{L_\alpha}\Delta\alpha + C_{L_{\dot{\alpha}}}\frac{\dot{\alpha}\bar{c}}{2V_0} + C_{L_q}\frac{q\bar{c}}{2V_0} + C_{L_\delta}\Delta\delta \tag{12.53}$$
$$C_D = C_{D_0} + C_{L_V}\frac{\Delta V}{V_0} + C_{D_\alpha}\Delta\alpha + C_{D_q}\frac{q\bar{c}}{2V_0} + C_{D_\delta}\Delta\delta \tag{12.54}$$
$$C_m = C_{m_0} + C_{m_V}\frac{\Delta V}{V_0} + C_{m_\alpha}\Delta\alpha + C_{m_{\dot{\alpha}}}\frac{\dot{\alpha}\bar{c}}{2V_0} + C_{m_q}\frac{q\bar{c}}{2V_0} + C_{m_\delta}\Delta\delta \tag{12.55}$$

Lateral

$$C_Y = C_{Y_0} + C_{Y_V}\frac{\Delta V}{V_0} + C_{Y_\beta}\Delta\beta + C_{Y_p}\frac{pb}{2V_0} + C_{L_r}\frac{rb}{2V_0} + C_{L_\delta}\Delta\delta \tag{12.56}$$

$$C_l = C_{l_0} + C_{l_V}\frac{\Delta V}{V_0} + C_{l_\beta}\Delta\beta + C_{l_p}\frac{pb}{2V_0} + C_{l_r}\frac{rb}{2V_0} + C_{l_\delta}\Delta\delta \tag{12.57}$$

$$C_n = C_{n_0} + C_{n_V}\frac{\Delta V}{V_0} + C_{n_\beta}\Delta\beta + C_{n_p}\frac{pb}{2V_0} + C_{n_r}\frac{rb}{2V_0} + C_{n_\delta}\Delta\delta \tag{12.58}$$

The coefficients C_{a_i} are the stability derivatives. These derivatives quantify the dependence of certain inputs (subscript i) and the forces and moments (subscript a). For example, if the coefficient is negative, when the input increases the force or moment decreases and vice versa. While with a positive coefficient the force or moment increases when the input increases. The magnitude of the coefficient influences the magnitude of the output force. The definition of each coefficient can be found in chapter 15 [Mulder et al., 2013].

12.4. PARAMETER ESTIMATION

In the previous section a general aircraft dynamic model is derived. The next step is to determine the parameters to complete the model. The methods to perform this task are explained in this section.

In subsection 12.1.1 three different categories of model identification are explained. Since the explained EOM is a possible model structure, the classification task reduces to either a state-parameter estimation problem or parameter estimation problem. Whether the state has to be estimated depends on the availability and quality of the sensors. Therefore, both the state and parameter estimation steps will be explained.

12.4.1. STATE ESTIMATION

To account for noise, sensor limitations and inaccuracy, a state estimation needs to performed. The most common state estimation method is the Kalman filter, according to [Klein and Morelli, 2006]. The Kalman filter is an optimal filter, meaning that it will estimate the minimum covariance error based on the available observations. Using statistical sensor data and a multitude of different sensors, a state estimation problem can be formulated. The linear filter process is set out as follows.

LINEAR KALMAN FILTER

The linear Kalman filter is based on the assumption that the equations of motion are linear, so the state-space form is:

$$\dot{\boldsymbol{x}} = \boldsymbol{A}\boldsymbol{x} + \boldsymbol{B}\boldsymbol{u} + \boldsymbol{w} \tag{12.59}$$

Where $\boldsymbol{A}$ are the system dynamics, $\boldsymbol{B}$ the control dynamics and $\boldsymbol{w}$ white noise. The sensor measurements (z) are linearly dependent on the states, so:

$$\boldsymbol{z} = \boldsymbol{H}\boldsymbol{x} + \boldsymbol{v} \tag{12.60}$$

Where H is the measurement matrix, and v is white measurement noise. Both eqs. (12.59) and (12.60) need to be discretised to be able to use the Kalman filter. The discretised versions are:

$$\underline{x}_{k+1} = \Phi_{k+1,k}\underline{x}_k + \Psi_{k+1,k}\underline{u}_k + \Gamma_{k+1,k}\underline{w}_{d,k} \tag{12.61}$$

$$\underline{z}_{k+1} = H_{k+1}\underline{x}_{k+1} + D_{k+1}\underline{u}_{k+1} + \underline{v}_{k+1} \tag{12.62}$$

The filter itself is set up in the following recursive steps:

1. One step ahead measurement prediction
2. One step ahead covariance prediction
3. Determine Kalman gain
4. Measurement update
5. Covariance matrix of state estimation error

Before these steps two initial conditions are determined:

$$\hat{x}(0|0) = \overline{x}_0 \tag{12.63}$$
$$\boldsymbol{P}(0|0) = \boldsymbol{P}_0 \tag{12.64}$$

Where $\hat{x}$ is the optimal estimate of the state and $\boldsymbol{P}$ is the covariance matrix. The the Kalman filter steps are defined as follows[Klein and Morelli, 2006].

- One-step ahead measurement prediction:

$$\underline{\hat{x}}_{k+1,k} = \Phi_{k+1,k}\underline{\hat{x}}_{k,k} + \Phi_{k+1,k}\underline{u}_k; \quad \underline{\hat{x}}_{0,0} = \underline{\hat{x}}_0 \tag{12.65}$$
$$\tag{12.66}$$

  Where $\underline{\hat{x}}_{k+1,k}$ is the state prediction, $\underline{\hat{x}}_{k,k}$ the current state.

- One-step ahead covariance prediction:

$$P_{k+1,k} = \Phi_{k+1,k}P_{k,k}\Phi^T_{k+1,k} + \Gamma_{k+1,k}Q_{d,k}\Gamma^T_{k+1,k}; \quad P_{0,0} = P_0 \tag{12.67}$$

  Where $P_{k+1,k}$ is the covariance prediction and $P_{k,k}$ the current covariance matrix. $Q_{d,k}$ is the white noise characteristic, defined as $E\left\{\underline{w}_{d,i}\underline{w}^T_{d,j}\right\} = Q_{d,i}$.

- Determine Kalman gain (K_{k+1}):

$$K_{k+1} = P_{k+1,k}H^T_{k+1}(H_{k+1}P_{k+1,k}H^T_{k+1} + R_{k+1})^{-1} \tag{12.68}$$

  Where R_{k+1} is the sensor noise covariance defined as: $E\underline{v}_i\underline{v}^t_j = R_i$.

- Measurement update:

$$\underline{\hat{x}}_{k+1,k+1} = \hat{x}_{k+1,k} + K_{k+1}\left(\underline{z}_{k+1} - H_{k+1}\hat{x}_{k+1,k}\right) \tag{12.69}$$

  Where $x_{k+1,k+1}$ is the optimal state estimate.

- Covariance matrix of state estimation error:

$$P_{k+1,k+1} = (I - K_{k+1}H_{k+1})\,P_{k+1,k} \tag{12.70}$$

  $P_{k+1,k+1}$ is the optimal covariance matrix

NON-LINEAR KALMAN FILTER

In addition to the linear Kalman filter, several different other Kalman filters exist. The most common non-linear Kalman filter is the Extended Kalman filter(EKF). The non-linear equations of motion are in this case:

$$\dot{\underline{x}}(t) = f(\underline{x}(t), \underline{u}(t), t) + G(\underline{x}(t), t)\underline{w}(t) \tag{12.71}$$

And the observation equation:

$$\underline{z}(t) = h(\underline{x}(t), \underline{u}(t), t) \tag{12.72}$$

For the EKF it is assumed that $f(\underline{x}(t), \underline{u}(t), t)$ and $h(\underline{x}(t), \underline{u}(t), t)$ are continuous and differentiable with respect to $\underline{x}$ and $\underline{u}$. The addition of the EKF compared to the linear Kalman Filter, is that the nonlinear state and observation equations will be linearised about the nominal values of $\underline{x}^*(t)$ and $\underline{u}^*(t)$. This is done by calculating the Jacobian of eqs. (12.71) and (12.72), which will need to be discretised. The remainder of the EKF is the same as the linear Kalman filter. The steps are set out as follows, the extra steps with respect to the linear Kalman filter are marked in bolt.

1. One-step ahead prediction:

$$\underline{\hat{x}}_{k+1,k} = \underline{\hat{x}}_{k,k} + \int_{t_k}^{t_{k+1}} f\left(\underline{\hat{x}}_{k,k}, \underline{u}_k^*, t\right) dt \tag{12.73}$$

2. **Calculate Jacobians:**

$$F_x\left(\underline{x}^*(t), \underline{u}^*(t), t\right) = \frac{\partial}{\partial \underline{x}} f(\underline{x}(t), \underline{u}(t), t)$$

and

$$H_x\left(\underline{x}^*(t), \underline{u}^*(t), t\right) = \frac{\partial}{\partial \underline{x}} h(\underline{x}(t), \underline{u}(t), t)$$

3. **Discretise the Jacobians**

4. Covariance matrix of state prediction error:

$$P_{k+1,k}\left(\underline{x}^*(t), \underline{u}^*(t), t\right) = \Phi_{k+1,k}\left(\underline{x}^*(t), \underline{u}^*(t), t\right) P_{k,k} \Phi_{k+1,k}^T\left(\underline{x}^*(t), \underline{u}^*(t), t\right) \tag{12.74}$$

$$+\Gamma_{k+1,k}\left(\underline{x}^*(t), \underline{u}^*(t), t\right) Q_{d,k}\left(\underline{x}^*(t), \underline{u}^*(t), t\right) \Gamma_{k+1,k}^T\left(\underline{x}^*(t), \underline{u}^*(t), t\right) \tag{12.75}$$

5. Calculate Kalman gain:

$$K_{k+1}\left(\underline{x}^*(t), \underline{u}^*(t), t\right) = P_{k+1,k}\left(\underline{x}^*(t), \underline{u}^*(t), t\right) H_x^T\left(\underline{x}^*(t), \underline{u}^*(t), t\right) \tag{12.76}$$

$$\left[H_x\left(\underline{x}^*(t), \underline{u}^*(t), t\right) P_{k+1,k}\left(\underline{x}^*(t), \underline{u}^*(t), t\right) H_x^T\left(\underline{x}^*(t), \underline{u}^*(t), t\right) + R_{k+1}\right]^{-1} \tag{12.77}$$

6. Measurement update:

$$\underline{\hat{x}}_{k+1,k+1} = \underline{\hat{x}}_{k+1,k} + K_{k+1}\left(\underline{x}^*(t), \underline{u}^*(t), t\right)\left[\underline{z}_{k+1} - \underline{h}\left(\underline{\hat{x}}_{k+1,k}, \underline{u}_{k+1}^*\right)\right] \tag{12.78}$$

7. Covariance matrix of state estimation error:

$$P_{k+1,k+1}\left(\underline{x}^*(t),\underline{u}^*(t),t\right)=\left[I_n-K_{k+1}\left(\underline{x}^*(t),\underline{u}^*(t),t\right)H_x\left(\underline{x}^*(t),\underline{u}^*(t),t\right)\right]P_{k+1,k}\left(\underline{x}^*(t),\underline{u}^*(t),t\right) \tag{12.79}$$

12.4.2. LINEAR PARAMETER ESTIMATION

After the states are estimated, the next step is to fit a model that can represent a system. The ordinary least squares and stepwise regression are discussed in this section.

ORDINARY LEAST SQUARES

For simple linear models the ordinary least squares (OLS) is a common method to estimate the parameters of a known model structure. For the following model:

$$\boldsymbol{y}=\boldsymbol{X}\boldsymbol{\theta} \tag{12.80}$$

$\boldsymbol{y}$ is the output vector and $\boldsymbol{\theta}$ are the model parameters. The OLS estimates the parameters by minimising the squared error between the measured output and the estimated output [Klein and Morelli, 2006]. The cost function that needs to be minimised is:

$$J(\boldsymbol{\theta})=\frac{1}{2}(\boldsymbol{y}-\boldsymbol{X}\hat{\boldsymbol{\theta}})^T(\boldsymbol{y}-\boldsymbol{X}\hat{\boldsymbol{\theta}}) \tag{12.81}$$

The derivative with respect to $\boldsymbol{\theta}$ is evaluated in order to minimise the cost function, so:

$$\frac{\partial J}{\partial \boldsymbol{\theta}}=-\boldsymbol{X}^T\boldsymbol{y}+\boldsymbol{X}^T\boldsymbol{X}\hat{\boldsymbol{\theta}}=\boldsymbol{0} \tag{12.82}$$

The OLS estimator will be:

$$\hat{\boldsymbol{\theta}}=(\boldsymbol{X}^T\boldsymbol{X})^{-1}\boldsymbol{X}^T\boldsymbol{y} \tag{12.83}$$

The most important properties of the OLS are:

- The OLS estimator is unbiased, meaning that $E(\hat{\boldsymbol{\theta}})=\boldsymbol{\theta}$.
- The OLS estimator is the best unbiased estimate for a linear model.
- The OLS estimator is consistent.

STEPWISE REGRESSION

The main weakness of the OLS is that it can only be performed when an adequate model structure is already known. The stepwise regression method does not rely on a predefined model structure with unknown parameters, instead it will determine a model by stepwise adding parameters which promise good performance, assess the performances of previously added parameters when new ones are added and delete them when they become redundant. It does this by combining two methods called Forward elimination and Backward elimination [Klein, 1989].

Forward selection

This method starts with only the independent constant term θ_0. One by one new terms will be added to the model, either until all regressors are added or until a selection criterion is satisfied. The order on which new terms are added is dependent on the simple correlation with the dependent variable, adjusted for mean value. The simple correlation between the regressor ξ_j and z is determined using

$$r_{jz} = \frac{\sum_{i=1}^{N} \left[\xi_j(i) - \bar{\xi}_j\right] [z(i) - \bar{z}]}{\sqrt{S_{jj} S_{zz}}} \tag{12.84}$$

Where S_{jj} is the centred sum of squares for ξ_j, calculated by

$$S_{jj} = \sum_{i=1}^{N} \left[\xi_j(i) - \bar{\xi}_j\right]^2 \tag{12.85}$$

and the centred sum of squares for S_{zz},

$$S_{zz} = \sum_{i=1}^{N} [z(i) - \bar{z}]^2 \tag{12.86}$$

When the partial F statistic of the regressor with the highest absolute simple correlation exceeds a preselected value (F_{in}) it will enter the model. The following regressor selected to enter will be the one with the highest simple correlation with the new model after the regressor of the previous step entered. So, for the second step the regressor with the highest correlation with $z - \theta_0 - \theta_1 \xi_1$ will enter when its partial F statistic passes F_{in}. The partial F statistic (F_0) for a model with p terms already in the model can be calculated with

$$F_0 = \frac{SS_R\left(\hat{\boldsymbol{\theta}}_{p+j}\right) - SS_R\left(\hat{\boldsymbol{\theta}}_p\right)}{s^2} \tag{12.87}$$

Here $SSR_R(\hat{\boldsymbol{\theta}}_p)$ is the sum of squares of the regression with p terms and $SS_R\left(\hat{\boldsymbol{\theta}}_{p+j}\right)$ is the sum of squares of the existing model with p terms and the jth regressor added. s^2 is the fit error variance which is computed as

$$s^2 \equiv \hat{\sigma}^2 = \frac{\boldsymbol{v}^T \boldsymbol{v}}{(N-p-1)} = \frac{\sum_{i=1}^{N} [z(i) - \hat{y}(i)]^2}{(N-p-1)} \tag{12.88}$$

In this equation it is assumed that the jth term is included in the regression. The addition of terms will continue until new regressors cannot pass F_{in} or all available regressors are added to the model.

Backward elimination

Backward elimination is the opposite of forward selection. Backward elimination starts with all the regressors already in the regression equation. In this case the partial F statistic of each term is determined and the term with the lowest statistic will be eliminated if it is lower than the predefined value F_{out}, so

$$F_0 = \min_j \frac{SS_R\left(\hat{\boldsymbol{\theta}}_p\right) - SS_R\left(\hat{\boldsymbol{\theta}}_{p-j}\right)}{s^2} < F_{\text{out}} \tag{12.89}$$

Where $SS_R(\hat{\boldsymbol{\theta}}_{p-j})$ is the sum of squares of the regression without the jth regressor term. Equally to the forward selection, the backward elimination will continue until F_{out} cannot be passed.

Stepwise regression

As mentioned before, the stepwise regression is a combination of forward selection and backward elimination. It starts the same as forward selection, the first regressor to enter is the one with the highest absolute simple correlation, Equation 12.84. The model will then look like

$$z(i) = \theta_0 + \theta_1 \xi_1(i) + v(i) \tag{12.90}$$

Where $v(i)$ is the residual, θ_j will be fitted using the OLS. If the partial F statistic of the new regression exceeds F_{in} the new model is accepted, so

$$F_0 = \frac{SS_R(\theta_1)}{s^2} > F_{in} \tag{12.91}$$

The next step is to construct new regressors in the candidate pool using the previous candidate pool by removing the part of the terms that are already modelled by the current regression. For example the new second regressor is modelled as

$$\xi_2(i) = a_0 + a_1\xi_1(i) \tag{12.92}$$

a_0 and a_1 are determined using the OLS. The new regressor will be the residual, so

$$v_2 = \xi_2(i) - \hat{a}_0 - \hat{a}_1\xi_1(i) \tag{12.93}$$

This will be performed for each other remaining regressor, every time a new term is added to the model. The second part of the stepwise regression is the elimination part. Every time a new term is added to the regression, the partial F statistic, Equation 12.89, of each selected regressor in the model is evaluated. When the F statistic of any of the regressors is lower than F_{out} it will be eliminated from the model. The regression is finished when candidate regressors cannot be added and selected regressor cannot be eliminated.

Modified stepwise regression

A regular stepwise regression often has the problem that the final model contains too many terms. This negatively influences the performance of the model, since it will overfit the data so it will not be able to represent extremer cases. Therefore, in aerospace, it is more common to use the modified stepwise regression (MSR). The regular stepwise regression starts with an empty regression and then fully depends on statistical methods to determine which terms will inter and exit the regression. The MSR gives preference to the linear regressors and terms the user finds important, for example C_{m_α}. This can be done in two ways, The first step of the MSR will be to only select the linear terms in the regression, after this the non-linear terms are evaluated. The linear terms are kept in the model irrespective of their statistical performance [Klein et al., 1983].

DATA PARTITIONING

The model identification methods mentioned above will produce continuous polynomial models. The results are, unfortunately, not valid for extreme cases, that are not close to the flight conditions of the performed manoeuvre. These models are not able to represent a wide range of conditions, like large variations in angle of attack or control deflection. Data partitioning can be used to produce models that represent a wide range of conditions [Batterson, 1981]. The data set will be split up in multiple partitions, each partition containing conditions that are important to be modelled. For example, when taking x, the set will be partitioned in m subsets, like this

$$y\left(\bar{x}_p, t\right) = \begin{cases} f_1\left[x_1(t), x_2(t), \ldots, x_{p-1}(t), x_{p+1}(t), \ldots, x_n(t)\right] \\ \qquad \text{for } x_{p0} < x_p < x_{p1} \\ f_2\left[x_1(t), x_2(t), \ldots, x_{p-1}(t), x_{p+1}(t), \ldots, x_n(t)\right] \\ \qquad \text{for } x_{p1} < x_p < x_{p2} \\ f_m\left[x_1(t), x_2(t), \ldots, x_{p-1}(t), x_{p+1}(t), \ldots, x_n(t)\right] \\ \qquad \text{for } x_{p_{m-1}} < x_p < x_{p_m} \end{cases} \tag{12.94}$$

Where

$$\overline{x}_p = \frac{x_{p_{i+1}} + x_{p_i}}{2} \tag{12.95}$$

The range, $\Delta x_p = |x_{p_i} - x_{p_{i+1}}|$ should be small enough such that

$$\overline{x}_p \approx x = \text{constant} \tag{12.96}$$

This means that the median of the subset is equal to the same point in the original set [Batterson and Klein, 1987]. It is important to note that by doing data partitioning the data set will not be continuous in time anymore. Different sections in time may have the same condition.

MULTIVARIATE ORTHOGONAL FUNCTIONS

When performing a linearisation of the EoM using a Taylor series expansion, as is done in Equation 12.41. In order to construct the regressors, higher order combinations of the various independent states are constructed. For example, α^2 or $\alpha^2\delta_e^3$. The issue that arises here is that the regressors become highly correlated. For a parameter estimation method it will then get more difficult to identify which regressor is responsible for which observed behaviour. Multivariate Orthogonal Functions is a method to make each regressor uncorrelated and isolate important unique behaviours in each regressor [Morelli, 1993].

12.4.3. NON-LINEAR PARAMETER ESTIMATION

Often it is not possible to fit the system behaviour in a linear model. At high angles of attack non-linear system behaviour is observed, since flow separation and vortices occur [R.Viet, 2019; Palermo, 2019]. Several methods are available to model these behaviours as mentioned in subsection 12.4.3. Garcia [2019] used simple polynomial splines to model the high angle of attack behaviours. Multivariate simplex splines, as proposed by De Visser [2011], with extra refinement at conditions where non-linearities occur would be a more advanced parametric method. A lot of interest has also been show to the use of neural networks to model system behaviour. Boëly and Botez [2010]; Akpan and Hassapis [2011] used neural networks to model fighter jet behaviour at high mach numbers and angle of attacks, good fitting performance was achieved. However, it was also mentioned that it hard to study stability performance, since the model itself is hard to analyse. Another aspect that has to be taken into account, especially for neural networks, is the complexity of the method. A simple polynomial splines model may already be sufficient in modelling the desired behaviours. Several methods are explained to develop models that can fit this non-linear behaviour in the following these methods are:

- Splines
- Neural network

SPLINES

Spline models are models that consist of multiple piecewise continuous functions connected to each other to form one continuous model. B-splines have been used extensively to model non-linear systems [Bruce and Kellett, 1998]. These splines consist of multiple polynomials expressed in terms of basis functions. It is stated that cubic splines are most commonly used with second order continuity at the knots, where the polynomials connect, this will in general render the connections invisible. The general representation of a nonuniform B-Spline, over the interval $0 < u < 1$, is defined as

$$f(u) = \sum_{i=0}^{m} b_{i,k}(u)\, p_i \tag{12.97}$$

Where $b_{i,k}$ is the kth order blending function for the ith control point and p_i are the coefficients. The shape of each blending function can be determined using the Cox-deBoor algorithm [Schumaker, 2007]. Equation 12.97 can also be extended to a multivariate spline representation, the 2-d case defined as:

$$f(u,v) = \sum_{i=0}^{n} \sum_{j=0}^{m} b_{i,k}(u) b_{j,l}(v) p_{i,j} \tag{12.98}$$

The major disadvantage of B-splines is that they can only interpolate on a rectangular mesh and cannot fit scattered data. Multivariate simplex splines are very well suited to model scattered data [De Visser, 2011]. It is shown that these models are more accurate in modelling non-linear systems than B-splines or polynomials. Another advantage mentioned is that the parameters that form the simplex splines are linear. Therefore, linear regression methods can be used to estimate these. A simplex spline consists out of multiple simplices joined together, each supporting a single B-form polynomial representing the data in their section. The spline polynomials are defined by barycentric coordinates, $\mathbf{b} \in \mathbb{R}^{n+1}$, which is a coordinate of the point $\mathbf{x} \in \mathbb{R}^n$. The Bernstein basis polynomial of degree d is defined by

$$B_\kappa^d(\mathbf{b}) := \frac{d!}{\kappa!} \mathbf{b}^\kappa \tag{12.99}$$

The single simplex t of degree d and dimension n is defined as

$$p(\mathbf{b}) = \sum_{|\kappa|=d} c_\kappa B_\kappa^d(\mathbf{b}) \tag{12.100}$$

Here c_κ is the B-coefficient. de Visser et al. [2009] states that the strength of multivariate simplex splines lies in the possibility to vary simplex sizes. So, models can be locally refined to achieve a better representation.

ARTIFICIAL NEURAL NETWORKS

The previously mentioned methods all yield clear mathematical models, where the user can relate system behaviour to parameters in the model. Neural networks, however, do not have this capability. Instead, they purely rely on input-output relationships, not needing to take any physical knowledge into account. Neural networks consists of multiple layers with several neurons each connected to the neurons of the previous and the following layer. When an individual neuron receives a signal, it will trigger an activation function (f^k) and give certain output to the next neuron which will do the same. To initiate the network, five parameters need to be chosen, input size, hidden layer size, output layer size, number of neurons in each layer and an identification data set. Each neuron is mathematically described as

$$d_i^k = f^k \left[\sum_{j=1}^{N} \left(w_{ij}^k d_j^{k-1} \right) + b_i^k \right] \tag{12.101}$$

With d_i^k the output, d_j^{k-1} the input, w_{ij}^k the weight and the bias b_i^k [Boëly and Botez, 2010] at the kth layer. A representation of a single neuron can be found in Figure 12.4.

Comparing neural networks to regression based models it was found that a neural network performs slightly better. Schlechtingen and Ferreira Santos [2011] found that both a regression based model and neural network managed to find defects, however, the neural network based model managed to detect them quicker. Similarly, Marquez et al. [1991], concluded that when a data set is "clean" both types of models perform similarly, neural networks prevail when the data set gets noisier.

12.5. MODEL PERFORMANCE

In order to judge the usability and accuracy of the estimated models, various measures can be used. In subsection 12.4.2 the partial F-statistic is already discussed when performing the stepwise regression. In order to judge the usability and accuracy of the estimated models or have additional performance parameters when doing a stepwise regression various additional measures can be used.

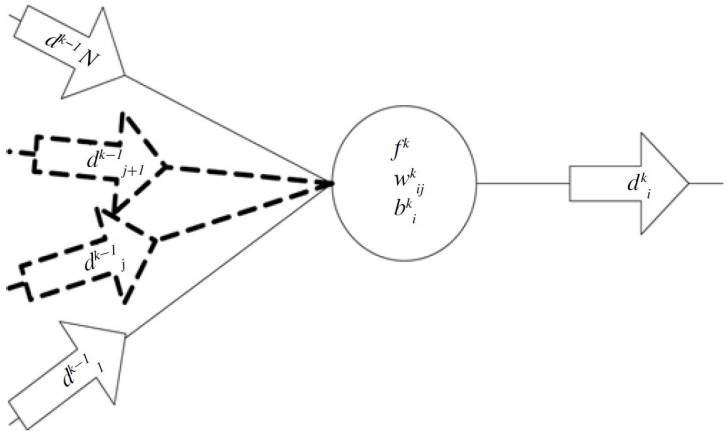

Figure 12.4: A single neuron [Boëly and Botez, 2010]

By only using the partial F statistic in stepwise regression the model may get too large or too small. i.e. the process of parameter selection may end prematurely if F_{in} is too large or if F_{out} is too small regressors with limited influence on the model may not be eliminated. The addition of other metrics are known to improve the model selection process [Klein and Morelli, 2006].

A principle often used in system identification to limit the size of the model is the principle of parsimony [Kashyap, 1977], which states:

> Given two models fitted to the same data with nearly equal residual variances, choose the model with the fewest parameters.

This means that a preference should be given to terms that significantly reduce the residual variance. The significance of the residual variance is settled by comparing the effect on the residual variance of individual terms with the variance of the measurement noise. If the magnitude of the residual variance does not exceed that of the measurement noise it is likely this term is modelling (part of) the measurement noise, which is a stochastic signal and should therefore not be included in the final model.

The coefficient of determination (R^2) assesses the overall fit of the model. For every term that is added to the model R^2 will increase, the change in R^2 can be used to judge the influence of adding terms. In the beginning R^2 will increase rapidly. However, eventually adding terms will will not significantly increase R^2, this can be a signal to stop the regression. An increase of less than 0.5% is often regarded as insignificant [Klein and Morelli, 2006]. R^2 is determined as follows

$$R^2 = \frac{SS_R}{SS_T} = 1 - \frac{SS_E}{SS_T} = \frac{\hat{\boldsymbol{\theta}}\boldsymbol{X}^T\boldsymbol{z} - N\overline{z}^2}{z^T z - N\overline{z}^2} \quad \text{where} \quad 0 \leq R^2 \leq 1 \tag{12.102}$$

Related to the R^2 is the F statistic, specified as

$$F_0 = \frac{SS_R/n}{SS_E/(N-p)} = \frac{\hat{\boldsymbol{\theta}}\boldsymbol{X}^T\boldsymbol{z} - N\overline{z}^2}{ns^2} \tag{12.103}$$

Combining this with Equation 12.102 yields the relationship

$$F_0 = \frac{(N-p)}{p-1}\frac{R^2}{1-R^2} \tag{12.104}$$

Using this metric the optimal amount of model terms can be found at the maximum F_0. Since when influential terms are added to the model, $\frac{R^2}{1-R^2}$ will dominate the equation. However, when the amount of

terms increases, $\frac{(N-p)}{p-1}$ will decrease more than $\frac{R^2}{1-R^2}$. The total F_0 will therefor decrease.

Another measure to judge the overall fitting performance of the model is the mean squared error (MSE), defined as

$$MSE = \frac{1}{N}\sum_{i=1}^{N} v(i)^2 \tag{12.105}$$

Where v(i) is the prediction error. The danger of this metric is that an increase of model terms will reduce the MSE, so overfitted models will be better according to this metric. In order to account for a growing amount of model terms the predicted squared error (PSE) is used [Morelli, 1993] and [Barron, 1984]. The PSE is defined as

$$PSE = \underbrace{\frac{1}{N}\sum_{i=1}^{N} v(i)^2}_{\text{MSE}} + 2\sigma_p^2 \frac{n}{N} \tag{12.106}$$

The first part of this equation is the MSE, the second part is a penalty to account for the amount of model terms. Where n is the amount of model terms in the model, σ^2_{max} is the highest error variance of the prediction data, defined as

$$\sigma^2_{max} = \frac{1}{N}\sum_{i=1}^{N} [\boldsymbol{z}(i) - \overline{z}]^2 \tag{12.107}$$

When adding terms to the model the PSE will be dominated by the MSE part in the beginning when the model is still small. The penalty factor will become more dominant with an increasing amount of model terms. The optimal amount of model terms, according to the PSE, is the amount with the lowest PSE.

12.6. SCALED AIRCRAFT

The eventual goal of the Flying-V project is to develop a full scale passenger aircraft. However, for current real world experiments a 4.6% scaled model is used. Several scaling effects need to be taken into account. Wolowicz and Bowman [1979] developed requirements for scaling aircraft. It is stated that when incompressible flow is assumed ($M < 0.3$) Froude scaling can be applied. Where for compressible flow ($M > 0.3$) Mach scaling is applied. The scaled version of the Flying-V is physically scaled using the Froude scaling rules. However, aerodynamically it is harder to scale the characteristics. Several plots were made that can be used to perform the Froude scaling by Wolowicz and Bowman [1979] to scale aerodynamic values. Unfortunately, these are only suitable for a minimum scale of 20%. Another research, performed by Wang et al. [2020], concluded that for a blended wing body in order to simulate stall characteristics, similarities between a scaled and full scale model, regarding Froude and Reynolds number scaling, only yielded meaningful relations at a scale of at least 50% of the full scale aircraft. Similarly, Haines [1994], concluded that clear relationships between a scaled and full scaled model cannot be found. The only method available to get a guesstimate of the characteristics of the full scale version using a scaled model is by using dimensionless models.

When performing flight test using a scaled airplane other considerations have to be taken into account as stated by Simmons et al. [2019]. The higher sensitivity to atmospheric disturbances and reduced data quality compared to larger aircraft pose extra challenges. They therefore proposed methods to improve model quality. It was found that the flight test data by itself was of poor quality due to high noise levels, measurement error and process noise are correlated and large perturbations were observed. They therefore aided the identification task by using knowledge gained from performing a VLM. This already gave an indication on which parameters may be important and which are not relevant. This method improved the fidelity of the longitudinal model. This method did not improve the fidelity of the lateral model, since

the data set was rich enough to accurately estimate a lateral model. It is important to note that the VLM method was used to aid the data set, because wind tunnel data was not available in this research.

12.7. SYSTEM IDENTIFICATION MANOEUVRES

Careful planning of flight manoeuvres can greatly benefit the model identification process. Important considerations to be made for flight testing, as described by Klein and Morelli [2006], are:

- Flight conditions, for example:
  - Trim angle of attack
  - Mach number
  - Aircraft configuration
  - Altitude
  - Power level
- Manoeuvre time length
- Control surfaces to be moved
- Input form

Typically, the flight conditions depend on the research objective, available resources and practical limitations of the experiment. For the other three considerations the objective is to excite the system such that the output data is sufficient to accurately model the system. This means that it should be possible to distinguish the deterministic signal from random noise. Klein and Morelli [2006] states that a signal-to-noise ratio (SNR) of ten or higher should provide good modelling results and a SNR as low as three may still be adequate. Another consideration is to ensure that the effects of control surfaces on aircraft behaviour are uniquely identifiable. Meaning that inputs should be planned such that the effects of control surfaces do not interfere with each other.

Single-Input manoeuvres are simple but offer accurate results. Since these are both deterministic and are only performed on one input-axis. The following input forms are the most common forms according to Klein and Morelli [2006]:

- Impulse
  - A quick input spike, it could be one sided, only one impulse in either positive or negative direction, or two sided, one impulse in positive directly followed by an impulse in negative direction.
  - Advantage:
    - Simple.
  - Disadvantage:
    - Low power manoeuvre.
- Frequency sweeps
  - A continuous sinusoid input with the frequency increasing in time. Commonly used when knowledge about the dynamic system is very limited or not available.
  - Advantage:
    - A comprehensive coverage of the frequency band, resulting in accurate models.
  - Disadvantages:
    - Sweeps take a long time.

        - Can only be applied to one input, very inefficient when multiple inputs have to be analysed.
        - Hard to maintain flight condition.
        - Frequency might pass through structural resonance frequency.

- Multisines
    - A sum of sinusoids with different frequencies, amplitudes and phase angles. Frequencies can be chose such that they cover frequencies of interest.
    - A common multisine is the Schroeder sweep.
    - Advantage:
        - Frequencies can be chosen using available knowledge to analyse frequencies of interest and/or avoid frequencies that can cause unwanted behaviours.
        - Schroeder sweep is generally considered as the superior frequency input for dynamic modelling.
        - Can be used with multiple inputs
- Doublets and Multisteps
    - Multiple steps of various sizes following each other. A doublet is a square wave, where one positive step is directly followed by a negative step. Common multistep inputs are the 3-2-1-1 and 2-1-1 manoeuvres. These sequences of numbers means that, for example for the 3-2-1-1, the first step is three seconds and positive, second two seconds and negative, third one second and positive and fourth one second and negative. Similarly, a doublet could be defined as a 1-1 or 5-5 multistep manoeuvre.
    - Similar to frequency sweeps or multisines. The timing of the steps are usually chosen to represent interesting frequencies.

Other manoeuvres could also be used to measure specific characteristics. For example the q-isolation pull-up or pushover, where the pitch rate is nonzero and the angle of attack approximately zero, as researched by Grauer et al. [2017]. This was performed to aid previously done test flights data in accurately separating C_{m_q} and $C_{m_{\dot{\alpha}}}$.

In recent years the research focus on test manoeuvres has shifted on more advanced multiple-input manoeuvres. Multiple-input manoeuvres offer the advantages of improved flight test efficiency, improved excitation of aircraft dynamics and identification of control interaction, according to [Morelli, 2021]. The main disadvantage of performing multiple-input manoeuvres is the danger of having correlated outputs. This issue is omitted by producing orthogonal optimised multisines, as is done by Morelli [2012]. These inputs are made such that the inputs are uncorrelated on both the time and frequency domain. It was found by Larsson et al. [2020] that the data acquired using multi-input has similar modelling performance as sequential single input manoeuvres while reducing the total manoeuvre time by almost 50%. This while maintaining practicality, versatility and robustness, according to Morelli [2021]. However, it is recommended to have these manoeuvres automated while a pilot is still in the loop. This to have accurate inputs while the pilot can focus on maintaining the desired flight conditions [Morelli, 2012].

13 | Flying-V model

The system identification will be done using flight data from a scaled version of the Flying-V. However, the estimated model will be developed to evaluate the handling qualities of the full scale version of the Flying-V. The possibilities to scale the aircraft states and models are discussed in this chapter.

13.1. Previous studies

13.1.1. Full-size Flying-V

Extensive research has been done on the preliminary aerodynamic sizing optimisation of the Flying-V by [Faggiano et al., 2017]. Using the initial sizing various aerodynamic analysis were performed on the full size model using computational methods. [Cappuyns et al., 2019] assessed the handling qualities using the Vortex Lattice Method(VLM) and lumped mass model. The results confirmed the lower centre of gravity range and trivial effects of a shorter tail arm compared to a conventional aircraft.

13.1.2. Windtunnel model

The next step is to physically analyse the performance of the aircraft. This will be done in wind tunnels or real flight. Unfortunately, performing these tests using a full size Flying-V is very costly, carries a lot of risk with it and it simply does not fit in a wind tunnel. Therefore, the analysis are done using a scaled model. [Garcia, 2019] performed an aerodynamic model identification on a scaled version of the Flying-V using wind tunnel data. A modified stepwise regression (MSR) was used to determine the model structure. It was found that in general global polynomials manage to establish a good model fit and for the majority of the data set the prediction capabilities were satisfactory. The polynomial models determined by Garcia [2019] are:

$$\begin{aligned} C_X = {} & C_{X0} + C_{X\alpha}\cdot\alpha + C_{X\alpha^2}\cdot\alpha^2 + C_{X\alpha^3}\cdot\alpha^3 + C_{X\alpha^4}\cdot\alpha^4 + C_{X\delta_1}\cdot\delta_1 + C_{X\delta_2}\cdot\delta_2 + \\ & + C_{X\delta_3}\cdot\delta_3 + C_{X\delta_1^2}\cdot\delta_1^2 + C_{X\delta_2^2}\cdot\delta_2^2 + C_{X\hat{V}}\cdot\hat{V} + C_{X\hat{V}^2}\cdot\hat{V}^2 \end{aligned} \tag{13.1}$$

$$C_Z = C_{Z0} + C_{Z\alpha}\cdot\alpha + C_{Z\alpha^2}\cdot\alpha^2 + C_{Z\alpha^3}\cdot\alpha^3 + C_{Z\delta_1}\cdot\delta_1 + C_{Z\delta_2}\cdot\delta_2 + C_{Z\delta_3}\cdot\delta_3 + C_{Z\hat{V}}\cdot\hat{V} \tag{13.2}$$

$$C_l = C_{l0} + C_{l\alpha}\cdot\alpha + C_{l\alpha^2}\cdot\alpha^2 + C_{l\alpha^3}\cdot\alpha^3 + C_{l\alpha^4}\cdot\alpha^4 + C_{l\delta_1}\cdot\delta_1 + C_{l\delta_2}\cdot\delta_2 + C_{l\delta_3}\cdot\delta_3 + C_{l\hat{V}}\cdot\hat{V} \tag{13.3}$$

$$\begin{aligned} C_m = {} & C_{m0} + C_{m\alpha}\cdot\alpha + C_{m\alpha^2}\cdot\alpha^2 + C_{m\alpha^3}\cdot\alpha^3 + C_{m\alpha^4}\cdot\alpha^4 + C_{m\delta_1}\cdot\delta_1 + C_{m\delta_2}\cdot\delta_2 + \\ & + C_{m\delta_3}\cdot\delta_3 + C_{m\delta_1^2}\cdot\delta_1^2 + C_{m\delta_2^2}\cdot\delta_2^2 + C_{m\delta_1\delta_2}\cdot(\delta_1\cdot\delta_2) + C_{m\alpha\delta_1^2}\cdot\left(\alpha\cdot\delta_1^2\right) + C_{m\alpha\delta_2^2}\cdot\left(\alpha\cdot\delta_2^2\right) + \\ & + C_{m\alpha^2\delta_1}\cdot\left(\alpha^2\cdot\delta_1\right) + C_{m\alpha^2\cdot\delta_2}\cdot\left(\alpha^2\delta_2\right) + C_{m\hat{V}}\cdot\hat{V} + C_{m\hat{V}\delta_1}\cdot\left(\hat{V}\cdot\delta_1\right) \end{aligned} \tag{13.4}$$

$$C_n = C_{n0} + C_{\alpha}\cdot\alpha + C_{\alpha^2}\cdot\alpha^2 + C_{\alpha^3}\cdot\alpha^3 + C_{\alpha^4}\cdot\alpha^4 + C_{\delta_1}\cdot\delta_1 + C_{\delta_2}\cdot\delta_2 + C_{\delta_1^2}\cdot\delta_1^2 + C_{\delta_2^2}\cdot\delta_2^2 + C_{\hat{V}}\cdot\hat{V} \tag{13.5}$$

The values of the coefficients can be found in tables 13.1 to 13.5.

Some model deficiencies were found for the angle of attack, because of the large range of measurement data. In order to account for this splines were used for the angle of attack. Data partitioning was recommended as an alternative, however, splines were used to maintain continuous models. They are as follows, with the coefficients in tables 13.6 to 13.10

$$\begin{aligned} C_X = {} & C_{X\alpha}\cdot\alpha + C_{X\alpha^2}\cdot\alpha^2 + C_{X\delta_1}\cdot\delta_1 + C_{X\delta_2}\cdot\delta_2 + C_{X\delta_3}\cdot\delta_3 + \\ & + C_{X\hat{V}}\cdot\hat{V} + C_{X\hat{V}^2}\cdot\hat{V}^2 + C_{X\alpha_{20}^2}\cdot(\alpha-\alpha_{20^\circ})_+^2 \end{aligned} \tag{13.6}$$

Table 13.1: Coefficients in X-direction corresponding to Equation 13.1

Parameter	Value ± confidence bounds
C_{X0}	$-2.029 \cdot 10^{-2} \pm (8.556 \cdot 10^{-4})$
$C_{X\alpha}$	$4.288 \cdot 10^{-2} \pm (2.662 \cdot 10^{-3})$
$C_{X\alpha^2}$	$9.792 \cdot 10^{-1} \pm (2.227 \cdot 10^{-3})$
$C_{X\alpha^3}$	$-1.617 \cdot 10^{-2} \pm (7.731 \cdot 10^{-2})$
$C_{X\alpha^4}$	$-1.519 \pm (1.639 \cdot 10^{-1})$
$C_{X\delta_1}$	$1.060 \cdot 10^{-2} \pm (6.473 \cdot 10^{-4})$
$C_{X\delta_2}$	$7.162 \cdot 10^{-3} \pm (1.193 \cdot 10^{-3})$
$C_{X\delta_3}$	$6.893 \cdot 10^{-4} \pm (1.294 \cdot 10^{-4})$
$C_{X\delta_1^2}$	$-3.928 \cdot 10^{-2} \pm (2.945 \cdot 10^{-3})$
$C_{X\delta_2^2}$	$-2.047 \cdot 10^{-2} \pm (4.027 \cdot 10^{-3})$
$C_{X\hat{V}}$	$8.727 \cdot 10^{-3} \pm (3.708 \cdot 10^{-4})$
$C_{X\hat{V}^2}$	$-3.075 \cdot 10^{-3} \pm (3.318 \cdot 10^{-4})$

Table 13.2: Coefficients in Z-direction corresponding to Equation 13.2

Parameter	Value ± confidence bounds
C_{Z0}	$-7.583 \cdot 10^{-2} \pm (5.310 \cdot 10^{-3})$
$C_{Z\alpha}$	$-1.943 \pm (1.564 \cdot 10^{-2})$
$C_{Z\alpha^2}$	$-1.026 \pm (1.288 \cdot 10^{-1})$
$C_{Z\alpha^3}$	$1.866 \pm (2.343 \cdot 10^{-1})$
$C_{Z\delta_1}$	$-1.353 \cdot 10^{-1} \pm (5.239 \cdot 10^{-3})$
$C_{Z\delta_2}$	$-8.462 \cdot 10^{-2} \pm (6.915 \cdot 10^{-3})$
$C_{Z\delta_3}$	$-5.012 \cdot 10^{-3} \pm (7.192 \cdot 10^{-4})$
$C_{Z\hat{V}}$	$3.747 \cdot 10^{-2} \pm (7.564 \cdot 10^{-3})$

$$\begin{aligned} C_Z = {} & C_{Z0} + C_{Z\alpha} \cdot \alpha + C_{Z\delta_1} \cdot \delta_1 + C_{Z\delta_2} \cdot \delta_2 + C_{Z\delta_3} \cdot \delta_3 + C_{Z\hat{V}} \cdot \hat{V} + \\ & + C_{Z\alpha_{11}^1} \cdot (\alpha - \alpha_{11^\circ})_+ + C_{Z\alpha_{17}^2} \cdot (\alpha - \alpha_{17^\circ})_+^2 \end{aligned} \tag{13.7}$$

$$\begin{aligned} C_l = {} & C_{l\alpha} \cdot \alpha + C_{l\delta_1} \cdot \delta_1 + C_{l\delta_2} \cdot \delta_2 + C_{l\delta_3} \cdot \delta_3 + C_{l\alpha_2^1} \cdot (\alpha - \alpha_{2^\circ})_+ + \\ & + C_{l\alpha_{20}^2} \cdot (\alpha - \alpha_{20^\circ})_+^2 + C_{l\delta_2\alpha_{14}} \cdot \delta_2 \cdot (\alpha - \alpha_{14^\circ})_+^0 + C_{l\delta_1\alpha_{23}} \cdot \delta_1 \cdot (\alpha - \alpha_{23^\circ})_+^0 \end{aligned} \tag{13.8}$$

$$\begin{aligned} C_m = {} & C_{m0} + C_{m\alpha} \cdot \alpha + C_{m\delta_1} \cdot \delta_1 + C_{m\delta_2} \cdot \delta_2 + C_{m\delta_3} \cdot \delta_3 + C_{m\hat{V}} \cdot \hat{V} + \\ & + C_{m\delta_1\delta_2} \cdot \delta_1\delta_2 + C_{m\delta_2\delta_3} \cdot \delta_2 \cdot \delta_3 + C_{m\delta_2^2} \cdot \delta_2^2 + C_{m\alpha\delta_2^2} \cdot \alpha \cdot \delta_2^2 + \\ & + C_{m\alpha_{20}^2} \cdot (\alpha - \alpha_{20^\circ})_+^2 + C_{m\alpha_{26}^2} \cdot (\alpha - \alpha_{26^\circ})_+^2 + \\ & + C_{m\delta_1\alpha_2} \cdot \delta_1 \cdot (\alpha - \alpha_{2^\circ})_+^0 + C_{m\delta_1\alpha_{23}} \cdot \delta_1 \cdot (\alpha - \alpha_{23^\circ})_+^0 + \\ & + C_{m\delta_2\alpha_{-7}} \cdot \delta_2 \cdot (\alpha - \alpha_{-7^\circ})_+^0 + C_{m\delta_2\alpha_{14}} \cdot \delta_2 \cdot (\alpha - \alpha_{14^\circ})_+^0 + \\ & + C_{m\delta_3\alpha_8} \cdot \delta_3 \cdot (\alpha - \alpha_{8^\circ})_+ \end{aligned} \tag{13.9}$$

$$\begin{aligned} C_n = {} & C_{n0} + C_{n\alpha} \cdot \alpha + C_{n\alpha^2} \cdot \alpha^2 + C_{n\delta_1} \cdot \delta_1 + C_{n\delta_2} \cdot \delta_2 + C_{n\delta_2^2} \cdot \delta_2^2 + \\ & + C_{n\hat{V}} \cdot \hat{V} + C_{n\alpha_8^1} \cdot (\alpha - \alpha_{8^\circ})_+ + C_{n\alpha_5^2} \cdot (\alpha - \alpha_{5^\circ})_+^2 \end{aligned} \tag{13.10}$$

The spline models achieved a good model fit, small confidence bounds and small parameter variances. For this analysis a half model of the airplane was used in a wind tunnel, therefore a model sideslip could not be estimated. In addition, the accuracy of the asymmetric moments, C_l and C_n, may be affected by this. Recommendations are done to use a Two-Step Method, so state estimation followed by parameter estimation, this to acquire a more accurate state estimation. This is especially needed when using in-flight

Table 13.3: Coefficients in the l-direction corresponding to Equation 13.3

Parameter	Value ± confidence bounds
C_{l0}	$3.584 \cdot 10^{-3} \pm (4.866 \cdot 10^{-4})$
$C_{l\alpha}$	$1.842 \cdot 10^{-1} \pm (1.895 \cdot 10^{-3})$
$C_{l\alpha^2}$	$-1.543 \cdot 10^{-2} \pm (4.737 \cdot 10^{-4})$
$C_{l\alpha^3}$	$3.215 \cdot 10^{-1} \pm (4.315 \cdot 10^{-2})$
$C_{l\alpha^4}$	$-8.141 \cdot 10^{-1} \pm (8.337 \cdot 10^{-2})$
$C_{l\delta_1}$	$1.842 \cdot 10^{-2} \pm (2.649 \cdot 10^{-4})$
$C_{l\delta_2}$	$1.450 \cdot 10^{-2} \pm (3.125 \cdot 10^{-4})$
$C_{l\delta_3}$	$9.893 \cdot 10^{-3} \pm (5.844 \cdot 10^{-4})$
$C_{l\hat{V}}$	$-3.036 \cdot 10^{-3} \pm (5.311 \cdot 10^{-4})$

Table 13.4: Coefficients in the m-direction corresponding to Equation 13.4

Parameter	Value ± confidence bounds
C_{m0}	$3.361 \cdot 10^{-2} \pm (2.788 \cdot 10^{-3})$
$C_{m\alpha}$	$-1.069 \cdot 10^{-1} \pm (5.938 \cdot 10^{-3})$
$C_{m\alpha^2}$	$-2.883 \cdot 10^{-1} \pm (6.506 \cdot 10^{-3})$
$C_{m\alpha^3}$	$-8.492 \cdot 10^{-1} \pm (1.839 \cdot 10^{-1})$
$C_{m\alpha^4}$	$4.088 \pm (3.731 \cdot 10^{-1})$
$C_{m\delta_1}$	$-1.482 \cdot 10^{-1} \pm (2.139 \cdot 10^{-3})$
$C_{m\delta_2}$	$-1.092 \cdot 10^{-1} \pm (1.433 \cdot 10^{-3})$
$C_{m\delta_3}$	$-6.377 \cdot 10^{-2} \pm (3.673 \cdot 10^{-3})$
$C_{m\delta_1^2}$	$1.039 \cdot 10^{-1} \pm (1.608 \cdot 10^{-2})$
$C_{m\delta_2^2}$	$3.400 \cdot 10^{-2} \pm (1.127 \cdot 10^{-2})$
$C_{m\delta_1\delta_2}$	$6.120 \cdot 10^{-2} \pm (1.248 \cdot 10^{-2})$
$C_{m\alpha\delta_1^2}$	$-5.459 \cdot 10^{-1} \pm (5.529 \cdot 10^{-2})$
$C_{m\alpha\delta_2^2}$	$-2.125 \cdot 10^{-1} \pm (4.211 \cdot 10^{-2})$
$C_{m\alpha^2\delta_1}$	$1.729 \cdot 10^{-1} \pm (4.450 \cdot 10^{-2})$
$C_{m\alpha^2\delta_2}$	$1.775 \cdot 10^{-1} \pm (3.443 \cdot 10^{-2})$
$C_{m\hat{V}}$	$8.071 \cdot 10^{-3} \pm (3.664 \cdot 10^{-3})$
$C_{m\hat{V}\delta_1}$	$2.203 \cdot 10^{-3} \pm (4.492 \cdot 10^{-4})$

data, since on-board sensors are less accurate and are not able to measure all the necessary states. In order to get a better sense of the noise involved in acquiring the data a Maximum Likelihood estimator is recommended. The noise statistics may be able to be determined and, when available, these can be compared to the variances and covariances of the OLS estimators. As mentioned before, the spline models managed to deliver a more accurate result than the polynomial models. More complex spline methods, like B-splines or Multivariate simplex splines could be used to get a more accurate representation of the system. Regarding the scaled wind tunnel model, it did not contain any winglets, engines and did not simulate any thrust influence. These can have implications on the accuracy of the model, especially for the force in the X-direction and moment around the Y-axis, C_m.

13.2. IN-FLIGHT MODEL

Previous studies, using simulation and wind tunnel data, have given an insight on the aerodynamic performance and handling qualities of the Flying-V. The next step is to perform flight tests and verify the previously acquired conclusions.

13.2.1. SCALED MODEL DESIGN

The Flying-V design used for the flight tests is a 4.6% scaled model, the same scale as used in the wind tunnel model discussed in subsection 13.1.2. Similar to that model, this one is also made with glass fibre

Table 13.5: Coefficients in the n-direction corresponding to Equation 13.5

Parameter	Value ± confidence bounds
C_{n0}	$2.636 \cdot 10^{-3} \pm (2.609 \cdot 10^{-4})$
$C_{n\alpha}$	$5.085 \cdot 10^{-5} \pm (4.599 \cdot 10^{-4})$
$C_{n\alpha^2}$	$9.565 \cdot 10^{-3} \pm (5.479 \cdot 10^{-4})$
$C_{n\alpha^3}$	$-2.732 \cdot 10^{-1} \pm (1.304 \cdot 10^{-2})$
$C_{n\alpha^4}$	$2.324 \cdot 10^{-1} \pm (2.823 \cdot 10^{-2})$
$C_{n\delta_1}$	$-1.097 \cdot 10^{-3} \pm (1.224 \cdot 10^{-4})$
$C_{n\delta_2}$	$-1.311 \cdot 10^{-3} \pm (2.030 \cdot 10^{-4})$
$C_{n\delta_1^2}$	$-6.060 \cdot 10^{-3} \pm (8.422 \cdot 10^{-4})$
$C_{n\delta_2^2}$	$-5.544 \cdot 10^{-3} \pm (6.520 \cdot 10^{-4})$
$C_{n\hat{V}}$	$-1.075 \cdot 10^{-3} \pm (2.293 \cdot 10^{-4})$

Table 13.6: Spline coefficients in the m-direction corresponding to Equation 13.6

Parameter	Value ± confidence bounds	Variance	VIF
$C_{X\alpha}$	$4.590 \cdot 10^{-2} \pm (3.49 \cdot 10^{-3})$	$9.003 \cdot 10^{-7}$	1.169
$C_{X\alpha_2}$	$7.484 \cdot 10^{-1} \pm (1.29 \cdot 10^{-2})$	$1.072 \cdot 10^{-6}$	46.946
$C_{X\delta_1}$	$8.103 \cdot 10^{-3} \pm (1.86 \cdot 10^{-3})$	$5.851 \cdot 10^{-7}$	1.331
$C_{X\delta_2}$	$6.727 \cdot 10^{-3} \pm (1.50 \cdot 10^{-3})$	$7.476 \cdot 10^{-7}$	1.419
$C_{X\delta_3}$	$7.246 \cdot 10^{-3} \pm (1.69 \cdot 10^{-3})$	$7.144 \cdot 10^{-7}$	38.009
$C_{X\hat{V}}$	$-2.276 \cdot 10^{-2} \pm (2.03 \cdot 10^{-3})$	$3.166 \cdot 10^{-6}$	9.810
$C_{X\hat{V}^2}$	$1.011 \cdot 10^{-2} \pm (1.66 \cdot 10^{-3})$	$4.334 \cdot 10^{-5}$	19.783
$C_{X\alpha_{20}^2}$	$-1.921 \pm (7.88 \cdot 10^{-2})$	$1.616 \cdot 10^{-3}$	4.127

shaped using Resin Liquid Infusion (RLI) with epoxy in a negative mould. At the leading and trailing edges Airex C70.75 foam panels are used. The ribs and spars are waterjet cut from earlier produced honeycomb reinforced glass fibre panels. The inside is left hollow to fit flight related components, like sensors, computers, batteries and servos. An image of the inside of the Flying-V can be found in Figure 13.1. The top and bottom half of the model are glued together using epoxy glue.

Since the intention of this model is to fly, it has more features added with respect to the half wing wind tunnel model. The important differences between the wind tunnel model and the flight model are:

- A whole aircraft instead of a half model
- Addition of landing gear
- Addition of engines
- Addition of winglets

13.2.2. DATA ACQUISITION

The purpose of flight testing is prove that the Flying-V is able to fly, but more importantly gather data to improve flight models and optimise future designs. In order to monitor the system and gather data a multitude of sensors are integrated. A Digital Airdata Computer (DADC) is responsible for the majority of the flight data. This an off the shelf μADC Air Data Computer Voyager from Aeroprobe. It is fitted with a five hole pitot tube, an Inertial Navigation System (INS) and a GPS module. Combining these the DADC accurately measures the airspeed, pitch, roll, heading, angle of attack and side slip angle, among others. The data is gathered at a sampling rate of 100 Hz. The specifications of the DADC can be found in Table 13.11 [García, 2020].

Table 13.7: Spline coefficients in the m-direction corresponding to Equation 13.7

Parameter	Value ± confidence bounds	Variance	VIF
C_{Z0}	$-8.554 \cdot 10^{-2} \pm (5.53 \cdot 10^{-3})$	$6.866 \cdot 10^{-6}$	42.245
$C_{Z\alpha}$	$-1.869 \pm (8.62 \cdot 10^{-3})$	$7.966 \cdot 10^{-6}$	46.476
$C_{Z\delta_1}$	$-1.284 \cdot 10^{-1} \pm (5.31 \cdot 10^{-3})$	$5.932 \cdot 10^{-6}$	1.363
$C_{Z\delta_2}$	$-7.395 \cdot 10^{-2} \pm (3.70 \cdot 10^{-3})$	$3.878 \cdot 10^{-3}$	4.860
$C_{Z\delta_3}$	$-4.303 \cdot 10^{-2} \pm (4.77 \cdot 10^{-3})$	$1.550 \cdot 10^{-4}$	15.576
$C_{Z\hat{V}}$	$3.126 \cdot 10^{-2} \pm (5.14 \cdot 10^{-3})$	$1.933 \cdot 10^{-5}$	8.590
$C_{Z\alpha^1_{11}}$	$-5.559 \cdot 10^{-1} \pm (2.44 \cdot 10^{-2})$	$7.350 \cdot 10^{-6}$	1.156
$C_{Z\alpha^2_{17}}$	$3.176 \pm (1.22 \cdot 10^{-1})$	$3.572 \cdot 10^{-6}$	1.247

Table 13.8: Spline coefficients in the m-direction corresponding to Equation 13.8

Parameter	Value ± confidence bounds	Variance	VIF
$C_{l\alpha}$	$1.959 \cdot 10^{-1} \pm (2.21 \cdot 10^{-3})$	$1.269 \cdot 10^{-6}$	27.538
$C_{l\delta_1}$	$1.891 \cdot 10^{-2} \pm (7.38 \cdot 10^{-4})$	$1.072 \cdot 10^{-7}$	1.425
$C_{l\delta_2}$	$1.690 \cdot 10^{-2} \pm (8.42 \cdot 10^{-4})$	$9.441 \cdot 10^{-5}$	1.689
$C_{l\delta_3}$	$9.542 \cdot 10^{-3} \pm (6.42 \cdot 10^{-4})$	$2.832 \cdot 10^{-7}$	2.897
$C_{l\alpha^1_2}$	$-1.077 \cdot 10^{-2} \pm (2.60 \cdot 10^{-3})$	$1.416 \cdot 10^{-7}$	1.288
$C_{l\alpha^2_{20}}$	$-6.556 \cdot 10^{-1} \pm (1.90 \cdot 10^{-2})$	$1.847 \cdot 10^{-7}$	2.944
$C_{l\delta_2\alpha_{14}}$	$-4.619 \cdot 10^{-3} \pm (1.04 \cdot 10^{-3})$	$1.755 \cdot 10^{-6}$	29.548
$C_{l\delta_1\alpha_{23}}$	$-4.795 \cdot 10^{-3} \pm (2.37 \cdot 10^{-3})$	$1.468 \cdot 10^{-6}$	1.104

CONTROL SURFACES

The control surfaces are controlled by servos. In total four different control surfaces on each side of the Flying-V need to be controlled, these are

- Inboard control surface
- Middle control surface
- Outboard control surface
- Rudder

Each needs their own servo. In total three different servos are used the important specification data can be found in Table 13.12 [García, 2020].

An accuracy of these servos is not given. Only for the Hitec Multiplex D954SW a resolution of 4096 is available[4]. Which would translate to an accuracy of $\frac{360}{4096} = 0.08789°$. It is likely that the other two servos have similar accuracy.

PROPULSION SYSTEM

Two ducted fans make up the external part of the propulsion system. In order to control and power these fans, two electronic speed controllers (ESCs) and two or four 12S LiPo batteries make the system complete. The specifics of the ducted fans can found in Table 13.13.

COMMUNICATION

In order to control and monitor the airplane in-flight wireless communication systems are used. An RC control link is responsible for the control of the airplane. The transmitter on the ground is a Duplex DS-14 and the receiver in the airplane a Duplex REX-12 produced by Jeti, both working at 2.4GHz. Telemetry, air data and system status are communicated using two RFD 868x radio modules produced by Pixhawk. These continually transmit to the ground station, ensuring the operators can access important data in real-time.

[4]URL https://hitecrcd.com/products/servos/d-series-servos/d954sw/product [cited 12/08/2021]

Table 13.9: Spline coefficients in the m-direction corresponding to Equation 13.9

Parameter	Value ± confidence bounds	Variance	VIF
C_{m0}	$2.440 \cdot 10^{-2} \pm (3.02 \cdot 10^{-3})$	$3.653 \cdot 10^{-4}$	4.960
$C_{m\alpha}$	$-1.461 \cdot 10^{-1} \pm (3.41 \cdot 10^{-3})$	$2.061 \cdot 10^{-6}$	43.964
$C_{m\delta_1}$	$-9.921 \cdot 10^{-2} \pm (7.30 \cdot 10^{-3})$	$5.728 \cdot 10^{-1}$	18.881
$C_{m\delta_2}$	$-8.065 \cdot 10^{-2} \pm (9.34 \cdot 10^{-3})$	$1.661 \cdot 10^{-5}$	7.801
$C_{m\delta_3}$	$-7.077 \cdot 10^{-2} \pm (4.85 \cdot 10^{-3})$	$2.595 \cdot 10^{-5}$	1.171
$C_{m\hat{V}}$	$1.383 \cdot 10^{-2} \pm (2.81 \cdot 10^{-3})$	$1.624 \cdot 10^{-2}$	22.655
$C_{m\delta_2^2}$	$4.729 \cdot 10^{-2} \pm (1.05 \cdot 10^{-2})$	$2.273 \cdot 10^{-5}$	27.494
$C_{m\alpha\delta_2^2}$	$-2.243 \cdot 10^{-1} \pm (3.75 \cdot 10^{-2})$	$6.131 \cdot 10^{-6}$	4.885
$C_{m\delta_1\delta_2}$	$4.165 \cdot 10^{-2} \pm (1.11 \cdot 10^{-2})$	$2.885 \cdot 10^{-5}$	5.039
$C_{m\delta_2\delta_3}$	$3.312 \cdot 10^{-2} \pm (1.08 \cdot 10^{-2})$	$8.540 \cdot 10^{-6}$	5.357
$C_{m\alpha_{20}^2}$	$5.545 \pm (2.50 \cdot 10^{-1})$	$2.537 \cdot 10^{-5}$	29.542
$C_{m\alpha_{26}^2}$	$-8.353 \pm (1.48 \cdot 10^{0})$	$3.035 \cdot 10^{-5}$	2.330
$C_{m\delta_1\alpha_2}$	$-4.691 \cdot 10^{-2} \pm (7.99 \cdot 10^{-3})$	$1.386 \cdot 10^{-5}$	7.560
$C_{m\delta_1\alpha_{23}}$	$5.040 \cdot 10^{-2} \pm (9.99 \cdot 10^{-3})$	$3.893 \cdot 10^{-6}$	2.823
$C_{m\delta_2\alpha_{-7}}$	$-3.080 \cdot 10^{-2} \pm (9.87 \cdot 10^{-3})$	$3.196 \cdot 10^{-5}$	1.602
$C_{m\delta_2\alpha_{14}}$	$3.383 \cdot 10^{-2} \pm (3.87 \cdot 10^{-3})$	$2.377 \cdot 10^{-6}$	48.083
$C_{m\delta_3\alpha_8}$	$1.476 \cdot 10^{-2} \pm (5.73 \cdot 10^{-3})$	$3.023 \cdot 10^{-6}$	4.656

Table 13.10: Spline coefficients in the m-direction corresponding to Equation 13.10

Parameter	Value ± confidence bounds	Variance	VIF
C_{n0}	$2.200 \cdot 10^{-3} \pm (2.68 \cdot 10^{-4})$	$7.940 \cdot 10^{-8}$	2.026
$C_{n\hat{V}}$	$-1.039 \cdot 10^{-3} \pm (2.31 \cdot 10^{-4})$	$7.877 \cdot 10^{-8}$	17.719
$C_{n\alpha}$	$-3.013 \cdot 10^{-3} \pm (5.50 \cdot 10^{-4})$	$1.863 \cdot 10^{-8}$	55.031
$C_{n\alpha^2}$	$5.844 \cdot 10^{-2} \pm (6.15 \cdot 10^{-3})$	$6.684 \cdot 10^{-9}$	1.181
$C_{n\delta_1}$	$-1.535 \cdot 10^{-3} \pm (2.33 \cdot 10^{-4})$	$1.417 \cdot 10^{-8}$	1.129
$C_{n\delta_2}$	$-1.251 \cdot 10^{-3} \pm (1.60 \cdot 10^{-4})$	$2.115 \cdot 10^{-6}$	171.828
$C_{n\delta_2^2}$	$-6.453 \cdot 10^{-3} \pm (5.52 \cdot 10^{-4})$	$1.391 \cdot 10^{-8}$	43.349
$C^1_{n\alpha_8}$	$-1.423 \cdot 10^{-2} \pm (2.85 \cdot 10^{-3})$	$9.836 \cdot 10^{-6}$	337.844
$C_{n\alpha_5^2}$	$-1.453 \cdot 10^{-1} \pm (5.90 \cdot 10^{-3})$	$9.054 \cdot 10^{-6}$	123.659

13.2.3. AVAILABLE DATA

An overview of the flight data gathered by the Flying-V can be found Table 13.14.

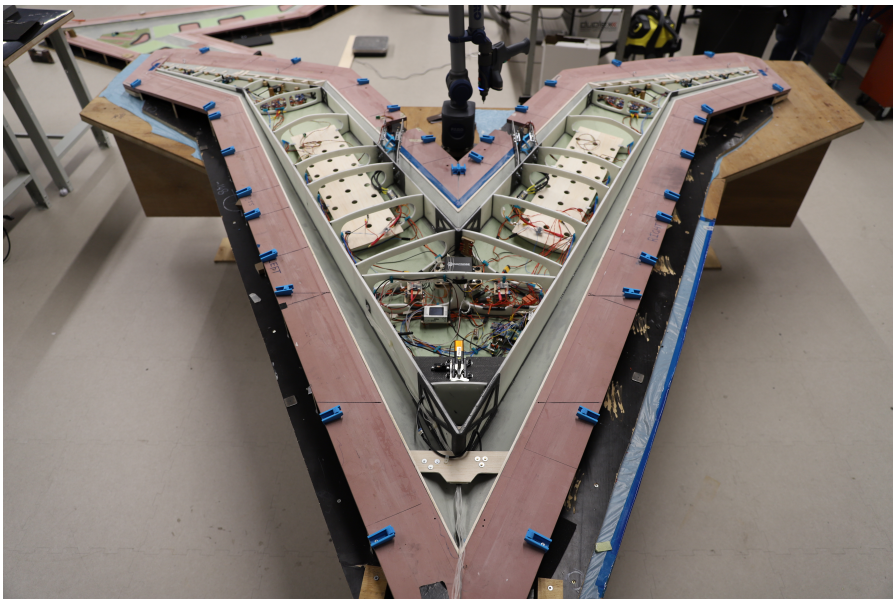

Figure 13.1: Inside of Flying-V during assembly

Table 13.11: Aeroprobe DADC specifications

Property	Value	Unit
Manufacturer	Aeroprobe	-
Model	Voyager	-
Airspeed range	16-62	-
Airspeed accuracy	±1.0	m/s
Airflow angle range (AoA & SSA)	±20	°
Airflow angle accuracy	±1.0	°
Barometric altitude resolution	1.0	m
Barometric altitude accuracy	± 24	m
Roll and pitch accuracy	0.3	°
Heading accuracy	1.0	°

Table 13.12: Servo specifications

	Value		Unit	
Manufacturer	Hitec Multiplex	Hitec Multiplex	Hitec Multiplex	-
Model	D954SW	D89MW	HS-5070MH	-
Control surface	Inboard	Middle & Rudder	Outboard	-
Max torque range	18-29	5.3-8.5	3.0-3.7	kg/cm
Operating voltage range	4.8-7.4	4.8-7.4	6.0-7.4	V
Idle current	30	30	3	mA
No load operating current	500	300	240	mA
Stall current	5200	2900	1300	mA
Speed (Seconds to 60°)	0.19-0.12	0.17-0.11	0.14-0.12	s

Table 13.13: Ducted fan specifications

	Value	Unit
Manufacturer	Schubeler Jets	-
Model number fan	DS-86-AXI HDS	-
Model number electric engine	HET800-68-685kV	-
Diameter	120	mm
Thrust static	60	N
Max voltage	52	V
Max current	108	A
Max RPM	33000	-

Table 13.14: Sensor data gathered by Flying-V

Data name	Unit	Sensor manufacturer
Angle of attack	°	Aeroprobe
Angle of sideslip	°	Aeroprobe
Airspeed	m/s	MS4525DO
Barometric altitude	m	Aeroprobe
GPS/GLONASS position	°	Ublox Neo-M8N
GPS position	°	PCTel 5012D-RD
GNSS/INS data	-	XSENS MTi-10-100
Temperature	$°C$	MLX90614

14 Conclusion

14.1. Conclusion Literature Study

The objective of this literature review was to research suitable methods for system identification on the Flying-V and investigate the limitations of using a scaled aircraft for this purpose.

Multiple methods to identify a model for the Flying-V are available. Each with its strengths and weaknesses, so determining which one is most suitable will be dependent on the data that will come available. Previous studies in the wind tunnel have shown that for low angles of attack an ordinary least squares(OLS) regression can yield accurate results. The model structure can then be determined using a stepwise regression. However, it was also found that at higher angles of attack, a linear method like the OLS will become increasingly inaccurate. Therefore, polynomial splines were used. These piecewise continuous functions managed to have a better approximation at higher angles of attack than the OLS method. An important aspect to take into consideration is the fact that for the wind tunnel analysis a half wing was used, which could only rotate around the y-axis. Consequently, forces in the y-direction could not be measured and rotation measurements around the x- and z-axis may be inaccurate. Since for the continuation of this project flight data will be used, forces and moments in and around all three Cartesian directions can be measured. In case the flight data yields nonlinear system behaviour, more advanced spline methods would be more appropriate, like B-Splines or Simplex Splines. Neural networks can also give accurate results, however, parametric methods are preferred since these are easier to be analysed by the user.

Using a 4.6% scaled version of the Flying-V will have consequences. The scaled version is physically scaled using Froude scaling, however, this method does not give any use full guides on how to relate a scaled version model to a full-scale model. In addition, Reynolds scaling and Mach scaling are also not feasible at this stage of the project, since these require extreme atmospheric conditions. The only method that may give remotely relatable results is by using dimensionless models. Another difficulty found with using a smaller aeroplane is the sensitivity to atmospheric disturbances and the reduced data quality since smaller less accurate sensors has to be fitted. A method to cope with this is to use previously gained knowledge from computational methods and wind tunnel testing to improve the quality of the model.

Bibliography

V. A. Akpan and G. D. Hassapis. Nonlinear model identification and adaptive model predictive control using neural networks. *ISA Transactions*, 50(2):177–194, 2011. ISSN 00190578. doi: 10.1016/j.isatra.2010.12.007. URL http://dx.doi.org/10.1016/j.isatra.2010.12.007.

A. Barron. Predicted Squared Error: A Criterion for Automatic Model Selection. In *Self-Organizing Methods in Modeling: GMDH Type Algorithms*, pages 87–104. New York, 1984.

J. G. Batterson. Estimation of Airplane Stability and Control Derivatives At High Angles of Attack. 2, 1981. ISSN 0018-9286. doi: 10.1109/JACC.1981.4232340.

J. G. Batterson and V. Klein. Partitioning of flight data for aerodynamic modeling of aircraft at high angles of attack. *14th Atmospheric Flight Mechanics Conference, 1987*, 26(4):444–451, 1987. doi: 10.2514/6.1987-2621.

J. Benad. the Flying V - a New Aircraft Configuration for Commercial Passenger Transport. *Deutscher Luft- und Raumfahrtkongress*, pages 1–8, 2015. URL http://www.dglr.de/publikationen/2015/370094.pdf.

N. Boëly and R. M. Botez. New approach for the identification and validation of a nonlinear F/A-18 model by use of neural networks. *IEEE Transactions on Neural Networks*, 21(11):1759–1765, 2010. ISSN 10459227. doi: 10.1109/TNN.2010.2071398.

P. D. Bruce and M. G. Kellett. Modelling and identification of nonlinear aerodynamic functions using B-splines. *IEE Conference Publication*, (455):907–912, 1998. ISSN 05379989. doi: 10.1049/cp:19980349.

T. Cappuyns, R. Vos, and K. Bender. *Handling Qualities of a Flying V Configuration*. PhD thesis, Delft University of Technology, 2019. URL http://resolver.tudelft.nl/uuid:69b56494-0731-487a-8e57-cec397452002.

C. C. De Visser. *Global Nonlinear Model Identification with Multivariate Splines*. C. C. de Visser, Delft, 2011. ISBN 9789085707707.

C. C. de Visser, Q. P. Chu, and J. A. Mulder. A new approach to linear regression with multivariate splines. *Automatica*, 45(12):2903–2909, 2009. ISSN 00051098. doi: 10.1016/j.automatica.2009.09.017. URL http://dx.doi.org/10.1016/j.automatica.2009.09.017.

S. A. V. Empelen. Engine Integration of the Flying V. 2020.

F. Faggiano, R. Vos, M. Baan, and R. Van Dijk. Aerodynamic design of a flying V aircraft. *17th AIAA Aviation Technology, Integration, and Operations Conference, 2017*, (June), 2017. doi: 10.2514/6.2017-3589.

A. R. Garcia. Aerodynamic Model Identification of the Flying V using Wind Tunnel Data (MSc Thesis). 2019. URL https://repository.tudelft.nl/islandora/object/uuid%3A79e01f29-1789-4501-8556-ca2bcf06f3ab?collection=education.

A. R. García. Flying V Scaled Model : Systems Report. Technical Report August, Delft University of Technology, Delft, 2020.

A. R. García, R. Vos, and C. C. de Visser. Aerodynamic model identification of the flying V from wind tunnel data. *Aiaa Aviation 2020 Forum*, 1 PartF:1–16, 2020. doi: 10.2514/6.2020-2739.

J. A. Grauer, E. A. Morelli, and D. G. Murri. Flight-Test techniques for quantifying pitch rate and angle-of-Attack rate dependencies. *Journal of Aircraft*, 54(6):2367–2377, 2017. ISSN 15333868. doi: 10.2514/1.C034407. URL https://doi.org/10.2514/1.C034407.

A. B. Haines. *Scale Effects on Aircraft and Weapon Aerodynamics*. Number July 1994. Essex, 1994. ISBN 9283507541.

N. Johnson. Effect of Winglet Integration and Rudder Deflection on Flying-V Aerodynamic Characteristics. 2021.

R. L. Kashyap. A Bayesian Comparison of Different Classes of Dynamic Models Using Empirical Data. *IEEE Transactions on Automatic Control*, 22(5):715–727, 1977. ISSN 15582523. doi: 10.1109/TAC.1977.1101594.

V. Klein. Estimation of aircraft aerodynamic parameters from flight data. *Progress in Aerospace Sciences*, 26 (1):1–77, 1989. ISSN 03760421. doi: 10.1016/0376-0421(89)90002-X.

V. Klein and E. A. Morelli. *Aircraft System Identification: Theory and Practice*. American Institute of Aeronautics and Astronotics, Blacksburg, Virginia, 1 edition, 2006. ISBN 1563478323.

V. Klein, J. G. Batterson, and P. C. Murphy. Airplane model structure determination from flight data. *Journal of Aircraft*, 20(5):469–474, 1983. ISSN 00218669. doi: 10.2514/3.44895.

M. Laban. *On-Line Aircraft Aerodynamic Model Identification*. 1994. ISBN 90-6275-987-4.

R. Larsson, A. Sobron, D. Lundström, and M. Enqvist. A method for improved flight testing of remotely piloted aircraft using multisine inputs. *Aerospace*, 7(9):1–25, 2020. ISSN 22264310. doi: 10.3390/AEROSPACE7090135.

L. Ljung. System Identification. In *Wiley Encyclopedia of Electrical and Electronics Engineering*, pages 1–19. John Wiley & Sons, Inc., Hoboken, NJ, USA, 2 edition, 5 2017. ISBN 0136566952. doi: 10.1002/047134608X.W1046.pub2. URL http://doi.wiley.com/10.1002/047134608X.W1046.pub2.

L. Marquez, T. Hill, R. Worthley, and W. Remus. Neural network models as an alternative to regression. *Proceedings of the Annual Hawaii International Conference on System Sciences*, 4:129–135, 1991. ISSN 15301605. doi: 10.1109/HICSS.1991.184052.

R. Martinez-Val. Flying Wings. A New Paradigm for Civil Aviation? *Acta Polytechnica*, 47(1), 2007. ISSN 1210-2709. doi: 10.14311/914.

E. A. Morelli. Nonlinear aerodynamic modeling using multivariate orthogonal functions. *Flight Simulation and Technologies, 1993*, 32(2):1–11, 1993. doi: 10.2514/6.1993-3636.

E. A. Morelli. Flight test maneuvers for efficient aerodynamic modeling. *Journal of Aircraft*, 49(6):1857–1867, 2012. ISSN 15333868. doi: 10.2514/1.C031699.

E. A. Morelli. Practical Aspects of Multiple-Input Design for Aircraft System Identification Flight Tests. pages 1–25, 2021. doi: 10.2514/6.2021-2795.

J. Mulder, W. v. Staveren, J. v. d. Vaart, E. d. Weerdt, A. i. t. Veld, and E. Mooij. Flight Dynamics - Lecture Notes. *Princeton University Press*, page 570, 2013. URL http://app.knovel.com/web/toc.v/cid:kpFD000016/viewerType:toc/root_slug:flight-dynamics/url_slug:kt00UQFX02?b-q=ailerons&b-within-title=true&b-group-by=false&b-search-type=tech-reference&b-sort-on=default.

M. Palermo. The Longitudinal Static Stability And Control Characteristics Of A Flying V Scaled Model. page 117, 2019. URL https://repository.tudelft.nl/islandora/object/uuid:6286f9e2-c24a-430c-a4fa-9fb67b9558b4?collection=education.

R.Viet. Analysis Of The Flight Characteristics Of A Highly Swept Cranced Flying Wing By Means Of An Experimental Test. page 142, 2019.

M. Schlechtingen and I. Ferreira Santos. Comparative analysis of neural network and regression based condition monitoring approaches for wind turbine fault detection. *Mechanical Systems and Signal*

Processing, 25(5):1849–1875, 2011. ISSN 08883270. doi: 10.1016/j.ymssp.2010.12.007. URL http://dx.doi.org/10.1016/j.ymssp.2010.12.007.

L. L. Schumaker. *Spline Functions: Basic theory*. 2007. ISBN 13 978-0-511-33206-7.

B. M. Simmons, H. G. McClelland, and C. A. Woolsey. Nonlinear model identification methodology for small, fixed-wing, unmanned aircraft. *Journal of Aircraft*, 56(3):1056–1067, 2019. ISSN 15333868. doi: 10.2514/1.C035160.

G. Wang, M. Zhang, Y. Tao, J. Li, D. Li, Y. Zhang, C. Yuan, W. Sang, and B. Zhang. Research on analytical scaling method and scale effects for subscale flight test of blended wing body civil aircraft. *Aerospace Science and Technology*, 106:106114, 2020. ISSN 12709638. doi: 10.1016/j.ast.2020.106114. URL https://doi.org/10.1016/j.ast.2020.106114.

C. H. Wolowicz and J. S. Bowman. Similitude Requirements and Scaling Relationships as Applied to Model Testing. *Most*, (August), 1979.

15 | Stability derivatives

15.1. Force and moment coefficients

Longitudinal parameters

$$C_X = \frac{X}{\frac{1}{2}\rho V^2 S} \quad C_Z = \frac{Z}{\frac{1}{2}\rho V^2 S} \quad C_m = \frac{M}{\frac{1}{2}\rho V^2 S\bar{c}}$$

Lateral parameters

$$C_Y = \frac{Y}{\frac{1}{2}\rho V^2 S} \quad C_l = \frac{L}{\frac{1}{2}\rho V^2 Sb} \quad C_n = \frac{N}{\frac{1}{2}\rho V^2 Sb}$$

Longitudinal stability derivatives

$$C_{X_u} = \frac{1}{\frac{1}{2}\rho V S}\frac{\partial X}{\partial u} \quad C_{Z_u} = \frac{1}{\frac{1}{2}\rho V S}\frac{\partial Z}{\partial u} \quad C_{m_u} = \frac{1}{\frac{1}{2}\rho V S\bar{c}}\frac{\partial M}{\partial u}$$

$$C_{X_\alpha} = \frac{1}{\frac{1}{2}\rho V S}\frac{\partial X}{\partial w} \quad C_{Z_\alpha} = \frac{1}{\frac{1}{2}\rho V S}\frac{\partial Z}{\partial w} \quad C_{m_\alpha} = \frac{1}{\frac{1}{2}\rho V S\bar{c}}\frac{\partial M}{\partial w}$$

$$C_{Z_{\dot\alpha}} = \frac{1}{\frac{1}{2}\rho V S\bar{c}}\frac{\partial Z}{\partial \dot w} \quad C_{m_{\dot\alpha}} = \frac{1}{\frac{1}{2}\rho V S\bar{c}^2}\frac{\partial M}{\partial \dot w}$$

$$C_{X_q} = \frac{1}{\frac{1}{2}\rho V S\bar{c}}\frac{\partial X}{\partial q} \quad C_{Z_q} = \frac{1}{\frac{1}{2}\rho V S\bar{c}}\frac{\partial Z}{\partial q} \quad C_{m_q} = \frac{1}{\frac{1}{2}\rho V S\bar{c}^2}\frac{\partial M}{\partial q}$$

$$C_{X_{\delta_e}} = \frac{1}{\frac{1}{2}\rho V^2 S}\frac{\partial X}{\partial \delta_e} \quad C_{Z_{\delta_e}} = \frac{1}{\frac{1}{2}\rho V S}\frac{\partial Z}{\partial \delta_e} \quad C_{m_{\delta_e}} = \frac{1}{\frac{1}{2}\rho V_2 S\bar{c}}\frac{\partial M}{\partial \delta_e}$$

$$C_{X_{\delta_t}} = \frac{1}{\frac{1}{2}\rho V^2 S\bar{c}}\frac{\partial X}{\partial \delta_t} \quad C_{Z_{\delta_t}} = \frac{1}{\frac{1}{2}\rho V S}\frac{\partial Z}{\partial \delta_t} \quad C_{m_{\delta_t}} = \frac{1}{\frac{1}{2}\rho V^2 S\bar{c}}\frac{\partial M}{\partial \delta_t}$$

Lateral stability derivatives

$$C_{Y_\beta} = \frac{1}{\frac{1}{2}\rho V S}\frac{\partial Y}{\partial v} \quad C_{l_\beta} = \frac{1}{\frac{1}{2}\rho V Sb}\frac{\partial L}{\partial v} \quad C_{n_\beta} = \frac{1}{\frac{1}{2}\rho V Sb}\frac{\partial N}{\partial v}$$

$$C_{Y_{\dot\beta}} = \frac{1}{\frac{1}{2}\rho V Sb}\frac{\partial Y}{\partial \dot v} \quad C_{n_{\dot\beta}} = \frac{1}{\frac{1}{2}\rho S b^2}\frac{\partial N}{\partial \dot v}$$

$$C_{Y_p} = \frac{2}{\frac{1}{2}\rho V Sb}\frac{\partial Y}{\partial p} \quad C_{l_p} = \frac{2}{\frac{1}{2}\rho V Sb^2}\frac{\partial L}{\partial p} \quad C_{n_p} = \frac{2}{\frac{1}{2}\rho V Sb^2}\frac{\partial N}{\partial p}$$

$$C_{Y_r} = \frac{2}{\frac{1}{2}\rho V Sb}\frac{\partial Y}{\partial r} \quad C_{l_r} = \frac{2}{\frac{1}{2}\rho V Sb^2}\frac{\partial L}{\partial r} \quad C_{n_r} = \frac{2}{\frac{1}{2}\rho V Sb^2}\frac{\partial N}{\partial r}$$

$$C_{Y_{\delta_a}} = \frac{1}{\frac{1}{2}\rho V^2 S}\frac{\partial Y}{\partial \delta_a} \quad C_{\ell_{\delta_a}} = \frac{1}{\frac{1}{2}\rho V^2 Sb}\frac{\partial L}{\partial \delta_a} \quad C_{n_{\delta_a}} = \frac{1}{\frac{1}{2}\rho V^2 Sb}\frac{\partial N}{\partial \delta_a}$$

$$C_{Y_{\delta_r}} = \frac{1}{\frac{1}{2}\rho V^2 S}\frac{\partial Y}{\partial \delta_r} \quad C_{l_{\delta_r}} = \frac{1}{\frac{1}{2}\rho V^2 Sb}\frac{\partial L}{\partial \delta_r} \quad C_{n_{\delta_r}} = \frac{1}{\frac{1}{2}\rho V^2 Sb}\frac{\partial N}{\partial \delta_r}$$

IV

CONCLUSION

16 Conclusion

The objective of this research was to develop a new aerodynamic model of the Flying-V using flight data. It was set up by, first, researching the possibilities and limitations of the different system identifications methods in order to find the most fitting solution for the current problem. Secondly, the aerodynamic system identification was performed using flight data. Then finally, using the new model the behaviour of the Flying-V can be analysed and compared with the previous wind tunnel studies.

The first research question is:

> Which methods are most suitable for aerodynamic system identification of the Flying-V using the available experimental flight data and information gained from previous studies?

This was treated in the literature review. Where various model structure determination methods were compared. A stepwise regression was chosen to determine the model structure, because previous studies have found this to be an ideal method to determine the structure of the polynomial models. The estimated polynomial models are especially useful in the early phases of the development of an aircraft.

After the model structure was determined the following question could be answered.

> What influence does the amount of input parameters and the individual parameters have on the model behaviour?

It was found that compared to the longitudinal polynomials, the lateral ones did use more parameters. This indicates that the lateral motions are more complex than the longitudinal ones. When analysing the influence of individual parameters C_{n_β}, the weathercock stability, stands out. For a conventional layout aircraft this stability parameter has a large influence on the directional stability of the aircraft. However, for the Flying-V this influence is small. When looking at the layout of the Flying-V compared to a conventional aircraft the rudder and arm to the rudder of the Flying-V are relatively small. This explains the small influence of C_{n_β}.

The final question was states as:

> What new information on handling and stability of the Flying-V can be gathered compared to the wind tunnel models?

For this the flight model was compared to the models found using the wind tunnel data. It became clear that the available engine model does not suffice for this in-flight use case. Especially C_X, and consequently C_D, suffer from the limited knowledge of the flight engine performance. Moreover, a large deviation was also found for C_m. This was partly due to the interaction with the engines. However, it is likely that the available data did not contain the information to fully evaluate the extent of C_m.

Altogether, taking the previously mentioned conditions into account, the presented models will give a realistic representation of the behaviour of the Flying-V. In conclusion, using the presented method, improved models will be able to be estimated when more data becomes available.

17 Recommendations

Following the conclusions recommendations for future research are presented in this chapter.

- The data set used for this analysis is fairly conservative when it comes to excitations. For future test flights it is recommended to perform manoeuvres with larger control surface deflections and aerodynamic angles. To improve the knowledge on, for example, control effectiveness and directional sensitivity.
- In the wind tunnel experiments it was found that at high angles of attack a pitch-break occurs and the aircraft can stall. Even though, this is hard to safely perform in test flights it is recommended to research this in-flight behaviours to improve future models.
- The currently available engine model does not manage to model the thrust at the evaluated flight states. For example currently the thrust is not influenced by the high angle of attack motions according to the model.
- Similarly, more data from a larger variety of identification manoeuvres would greatly enrich the available information for future iterations of the currently discussed aerodynamic model.
- It was also found that there is a possible interaction between longitudinal and lateral states. It is expected that this is from an influence between the rudder and the wing. However, more knowledge of these interactions will result in improved future models of the Flying-V and a better understanding of the implications of this phenomena.
- For the method verification the Citation-II DASMAT model is used. To improve the verification a direct comparison of parameters can be performed. Ideally the parameters estimated by the DASMAT model should converge around the parameter values estimated using the model from the stepwise regression.